SPRINGER BRIEFS IN APPLIED SCIENCES AND TECHNOLOGY · POLIMI SPRINGER BRIEFS

Fabio Borghetti
Marco Derudi
Paolo Gandini
Alessio Frassoldati
Silvia Tavelli

Tunnel Fire Testing and Modeling

The Morgex North Tunnel Experiment

POLITECNICO
DI MILANO

EXTRAS ONLINE

Springer

SpringerBriefs in Applied Sciences and Technology

PoliMI SpringerBriefs

More information about this series at http://www.springer.com/series/11159
http://www.polimi.it

Fabio Borghetti · Marco Derudi
Paolo Gandini · Alessio Frassoldati
Silvia Tavelli

Tunnel Fire Testing and Modeling

The Morgex North Tunnel Experiment

Springer

Fabio Borghetti
Department of Design
Politecnico di Milano
Milan
Italy

Marco Derudi
Department of Chemistry,
Material and Chemical Engineering
"Giulio Natta"
Politecnico di Milano
Milan
Italy

Paolo Gandini
Department of Design
Politecnico di Milano
Milan
Italy

Alessio Frassoldati
Department of Chemistry,
Material and Chemical Engineering
"Giulio Natta"
Politecnico di Milano
Milan
Italy

Silvia Tavelli
Department of Chemistry,
Material and Chemical Engineering
"Giulio Natta"
Politecnico di Milano
Milan
Italy

Additional material to this book can be downloaded from http://extras.springer.com

ISSN 2191-530X ISSN 2191-5318 (electronic)
SpringerBriefs in Applied Sciences and Technology
ISSN 2282-2577 ISSN 2282-2585 (electronic)
PoliMI SpringerBriefs
ISBN 978-3-319-49516-3 ISBN 978-3-319-49517-0 (eBook)
DOI 10.1007/978-3-319-49517-0

Library of Congress Control Number: 2016958493

Printed on acid-free paper

This Springer imprint is published by Springer Nature
The registered company is Springer International Publishing AG
The registered company address is: Gewerbestrasse 11, 6330 Cham, Switzerland

Preface

Fires in buildings, industrial plants, as well as in road, railway and underground tunnels are considerable threats for human safety. The importance of safety in road and railway tunnels and, more specifically, the concern for the risks associated with fires has grown after some recent tunnel disasters.

In this book the authors present the experience and discuss the results obtained during the experimental and modeling activities carried out within the research project "IMPROVED CFD MODELS FOR TUNNEL FIRE RISK ANALYSIS" promoted and funded by the Politecnico di Milano.

The project is the result of initiatives carried out in the field of enclosed fire dynamics and tunnel fire safety, tackling the problem from both a transportation engineering and combustion point of view. For these reasons, the activities saw the synergic cooperation of researchers of the transportation and chemical engineering departments of the Politecnico di Milano. Moreover, the project saw the active participation of public and private entities, such as *Corpo Valdostano Vigili del Fuoco* (fire fighters of Valle d'Aosta region) and the RAV company (Raccordo Autostradale Valle d'Aosta S.p.A.), which owns and operates the tunnel where the real scale tunnel fire experiments were performed.

In this book, the authors describe in detail how they planned, designed, organized and performed the experimental activity related to full-scale fire tests inside the Morgex North tunnel, a road tunnel actually in use on the A5 Aosta—Mont Blanc highway (Italy). The entire organization of the experimental activity, from preliminary evaluations to the solutions found for managing operational difficulties and taking into account potential safety issues are described in this book. Pictures, figures and tables containing the technical details are used to illustrate the activity and allow the reader to find advice on several technical and safety issues for both the infrastructure and workers involved, on how to manage them effectively and to develop appropriate policies and procedures.

This text is targeted at researchers and engineers involved in the field of safety engineering, in particular the modeling of tunnel fires dynamics and fire safety in tunnels, but also the design of safety management systems for both normal operation and emergency conditions resulting from a relevant fire event. These include,

for example, tunnel managers, emergency services, risk analysts, designers of plants and equipment, as well as students in the field of risk management and prevention and safety engineering.

The book has two main purposes. The first is to provide a detailed technical guidance on the organization of a controlled real scale tunnel fire test, specifically in the case of a tunnel which is normally open to traffic, highlighting the solutions adopted to effectively protect the tunnel infrastructure during the test while ensuring minimal traffic disruption.

The second is to collect all the experimental results related to the Morgex North fire tests in a single document with the complete details of the measured quantities and corresponding theoretical and modeling predictions. Hence, the complete fire test results are also discussed with particular attention to the evaluation of the fire heat release rate and the comparison of the values of temperature and pollutants composition, measured in several sections of the tunnel, with predictions made using semi-empirical models and CFD (Computational Fluid Dynamics) simulations. Gas concentrations and temperatures were measured both upstream and downstream of the fire, with the aim of investigating the effect of different emergency ventilation strategies on smoke backlayering and in general on the fire dynamics.

A peculiar aspect of the Morgex fire tests refers to the geometry of the tunnel and the characteristic of the accidental scenario: the presence of a bypass zone ahead of the fire region and an obstacle representing a semi-trailer located immediately downstream of the fire zone make this experiment a challenging test-case for CFD modeling of tunnel fires with longitudinal ventilation. Moreover, the Particulate Matter (PM) concentration and size distribution were measured and can be used to validate the combustion model of CFD codes with particular attention to PM formation and thermal effects.

In essence this book provides guidance to the reader on the following aspects:

- How to design a real scale fire test in a tunnel.
- Which kind of instruments can be used.
- Where to place the instruments and devices.
- How to protect these instruments from fire, thermal effects, smoke deposition, etc.
- How to protect the tunnel and its infrastructures and selection criteria for materials to be used.
- How to organize a rapid preparation and disassembling of the experimental setup.
- How to manage the safety issues and the presence of technical personnel and external observers.
- The impact of active ventilation strategies on fire dynamics with temperature and smoke composition analyses.
- Which is the accuracy of semi-empirical models and CFD simulations.

The book is organized into chapters and annexes as follows:

- Chapter 1 contains a general brief overview about safety in road tunnels.
- Chapter 2 illustrates the aim of this research project and the partners involved.
- Chapter 3 describes the tunnel geometry and the accidental scenario, and gives details on the preparation of the fire tests.
- Chapter 4 describes the results of the fire tests and the comparison with the predictions of semi-empirical correlations for tunnel fires and CFD simulations.
- Chapter 5 describes a methodology for the quantitative assessment of the severity of the fire consequences on the users safety.
- Annex A—Sections of encoded measuring instruments.
- Annex B—Selected experimental results of the Morgex fire tests.

Milan, Italy

Fabio Borghetti
Marco Derudi
Paolo Gandini
Alessio Frassoldati
Silvia Tavelli

Acknowledgments

The authors wish to thank Politecnico di Milano for the financial support (Progetto 0 per mille Junior—CUP code D41J10000490001). They also acknowledge the fruitful cooperation with the Corpo Valdostano dei Vigili del Fuoco and thank the RAV—Raccordo Autostradale Valle d'Aosta SpA team for their hospitality and competence.

Contents

Abbreviations

AMSL	Above Mean Sea Level
CCTV	Closed Circuit Television
CFD	Computational Fluid Dynamics
DG	Dangerous Goods
FDS	Fire Dynamics Simulator
FED	Fractional Effective Dose
HRR	Heat Release Rate
KHI	Key Hazard Indicator
KPI	Key Performance Index
LEL	Lower Explosive Limit
MPV	Multi-purpose Vehicle
PM	Particulate Matter
RAV	Raccordo Autostradale Valle d'Aosta
TERN	Trans European Road Network
UPS	Uninterruptible Power Supply

Chapter 1
Safety in Road Tunnels

Abstract This chapter briefly presents the main issues related to the safety inside road tunnels. Fires, events with potentially catastrophic consequences within these infrastructures, are concisely introduced.

Safety in road tunnels has a significant social relevance as a result of several accidents recently occurred in tunnels belonging to the Trans-European Road Network (TERN).

The consequences of an accident in confined space, such as a road tunnel, can be much more significant compared to those typically occurring in open air contexts. While the probability of an accident inside a tunnel is lower than in open air environments [1], because the users generally drive more carefully and the visibility and meteorological conditions are constant, it is important to notice that the potential consequences for the tunnel users and also the potential damages to the structures are significantly larger. In this context, fire safety engineering in tunnels is essential in order to ensure safe conditions for road tunnel users. A comprehensive overview on how fires develop and how they are influenced by different physical parameters such as flammability, ventilation, and tunnel geometry is given by Ingason et al. in their recent book [2]. It also contains an overview of the relevant tunnel fire experiments of the last decades.

Road traffic authorities and tunnel managers in particular have two significant concerns. Firstly, it is important to notice that tunnels, which are expensive to build and operate, often provide non-redundant network connections and therefore have a vital role in the whole transportation system. For this reason, no effective alternative route is likely to exist in the event of disrupted tunnel operation. The second concern of tunnel owners/managers is to guarantee the effective and safe use of their tunnels to transport people and goods, and also plan emergency procedures and provide assistance in the event of severe emergencies [3]. Among the possible accidental scenarios in tunnels, vehicle fires in particular pose significant risk of injuries not only for the users of the infrastructure, but also for the rescue teams.

The relevant events occurred in European road tunnels such as those of the Mont Blanc Tunnel (1999) (Fig. 1.1), the Gotthard Tunnel (2001), the Tauern Tunnel

F. Borghetti et al., *Tunnel Fire Testing and Modeling*,
PoliMI SpringerBriefs, DOI 10.1007/978-3-319-49517-0_1

Fig. 1.1 Pictures of the accident occurred in the Mont Blanc Tunnel (1999)

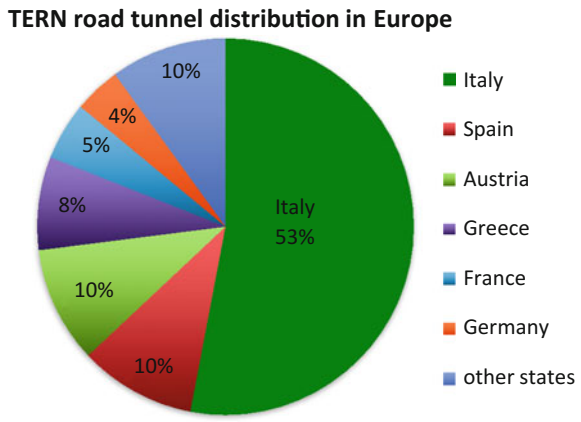

Fig. 1.2 TERN road tunnel distribution in Europe

(2002) and the Frejus Tunnel (2005), increased the attention about safety issues in tunnels, underlining the importance of these infrastructures from the human, economic and cultural point of views. Moreover, such events demonstrated the need and urgency to adapt the existing road tunnels to higher safety standards.

Italy, especially for its complex orography, is characterized by a high number of road tunnels compared to other European countries. Figure 1.2 shows the distribution of the operational road tunnels belonging to the TERN,[1] for each Member State to June 2013 [4]. It shows that Italy hosts more than fifty percent of all European tunnels with a length greater than 500 m belonging to TERN (green).

Figure 1.3 shows the features of some typical fires related to light vehicles (cars), buses, heavy vehicles and vehicles used for the dangerous goods transportation (e.g. road tankers or trailers). For each type of fire, Fig. 1.3 shows an

[1]The Trans European Road Network is composed by motorways and high-quality roads, whether existing or future, strategic for long distance traffic and ensure the interconnection with other modes of transport or allow to link regions in Europe. This network also provides users a uniform and continuous level of service, comfort and safety.

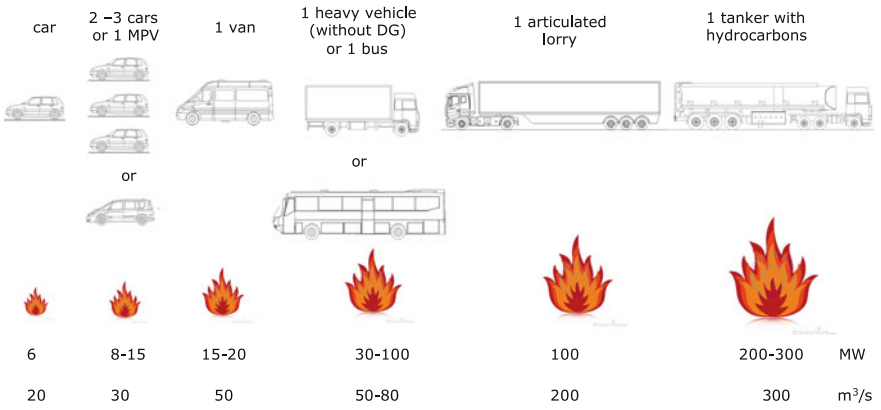

Fig. 1.3 Estimated HRR and smoke generation rates for typical road tunnel accidental scenarios

indication about the maximum achievable fire intensities, in terms of heat release rate (HRR), and the corresponding smoke generation rates [5–9].

In case of fire, but more broadly, the design of tunnel safety requires an overall analysis of the *tunnel system* [10] which includes mutual interactions among the elements mentioned in Fig. 1.4.

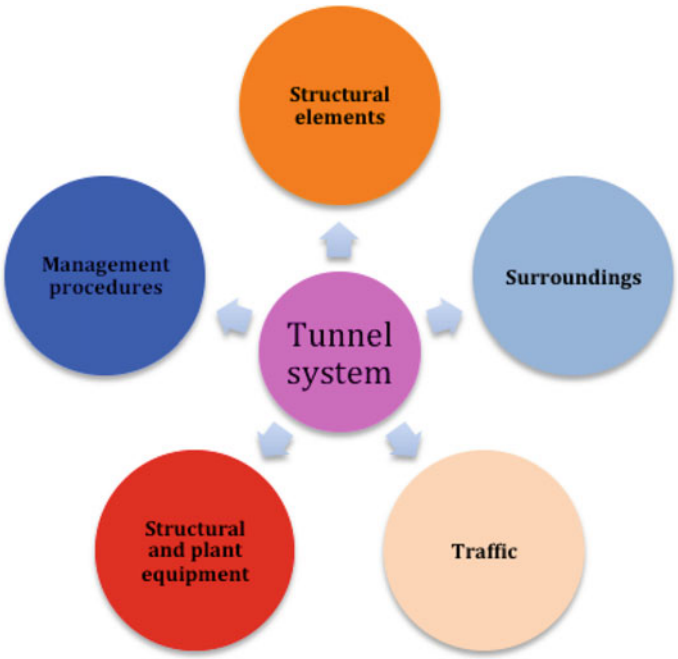

Fig. 1.4 Relationship among tunnel system elements [10]

The application of fire safety approaches to the tunnels is a complex issue. It requires a multi-disciplinary approach and broad knowledge of different aspects. It is then the result of the integration of infrastructural measures and tunnel operations with the human behaviour, the preparedness of the personnel and strategies for incidents management. Reducing risk and ensuring the safety of a tunnel require the implementation of complex systems able to reduce the occurrence or to control and mitigate the consequences of possible accidents. These systems determine the structural reaction to emergency conditions inside the tunnel and the response of the users exposed to accidental events [9, 11–13].

The use of the *Bow-tie diagram* technique [1, 14, 15], recognized in the literature of the industrial process safety, helps to identify two types of measures for the tunnel system, as shown in Fig. 1.5:

- on the left side: preventive measures, aimed to reduce the rate of occurrence of possible critical and unwanted events (top events);
- on the right side: protection measures, aimed to mitigate the possible consequences that can be produced by the critical event (top event).

Usually, critical events that require the assessment of the safety level of the tunnel are characterized by low probability of occurrence and severe consequences [15]. A list of typical critical events occurring inside tunnels can be summarized as follows:

- collision events or other events that result in a fire;
- collision events or other events which produce the release of flammable liquids;
- events of deflagration and/or detonation;
- events of release of toxic or other hazardous materials.

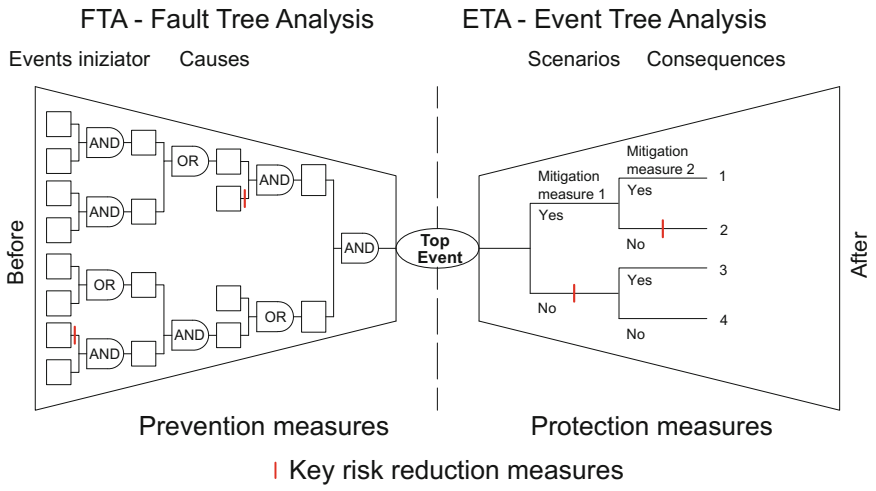

Fig. 1.5 Sketch of the Bow-tie approach used for safety evaluations in process systems

References

1. Beard, A., Carvel, R.: The Handbook of Tunnel Fire Safety. Thomas Telford Publishing (2005)
2. Ingason, H., Li, Y.Z., Lönnermark, A.: Tunnel Fire Dynamics. Springer, New York (2015)
3. Parsons, Brinckerhoff, Quade, and Douglas, TCRP Report 86/NCHRP Report 525, Transportation Security, Vol. 12: Making Transportation Tunnels Safe and Secure. Transportation Research Board, Washington DC (2006)
4. Senato della Repubblica Italiana, Relazione concernente lo stato di attuazione degli interventi relative all'adeguamento delle gallerie stradali della Rete Transeuropea, Ministero delle Infrastrutture e dei Trasporti (2013) (in Italian)
5. Cheong, M.K., Spearpoint, M.J., Fleischmann, C.M.: Design fires for vehicles in road tunnels. In: Proceedings of 7th International Conference on Performance-Based Codes and Fire Safety Design Methods, Auckland, New Zealand, pp. 229–240 (2008)
6. PIARC, Fire and smoke control in road tunnel, Permanent International Association of Road Congress (1999)
7. NFPA 502, Standards for road tunnels, bridges and other limited access highways, 2004 Ed., National Fire Protection Association, Quincy, Massachusetts (2004)
8. BD 78/99—Design manual for roads and bridges, The Highways Agency (1999)
9. Maevsky, I.Y.: Design Fires in Road Tunnels, A Synthesis of Highway Practice, NCHRP Synthesis 415 (2011)
10. European Union, Directive 2004/54/CE: Minimum levels of safety in European road tunnels (2004)
11. ANAS, Linee Guida per la progettazione della sicurezza nelle Gallerie Stradali secondo la normativa vigente (2009) (in Italian)
12. Van Weyenberge, B., Deckers, X., Caspeele, R., Merci, B.: Development of a risk assessment method for life safety in case of fire in rail tunnels. Fire Technol. **52**, 1465–1479 (2015)
13. Ronchi, E., Colonna, P., Capote, J., Alvear, D., Berloco, N., Cuesta, A.: The evaluation of different evacuation models for assessing road tunnel safety analysis. Tunn. Undergr. Space Technol. **30**, 74–84 (2012)
14. PIARC, Integrated approach to road tunnel safety (2007R07). World Road Association. La Défense cedex, France (2007)
15. Gehandler, J.: Road tunnel fire safety and risk: a review. Fire Sci. Rev. **4**, 2–27 (2015)

Chapter 2
The Research Project and Partners Involved

Abstract In this chapter the authors introduce how fires in tunnels can be studied using CFD models, explaining the reasons behind the research project and the importance to perform full-scale fire tests in order to better understand and investigate these events. Finally, the subjects involved in project (Politecnico di Milano, Corpo Valdostano dei Vigili del Fuoco, RAV—Autostrade Spa) are presented.

The severe fires in Europe, such as those of the Mont Blanc, Gotthard and Tauern tunnels, have clearly displayed the importance of adapting tunnels to higher safety standards. As already mentioned, fires in tunnels are a threat not only for the safety of users but also for rescue teams. Moreover, it is also important to take into account that damage to the infrastructure and the associated prolonged closure of the tunnel would result in significant economic losses. Furthermore, dangerous goods are also transported through many of these tunnels. These issues push public authorities and tunnel designers/managers to pay increasing attention to the risks related to fires. An important step towards safety for tunnels in EU is the Tunnel Directive 2004/54/EC [1], which indicates that a risk analysis is required for existing tunnels that are considered below the minimum safety standards.

In this framework, an important role can nowadays be played by computer simulations and fire models. For example, a proper design of a ventilation system is highly dependent on the geometrical and physical configuration of the tunnel. Moreover, the ventilation can also influence the Heat Release Rate of the fire and the spread of the fire to adjacent vehicles [2, 3]. Given the impossibility to perform a high number of experimental tests for each tunnel configuration, it is necessary to rely on the possibility to simulate the fire and smoke dynamics, as well as their consequences. Computational Fluid Dynamics (CFD) simulations are commonly used to support the design of fire-safe tunnels, because they are more cost-effective than conducting large-scale fire experiments and therefore allow to analyze several different possible fire scenarios. Nevertheless, the CFD models must be carefully tested to identify their possible limitations and prove that simulations provide reliable results. Performing full-scale tests that can reasonably replicate a real event with well-characterized boundary conditions (e.g. geometry, devices and systems

F. Borghetti et al., *Tunnel Fire Testing and Modeling*,
PoliMI SpringerBriefs, DOI 10.1007/978-3-319-49517-0_2

installed, etc.) helps validating and improving the CFD codes, but also allows to test the safety system of a real tunnel. In fact, experimental data measured during these tests are useful not only for the understanding of the physics related to tunnel fires, but also for verifying assumptions, validate computational models, and assess the effectiveness of the tunnel design. Moreover, they are also important for tunnel operators to verify in practice their emergency response plans and procedures. Each tunnel has unique safety requirements, which depends on its design, in terms of geometry, size, height and level of traffic. It is therefore important to perform new tunnel fire tests, especially with high HRR [4].

This need has led to a fruitful collaboration between researchers of the Politecnico di Milano, the Corpo Valdostano dei Vigili del Fuoco, and two tunnel owners of the Valle d'Aosta region, in northern Italy, in the framework of the project "Improved CFD models for tunnel fire risk analysis" (project number D41J10000490001), financially supported by Politecnico di Milano.

A first preliminary fire test was organized during the training experimental activity performed in the Gran San Bernardo road tunnel [5], which connects Italy and Switzerland, where a firefighters brigade of Valle d'Aosta performed one of the regular safety and training exercises as part of a bi-national safety exercise on June 16th, 2011. One of the most relevant elements of this safety exercise was the need to reproduce conditions similar to the real emergency situations, to better study the critical points of the intervention procedures in use. A new fire test entirely dedicated to fire research and tunnel safety, and not associated to the traditional regular safety exercises, was then organized in the Morgex North tunnel in July 2012.

This book describes in detail all the phases related to the Morgex fire tests, from the design of the fire scenario, the setup of the test, the experimental results and the successive modeling activities.

In this work two full-scale fire tests were performed; during these transient experiments, both the HRR and ventilation velocity were measured as a function of time in the Morgex North tunnel of the A5 Aosta-Monte Bianco highway (Valle d'Aosta region, Italy). It is important to notice that normally in a real tunnel fire, the HRR varies with time. At the same time, the ventilation velocity across the fire site also varies with time due to the intervention of the emergency ventilation system immediately after the fire is detected. Therefore, characteristic values such as the flame angle, back-layering length and maximum smoke temperature become transient values. Despite the fact that the behaviour of a real tunnel fire is highly dynamic, the experimental data from both model-scale and large-scale tests are usually obtained in a quasi-steady state condition [6].

The Morgex fire tests are controlled dynamic fire events where characteristic quantities (such as the fire HRR, the temperature distribution, smoke movement and pollutants concentration inside the tunnel) were measured with the aim to assess, in a successive analysis, the quality of the tunnel design and to further validate fire models. This book describes how the fire scenario was designed and created, how the experimental data gathered can be analyzed and compares them to other

full-scale tunnel fire experiments, semi-empirical models and CFD predictions. During the fire test, it was possible to measure temperature, air velocity, O_2, CO, CO_2 and PM (Particulate Matter) levels in several locations within the tunnel. This fire scenario was organized to simulate the fire of a heavy vehicle semi-trailer and thus reproduce conditions similar to possible actual emergency situations, including the time-varying emergency ventilation strategies. Thanks to the presence of some diesel oil pool fires, able to generate a large amount of dense smoke, it was possible to test the safety procedures, such as the effectiveness of the longitudinal ventilation system on the control of the smoke movement.

2.1 The Subjects Involved in the Test

Three subjects were involved in this real-scale experimental campaign about tunnel fires, with different objectives and separate responsibilities, which can be summarized as follows:

Politecnico di Milano:

- Further validation of the CFD code FDS using new experimental data and sensitivity analysis of model predictions to boundary conditions.

Two groups of Politecnico participate to the project. One belongs to the *Laboratorio Mobilità e Trasporti*,which is a center of competence of the Italian national civil protection for transportation safety and management, and the second is a research group of the Department of Chemistry, Material and Chemical Engineering "G. Natta" of Politecnico.

Corpo Valdostano dei Vigili del Fuoco:

- Test safety procedures in a tunnel in Valle d'Aosta in the case of a relatively large fire ($\sim$15 MW);
- Gain experience and data during a real fire test, useful to define and improve the intervention procedures;
- Evaluate the best strategies for intervention of rescue teams.

RAV—Autostrade Spa:

- Test the effectiveness of the ventilation system, using the ventilation setup and performance characteristics described in the risk analysis project of the Morgex North tunnel;
- Check the response of the operators and emergency systems to the presence of a tunnel fire and gain familiarity with the equipment and with each other.

The entities and authorities that participated in the Morgex fire test are described in the following paragraphs in more detail.

2.1.1 Politecnico di Milano

Politecnico di Milano is one of the most outstanding universities in the world, according to QS World University Ranking. Founded in 1863, Polimi is the largest School of Architecture, Design and Engineering in Italy, with 3 main campuses located in Milan and 5 campuses based in the North of Italy.

Thanks to a strong internationalization policy, several study programmes are taught entirely in English, attracting an ever-increasing number of talented international students from more than 100 countries. Teaching is increasingly related to research, a key commitment that enables to achieve results of high international standards, while creating connections with the business world. Strategic research is carried out mainly in the fields of energy, transport, planning, management, design, mathematics and natural and applied sciences, information and communication technologies, built environment, cultural heritage, with more than 250 laboratories. Many important scientists and architects studied and taught here; among them Achille Castiglioni, Gio Ponti, Renzo Piano and Aldo Rossi, both Pritzker Prize in 1990 and 1998 respectively, and Giulio Natta, Nobel Prize in Chemistry in 1963.

2.1.2 The Aosta Valley Fire Department

The Aosta Valley Fire Department, pursuant to regional law No. 37 of 10 November 2009—New provisions on the organisation of fire prevention services in the Valle d'Aosta/Vallée d'Aoste Region, is a fundamental component and an operational structure of the civil protection service, in terms of article 11 of Law No. 225 of 24 February 1992 (Establishment of the nationwide civil protection service) and regional law No. 5 of 18 January 2001 (Organization of regional civil protection activities). It replaces, within the regional territory, the national Fire Department, and discharges the tasks and functions allocated to it. The Aosta Valley Fire Department additionally carries out the functions relating to airport fire protection services, at the regional airport, according to the legislation in force in that field. Accordingly, the fire protection functions and responsibilities resting on the Ministry of internal affairs or the Minister of internal affairs are respectively entrusted to the regional Administration and to the President of the Region. Moreover, in coordination with the same structures of the Ministry of internal affairs, the Aosta Valley Fire Department (CVVVF in Italian) ensures, within the limits of its powers, the technical direction of relief efforts within the scope of civil defence operations.

The responsibilities of the Aosta Valley Fire Department consist in:

- Fire prevention;
- Public aid;
- Civil protection activity;
- Training.

The Aosta Valley Fire Department, with a view to safeguarding the safety of persons and the integrity of goods, guarantees the technical interventions characterized by the requirement of immediacy of performance in respect of which technical professionalism, of a highly specialized content as well, and suitable instrumental resources, are demanded.

2.1.3 RAV—Aosta Motorway Company

The connection of the Italian motorway network from Aosta to the Mont Blanc tunnel, carried out by RAV—Aosta Motorway Company, is an example of very advanced mountain highway engineering, capable of combining the most modern technical solutions with deep respect for the territory and the environment; to cope with the natural physiological increase in traffic volumes, without at the same time causing harm to the several inhabited centres and the tourist settlements of the High Valley, freeing them from traffic, especially from the heavy type. Precisely in order to build the missing segment of the complete connection, via the Mont Blanc Tunnel, of the Italian motorway network, 1983 witnessed the foundation of the Aosta Motorway Company (R.A.V.) with the aim of designing, implementing and managing the highway between the city of Aosta and the Mont Blanc Tunnel. The company, held for 58% by the Società Italiana per il Traforo del Monte Bianco S.p. A. (Italian Company for the Mont Blanc Tunnel) and for 42% by the Autonomous Region of Aosta Valley (Valle d'Aosta), became operational for all intents and purposes in 1988 by virtue of a concession for the work granted by ANAS, pursuant to a specific convention concluded on 11 November 1987 and made executive by Inter-ministerial Decree of 23 March 1988. In 1999, the Concession has been renewed through the conclusion of a new convention, made executive as a result of registration with the Court of Auditors in February 2000.

References

1. European Union, Directive 2004/54/CE: Minimum levels of safety in European road tunnels (2004)
2. Beard, A., Carvel, R.: The Handbook of Tunnel Fire Safety. Thomas Telford Publishing (2005)
3. Ingason, H., Li, Y.Z., Lönnermark, A.: Tunnel Fire Dynamics. Springer, New York (2015)
4. Maevsky, I.Y.: Design Fires in Road Tunnels, vol. 415. A Synthesis of Highway Practice, NCHRP SYNTHESIS (2011)
5. Frassoldati, A., Cuoci, A., Borghetti, F., Gandini, P., Juglair, R., De Bacco, G., Deffeyes, M., Castellan, M.: Proceedings of the XXXIV Meeting of the Italian Section of the Combustion Institute, Rome (2011). Doi:10.4405/34proci2011.III23
6. Li, Y.Z., Ingason, H.: Maximum ceiling temperature in a tunnel fire. SP Rep. **51** (2010)

Chapter 3
The Fire Tests in the Morgex North Tunnel

Abstract After presenting the Morgex North tunnel, location of the full-scale fire tests, the choices made for the implementation of the fire test, made up by two fire scenarios, are deeply described. The idea of this part of the book is to give possible stakeholders useful suggestions in order to guide them in the preparation of a similar experience. Indications are given about fire scenarios and their preparation, safety issues, materials and equipment, preparation and location of measuring instruments.

3.1 The Morgex Tunnel Infrastructure

The tunnel used for the tests was the Morgex North tunnel, which is the eighth in a homogeneous series of 10 tunnels located along the highway which connects the town of Aosta with the Mont Blanc tunnel. Since the tunnel was in use, it was necessary to balance the consequences induced by a fire with a significant HRR test with the aim to preserve the practicality and efficiency of the infrastructure and its equipment, in order to grant an essential public service, just after the test.

As already hinted at earlier, the Project has witnessed an experimental activity aimed at acquiring data on fire accidents simulated in full-scale. Given that the Mobility and Transports Lab has been collaborating for years with the Aosta Valley Fire Department around issues related to safety in tunnels and the transportation of dangerous goods by road, it was once again possible to consolidate this synergy by jointly organizing an additional test, besides the one that took place at the Gran San Bernardo in June 2011.

As regards the infrastructure to be used in the test, it was decided to involve RAV SpA, which manages a large number of highway tunnels in the A5 Aosta–Mont Blanc motorway, and which expressed an intention to take part in the Project in order to check, through full-scale fire tests, and by resorting to objective and independent measurements, the efficacy of mechanical ventilation systems installed in barrel vaults.

F. Borghetti et al., *Tunnel Fire Testing and Modeling*,
PoliMI SpringerBriefs, DOI 10.1007/978-3-319-49517-0_3

Given that the tunnel was in operation, it was compulsory to contemplate the consequences brought about by a fire test of significant intensity, along with the inescapable obligation to preserve the stability and efficiency of the infrastructure and the relevant equipment operating on behalf of an essential public service.

During the period of implementation of the test, the road SS 26 Dir was closed to traffic inside the Courmayeur territory (a town close to the Morgex tunnel), thereby entailing a no thoroughfare for vehicles with a mass exceeding 3.5 ton on the ordinary roads of the same municipality.

The A5 Aosta–Mont Blanc highway accordingly represented the only viable link for commercial traffic to and from France. Following the suspension of highway traffic, as in the case of the previously mentioned fire tests, it was necessary to envisage the temporary ban of heavy vehicles inside the regulation areas of Aosta and Passy (France) and ensure fulfilment of the pressing need to restore highway traffic within the shortest time possible.

3.1.1 Location

The tunnel is located in the second functional highway section, between the municipalities of Morgex and Courmayeur, close to the Mont Blanc (Fig. 3.1). The traffic interruption in the tunnel, needed to perform the tests, did not affect significantly the practicality of the highway because of the low traffic, since the test was performed during the night. A tunnel located on the first section would have instead led to the closure of the entire highway from the town of Aosta to Courmayeur.

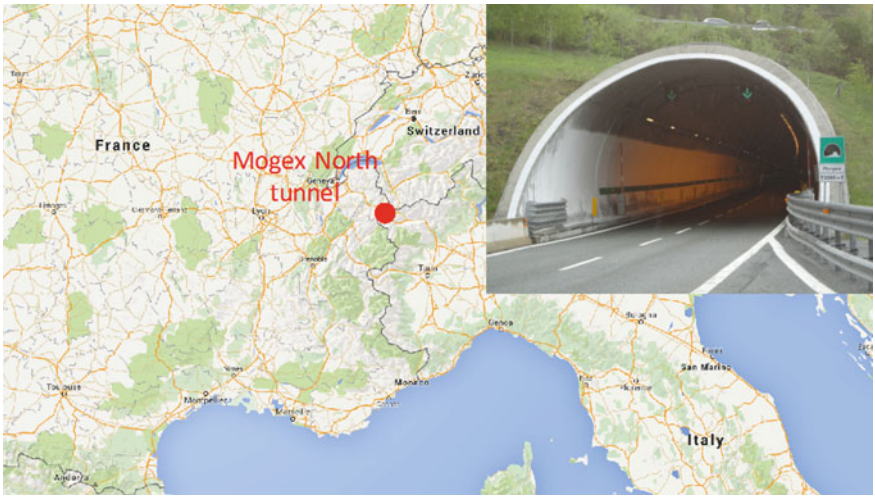

Fig. 3.1 Location and entrance of the Morgex North tunnel

Moreover, the exit of the North bore is located in an elevated and isolated position, far from any civil settlement and/or other infrastructures. For this reason, no impact could have arisen from smoke and exhausts pushed outside the tunnel by the ventilation system.

3.1.2 Main Features of Morgex North Tunnel

Table 3.1 briefly summarizes the main features of the Morgex North Tunnel.

Figure 3.2 shows the Morgex North tunnel synoptic representation, with particular reference to the location of the fire.

3.1.3 Structural and Geometric Data

Table 3.2 reports all the relevant structural and geometric data of the Morgex North Tunnel.

3.1.4 Devices and Equipment

Table 3.3 reports the main devices and equipment of the Morgex North Tunnel.

Table 3.4 describes the monitoring and detection systems of the tunnel.

The fire tests inside the tunnel, described in this volume, were designed for two different activation strategies of the ventilation system:

Table 3.1 Main features of Morgex North tunnel

Highway company	R.A.V.—Raccordo Autostradale Valle d'Aosta—SpA
Highway	A 5
European Route	E 25
Region/Province	Valle d'Aosta/Aosta
Municipality	Morgex
Opening year	2002
Starting point	131 km + 560 m
Ending point	133 km + 854 m
Total length	2294 m
Average height (AMSL)	979 m
Traffic (year 2011)	3474 (vehicles/day for each fornix)
	22% of heavy vehicle (>3.5 ton)

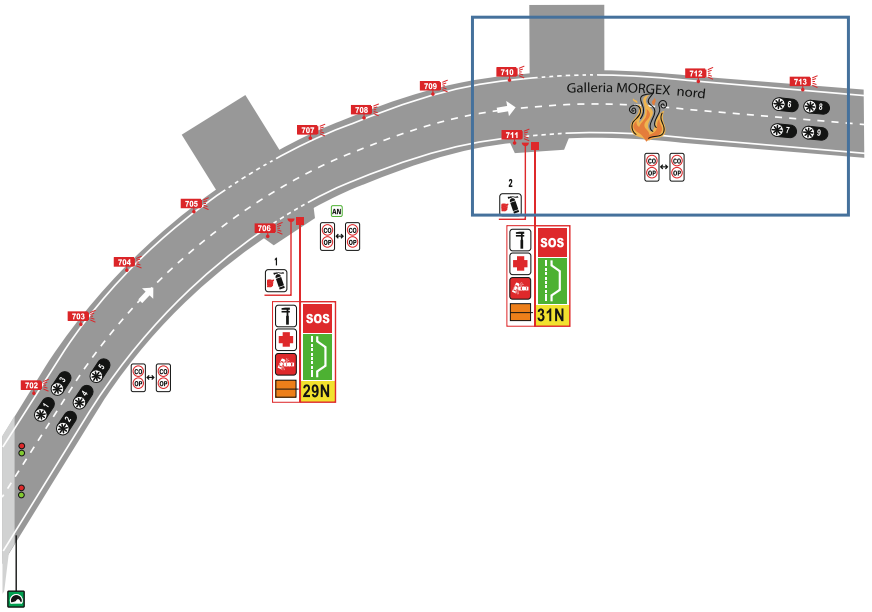

Fig. 3.2 Morgex North tunnel synoptic representation and fire position

Table 3.2 Structural and geometric data

Covering	Concrete/ribs and concrete
Section area	65 m^2
Width road platform	10.50 m
Height	7.2 m (maximum height)
Direction	One-way
Platform width	8.50 m
Number of lanes	2
Lane width	3.75 m
Quay	0.50 m (right and left)
Sidewalks width	1.00 m raised 0.30 m (right and left)
Planimetric	Curved internal part; straight entry and exit
Average slope	3.2%
Internal by-pass	n. 2 (carriageable)
Emergency lay-by	n. 2 (length 80 m and width 3.0 m)

- 9 fans in use (average expected air velocity over 5.0 m/s) for the first accidental scenario;
- 5 fans in use (minimum expected air velocity about 2.5 m/s) for the second accidental scenario.

Table 3.3 Devices and equipment

Lighting	Continuous on the left side
	1 row
	3 circuits
Emergency lighting	UPS
	Single lamp power: 58 W
	Lamp type: Neon
Entrance Lighting	Both side along 200 m
	2 levels step with the luminance sensor
	Lamp type: sodium
Ventilation	Type: longitudinal with silenced fans
	N° fans: 9
	Total of 5 fans ventilation groups: 4 double fans and 1 single
	Power per fan: 30 kW
	Fan diameter: 1 m
	Airflow per fan: 28 m^3/s
	Total airflow rate: 252 m^3/s
Environmental detectors	3 opacimeters
	3 CO analyzers
	1 anemometer

Table 3.4 Monitoring and detection systems

Control room	Active 24 h a day
CCTV	12 internal cameras
	1 external camera (entry)
Traffic analysis	Automatic detection of: slow-moving traffic, stopped vehicle, queue, against the flow
Broadcasting	Radiating cable on the right side
	Frequency guaranteed for RAV, Traffic Police, Fire Department
Telephony	GSM/UMTS
Traffic lights	Arrow/cross signs at the entrance on each lane
SOS	2 for each emergency lay-by with voice channel
Extinguishers	2 for each emergency lay-by

3.2 Accidental Scenario

The accidental scenario was designed with the aim to reproduce a possible fire of a heavy vehicle (a semi-trailer truck blocking the right lane), as a consequence of the fire ignition on board of the trailer of the vehicle due to a technical failure and/or an overheating of some mechanical parts. After the ignition, the semi-trailer catches fire, causing a fire which generates a dense smoke plume that quickly spreads inside the confined tunnel environment. This fire scenario was organized to reproduce

Fig. 3.3 Roll-off container used for the real-scale fire test

conditions similar to real emergency situations, including the activation of the time-varying longitudinal ventilation system. Two different fire scenarios were realized, the first one used 9 tail fans, the second 5 fans.

Thanks to the presence of six large diesel oil pool fires, able to generate a large amount of dense smoke, it was possible to test the tunnel safety systems, such as the effectiveness of the ventilation system to control the smoke dispersion. A roll-off container (Fig. 3.3) was used to reproduce the expected aerodynamic effect of the road tractor on the smoke movement. Figure 3.4 shows the position of the container and the six pool pans used to generate a fire with a HRR of about 15 MW inside the tunnel. This fire size corresponds approximately to that of a small Van, as previously shown in Fig. 1.3.

For organizational reasons, heavy and/or light vehicles were not placed on the accident site. This choice is justified by the fact that during each fire test, the procedures of emergency services were not tested and evaluated. The evaluation of these procedures, in fact, would have not been compatible with the fire scenario due to the equipment and instruments installed inside the tunnel.

Figure 3.4 shows a representative layout of the accidental scenario: the 6 pans used to simulate the fire source, covering an area of approximately 6 m × 2.5 m, 6 m away from the roll-off container. The six pans are contained inside an ideal rectangle on the right lane. The roll-off container is placed at a distance of 6 m from the downstream pans. The total area directly defining the fire scenario corresponds to a rectangle having the longer dimension equal to 18 m and the shorter dimension equal to 2.5 m.

3.3 Fire Scenario

The fire scenario was realized using six pool pans filled with diesel oil as shown in Fig. 3.4. Each stainless steel pan has a diameter of 1.2 m and was filled with 60 L of fuel. In this way, neglecting the interactions between the pool fires and the

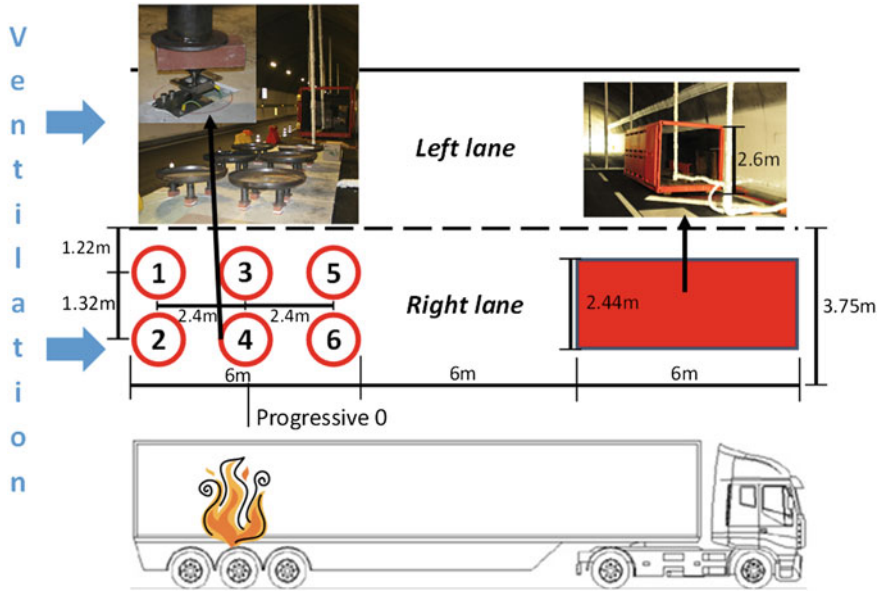

Fig. 3.4 Relative position of the pool pans and the roll-off container, usually used by fire brigades (*Corpo Valdostano Vigili del Fuoco*) to generate smoke in controlled fire conditions. Pool #4 was set on load cells to measure the weight loss of fuel during the fire tests

thermal radiation feedback of the walls, using literature correlations the six pans were estimated to develop an average HRR of approximately 10 MW. The use of load cells to record the weight loss of pan #4 (Fig. 3.4) during the various stages of the fire event (ignition, growth period, fully developed fire, and extinction) allowed for estimating the average and the actual instantaneous HRR of the investigated fire scenarios.

Literature correlations which provide the diesel oil burning rate (kg m^{-2} s^{-1}) as a function of the pool diameter (D) were used to design the fire scenario:

$$m = m_{\infty} \cdot \left(1 - e^{-k'D}\right)$$

where m_{∞} is the asymptotic value of the mass burning rate and k' an empirical parameter.

The burning rates of fires in the radiation-dominated region may be estimated using the parameters presented in Table 3.5. This correlation expresses the HRR of the fire as a function of the pool diameter, but it refers to isolated fires and it is not able to take into account the interactions among several adjacent pool fires, as in the case of the Morgex experiments; therefore this correlation was expected to underestimate the effective HRR of the fire. The literature parameters of the correlation are shown in Table 3.5 while Fig. 3.5 shows a comparison among the calculated values and literature experimental results, evidencing clearly that the

Table 3.5 Parameters of the correlation for diesel oil pool fires

m_∞	k'	Reference
0.0555	0.935	Used in this work
0.054	1.30	Rew et al. [1]
0.057	0.57	Chartis et al. [2]
0.034	2.8	Babrauskas [3]

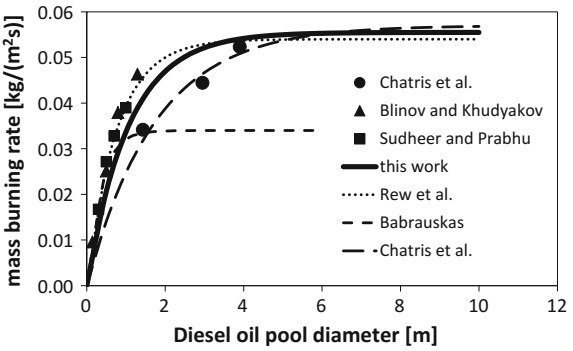

Fig. 3.5 Comparison of experimental data [1–3] and literature results with the one used to design the fire scenario (*this work*)

specific burning rate of large pools is larger than the one of small fires. The values used to design the fire scenario and to estimate the number of pools and total HRR were confirmed by a preliminary fire test made using a single pan.

Using the average correlation of Table 3.5, and thus neglecting interactions among pool fires, as previously mentioned a total HRR of about 10 MW can be estimated; then, the measurements performed during the fire tests allowed to determine that the actual average HRR of the fire was approximately 15 MW. The difference is largely a consequence of the interactions among the pools which were clearly observed during the test. Moreover, it is important to notice that the development of a fuel oil pool fire is a dynamic process, while the parameters of Table 3.5 refer to a fully developed fire. The instantaneous value of burning rate varies as a function of time and pool fire diameter. Typically, after an initial transient period at the beginning (fire growth), there is a fully developed fire before the flame extinguishment [2], but the behaviour may be even more complex: in the initial stages of a fire there are a number of non-steady effects due to the heating of the fuel, and heat losses to the sides and base of the pans. These effects tend to produce a steady increase in the burning rate [4] which was also observed in the Morgex experiments and discussed in the following sections. Other non-steady effects can be highlighted when the fuel level diminishes, as well as during the last stages of the fire, when the fuel is consumed, the fuel layer becomes very thin and the heat transfer is greatly enhanced. A modification of the ventilation velocity also affects the evolution of both the burning velocity and the HRR. Finally, the fuel mixture varies its composition during the combustion process, leading to complete absence of steady-state burning condition [4].

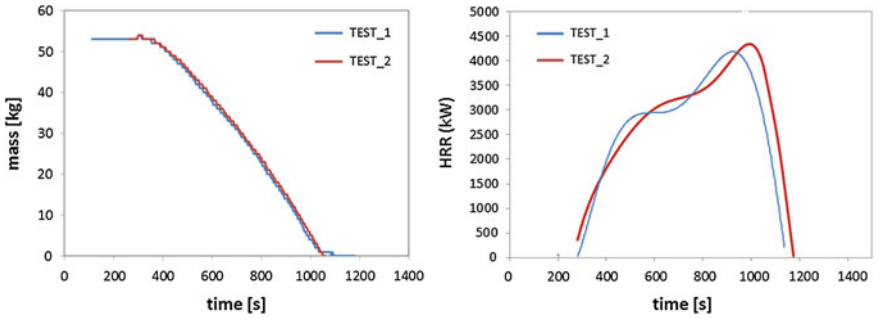

Fig. 3.6 *Left panel* Measured diesel oil weight as a function of time. Initial pool fuel content was 60 L (density 0.88 kg/L). *Right panel* Estimated Heat Release Rate

Figure 3.6 shows the measured weight losses of pan #4 as a function of time for the two investigated scenarios (9 or 5 fans were used for the emergency ventilation, respectively). The weight loss of the central pan located right side was recorded, as shown in Fig. 3.4. It is possible to observe that different ventilation velocity conditions did not change significantly the fuel consumption rate and the corresponding HRR. This results is consistent with the measurements of Chatris et al. [2] and could be explained considering the relatively small difference in ventilation velocity between fire tests #1 and #2.

A significant interaction among pools was visible during the two tests. The four pools located downstream (#3–6 in Fig. 3.4) showed a more intense fire (larger HRR) and consequently they burnt for a shorter time. These four pools extinguished, due to the complete fuel consumption, almost at the same time after about 15 min. On the contrary, the burning rate of the two pools located upstream was visibly less intense and more consistent with the values predicted by means of the correlations of Table 3.5. These two pans extinguished after about 20 min. This value is close to the measured fire duration of an isolated pan which was obtained during a preliminary open-field test a few days before the tunnel fire tests. Prior to implementing the tests, in fact, it was necessary to conduct a preliminary fire experiment by using a single steel tank, as evinced by Fig. 3.7.

This fire test has been performed using 20 L of diesel fuel and a small amount of heptane to facilitate the pool fire ignition. The first objective of the test consisted in checking the thermal resistance of the pans to high temperatures, by monitoring their feet deformations. This way, it was possible to ensure a correct alignment of feet of the pan during the test, which would have otherwise caused the same to slide from the load cells and the fuel to flip over. It was possible to ascertain that the combustion time of 20 L of diesel found inside the tank was equal to approximately 7 min. Such a temporal value is in line with the estimates made thanks to the correlation presented in Table 3.5.

Assuming for the diesel fuel a combustion enthalpy of $\sim$42,000 kJ/kg, on the basis of the measured mass burning rate, it is possible to calculate an average HRR of 3 MW for the four downstream pools. As already discussed, the two upstream

Fig. 3.7 Preliminary fire test using 20 L of diesel fuel

pools were characterized by longer fire duration (∼20 min), with an average HRR of 1.8 MW. It is interesting to notice that this value, which can be also estimated with the parameters of the correlation presented in this work (Table 3.5), is consistent with the measurements of Ingason [5], who studied a diesel oil pool fire of similar size. The average total HRR of the fire can be estimated as $Q = (4 \times 3\ \text{MW} + 2 \times 1.8\ \text{MW}) = 15.6\ \text{MW}$. This is a nominal value, which assumes unity combustion efficiency. In the case of a longitudinal and well ventilated fire, a combustion efficiency of 0.9 can be expected [6], which corresponds to a mean HRR of 14 MW. It is important to notice that this is an average value that underestimates the peak heat release which was observed when the six pools reached the maximum HRR. In fact, the instantaneous mass burning rate tended to increase with time due to the progressive heating of the diesel oil pool as shown in Fig. 3.6. For this reason a HRR peak value of about 15 MW was reached.

3.3.1 Fire Test Risk Management and Safety Issues

It is important to notice that one of the major difficulties in the preparation of these fire tests was associated to the fact that the tunnel is part of an important highway, which connects northern Italy to France through the Mont Blanc tunnel. For this reason, the Morgex North tunnel remained in operation also during the construction works needed to prepare and install all the equipment, instruments, insulation materials etc. (only the right lane of the tunnel was temporary closed) to be used during the fire tests. Figure 3.4 shows the pool pans and also the insulation material used to protect the road to avoid overheating and damage of the asphalt pavement. Tunnel lights, the radiant cable as well as other infrastructures were properly protected by insulation especially in the fire region.

Significant efforts were made to define a fire scenario in compliance with safety requirements and the need of a quick preparation and disassembling of the experimental setup; in fact, the tunnel remained completely closed to traffic only for a few hours during the night between 2 and 3 July, 2012. Thanks to the careful design and preparation of the fire tests, the proper use of insulation material and the efficiency of the ventilation system, the tunnel was not damaged by the thermal effects of the fire and it was opened to the traffic flow almost immediately after Fire Test #2.

The organisation of the test included an important phase dedicated to safety issues. The tests in fact saw the presence of technical observers capable of witnessing the two accidental scenarios.

Locating the test inside the tunnel has also been dictated by specific safety requirements, such as positioning the fire some tens of metres away (approximately 50 m) downstream of the driveway linking the two pavements. This way, the area set aside for observers would have ensured, if need be, a rapid evacuation of persons in case of danger. Such a solution further enabled the transport of observers on buses to the southern roadway near the bypass.

The safety management during the test has been ensured by the presence of the Aosta Valley Fire Department personnel, including their vehicles as illustrated in Fig. 3.8.

The ICE & FIRE company (http://www.ice-fire-italia.com) also contributed to the implementation of the fire tests by providing assistance and support in managing technical observers.

In order to be able to provide real-time information to the observers, an audio sound system has been set up. This way, before starting the test, the accidental scenario has been described to the invited observers, thereby preparing them to observe the scenario and the fire tests while ensuring their safety.

During the execution of the test, some real-time values of the measured parameters have been communicated, such as for instance the peak temperature reached in the vault above the fire, that helped organisers to monitor the state of the infrastructure and the surrounding environment, thereby preserving it from any irreversible damage.

Fig. 3.8 Rescue vehicles used during the fire test

3.4 Materials and Equipment Used in the Fire Tests Design

The fuel selected (diesel) complies with a number of characteristics making it suitable for the tests. First of all, it can be found easily and does not entail any specific problem associated with its transport and storage. Secondly, given its low volatility, it does not pose relevant safety problems, whether in its transport or in its use within a closed and poorly ventilated environment such as a road tunnel.

Besides, being a liquid fuel, its representation inside computational fluid dynamics (CFD) codes is less complex, for instance, than that of a solid fuel, concerning which it is necessary to characterize not only its combustion flame speed during the gas phase but also the pyrolysis reaction rate. Diesel, moreover, is a fuel largely used both for the traction of light vehicles and for light and heavy commercial vehicles, hence it is representative of a possible fire involving the release of fuel from a tank of such a kind of vehicle in a tunnel.

The main features of the pans used during the fire test are reported below and in Fig. 3.9:

- made of carbon steel;
- 1200 mm diameter;
- 4 mm thick steel;
- 4 support feet;
- 2 handles.

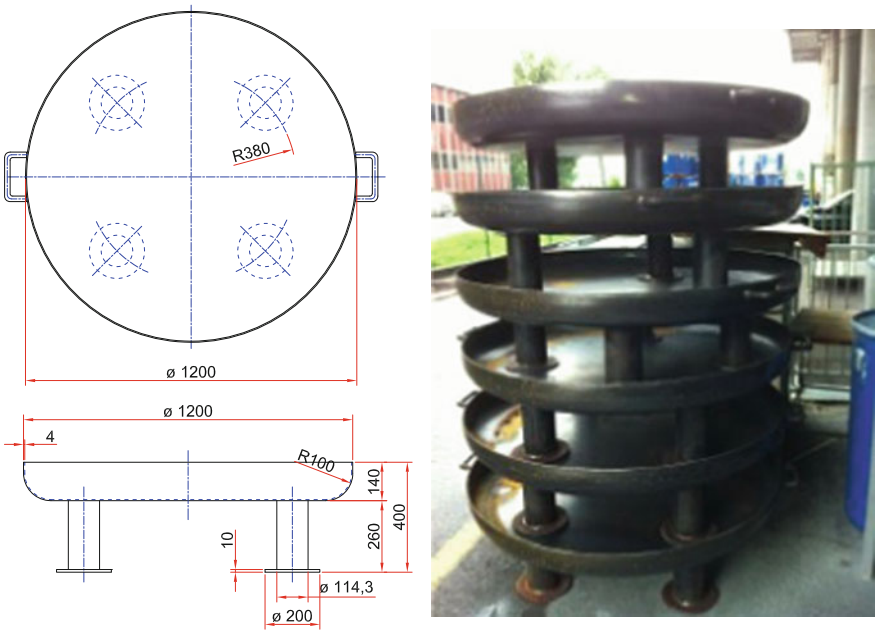

Fig. 3.9 Carbon steel pans used to create the liquid pool fires during the fire experiments

3.5 Measured Parameters

The test involved the measurement of the following parameters for a set of equipped sections inside the tunnel:

- Air and gas temperatures;
- Air velocity;
- Air and gas opacity [in terms of light absorption coefficient k (m^{-1})];
- Gaseous components (O_2, CO, CO_2).
- Total Particulate Matter (TPM) and Particle Size Distribution.

Furthermore, the weight loss of one of the six pans containing the fuel, was measured in real-time, to allow the evaluation of the instantaneous fuel consumption and fire HRR.

3.6 Tunnel Sections Equipped for the Measurements

The working group identified the tunnel cross-sections, located upstream and downstream of the fire, where measuring instruments were installed.

In order to uniquely determine the sections equipped with the instruments, a criterion was established in order to provide the identification of each section with a letter and a progressive number.

The sequence of the sections accordingly make reference to these coordinates. In particular, the negative ones are placed upstream of the fire (towards the entrance of the tunnel), whereas the positive ones are placed downstream of it (towards the tunnel exit) as described in Sect. 3.2 (Fig. 3.4).

In total 14 control sections were defined, arranged in the upstream part and downstream part of the fire area, with measuring instruments positioned with special props or metal supports adjustable in height.

The equipped sections are summarized in Table 3.6 and reproduced in detail in the Annex A. The positions of individual instruments were defined in terms of transverse coordinates and height above the ground, within each equipped section.

In each section, the props or vertical supports were located in three different location:

- lane (2.1 m from the right sidewalk);
- middle section of the road (0.4 m from the centerline on the lane);
- passing lane (2.1 m from the left sidewalk).

This solution granted an effective organization of the accidental scenarios on the right lane, allowing to arrange the supports in safety conditions, with the passing (left) lane still open to traffic.

Table 3.6 Tunnel sections equipped with monitoring devices and instruments

Number of section	Section − Progressive
1	A: − 443 m
2	B: − 53 m
3	C: − 23 m
4	D: − 8 m
5	E: 0 m − fire
6	F: + 6.5 m
7	G: + 10 m
8	H: + 12 m
9	I: + 18 m
10	L: + 33 m
11	M: + 53 m
12	N: + 103 m
13	O: + 153 m
14	P: + 198 m

After the closure of the tunnel, it was possible to quickly arrange the supports provided in the passing lane, reducing the total time needed to setup all the measuring devices and instruments.

As already mentioned, during the execution of the tests, some real-time measurements were performed to help the organisers to monitor some critical quantities (such as the maximum temperature above the fire but also the air quality for the technical observers). In particular, Section B was specifically devoted to monitor the air quality and thus ensuring a safe place for the observers. These values were monitored with different detectors only for safety reasons (Fig. 3.10), in the area where the observers were located, and therefore not recorded.

Moreover, sections A and P only contain the fixed instruments belonging to the tunnel equipment (anemometers, carbon monoxide detectors, and opacimeters installed on the tunnel side walls) (Fig. 3.11).

Fig. 3.10 Box containing the instruments used for real-time monitoring of the air quality in the observers area

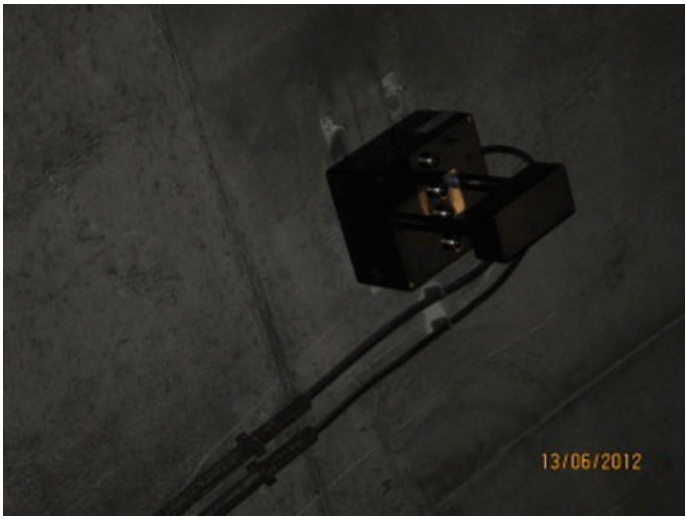

Fig. 3.11 Picture of one of the anemometers belonging to the tunnel ordinary equipment

The height of each instrument from the driveway (pavement) can assume the following values in the three transverse positions:

- 1.6 m;
- 3.5 m;
- 5.0 m;
- 6.6 m.

These positions were assumed to grant a representative coverage of the section, for what concern in particular the temperatures distribution. At 1.6 m height it is possible to measure temperature, smoke and gas compositions at man height, while at 6.6 m it is possible to investigate what happens in the tunnel vault.

The measuring instruments positions in each section were uniquely identified by an alphanumeric code, as illustrated in Fig. 3.12 where:

- the first letter represents the section reference as a function of a progressive coordinate (e.g., section A = −443 m with respect to the fire center location);
- the second letter identifies the transverse coordinate (M = lane, C = centerline; S = passing lane);
- the number defines the height from the driveway according to a defined criterion and reported in the following.

The height of each monitoring device or instrument was coded as follows:

- numbers 1, 4, and 7 = 6.6 m above the ground;
- number 1 BIS = 5 m above the ground (present only in some sections and in lane);

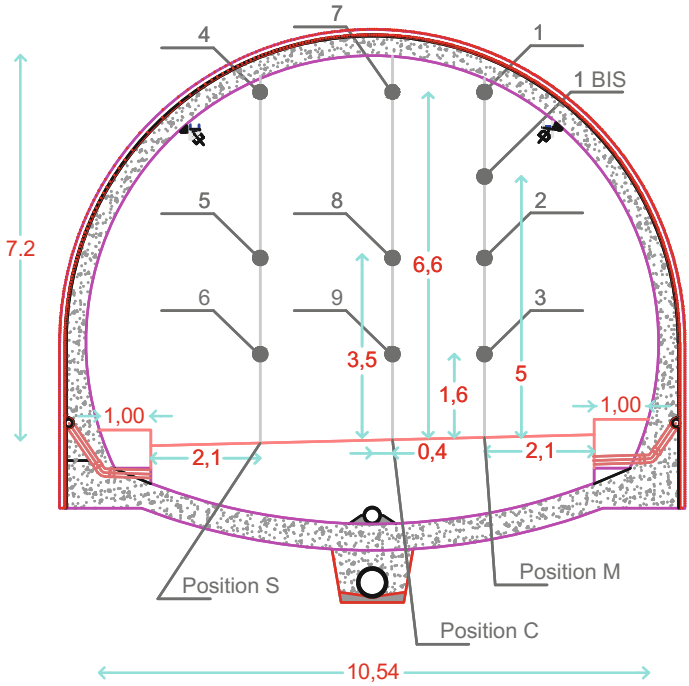

Fig. 3.12 Example of possible measuring positions. Size in meters

- numbers 2, 5, and 8 = 3.5 m above the ground;
- numbers 3, 6, and 9 = 1.6 m above the ground.

3.7 Preparation of the Accidental Scenario

In this section, the activities related to the preparation of the accidental scenario are described.

The underprops and supports used to sustain the measuring devices and probes were prepared using an insulating material consisting of wool sheets made by alkaline earth silicate capable of ensuring a high degree of thermal insulation. The technical specifications are set out in Table 3.7.

The insulating material has been used for two purposes:

- Protecting the underprops, supports and instrument cables from flames, smoke and thermal effects;
- Avoiding contact between thermocouples and underprop/support in order to avoid signal interferences during the measurement phase.

Table 3.7 Features of protection materials

Protection materials	Features
Gypsum plasterboards	Thickness: 18 mm
	Fire class reaction: A2-s1, d0 (UNI CEI EN ISO 13943: 2004)
Alkaline earth silicate wool	Thickness: 50 mm
	Density: 169 kg/m^3
	Thermal conductivity @ 400 °C: 0.09 Wm^{-1} K^{-1}
	Thermal conductivity @ 600 °C: 0.15 Wm^{-1} K^{-1}
	Thermal conductivity @ 800 °C: 0.21 Wm^{-1} K^{-1}
	Thermal conductivity @ 1000 °C: 0.29 Wm^{-1} K^{-1}

Figure 3.13 shows the activity of setting up underprops/supports prior to the installation of the different measuring tools.

As already mentioned, the same insulating material was also used for the protection of the equipment found in the tunnel with a view to preserving their integrity and correct functioning.

It was therefore necessary to carry out the cladding of the radiative cracked cable on the right-hand side of the tunnel for a length, upstream and downstream of the fire, sufficient to ensure protection from thermal effects, as illustrated in Fig. 3.14.

Besides the radiative cracked cable, it was also necessary to protect the lamps located on the-left hand side of the tunnel. The said activity has been carried out with the tunnel closed and the traffic interrupted in order to ensure the safety of users and operators involved in the preparation of the experimental campaign.

The phase of preparation of the underprops and protection of the installations has been implemented through the aid of hydraulic baskets and platforms capable of reaching suitable heights to carry out the single machining operations. Figures 3.15 and 3.16 illustrate the activities of positioning the props and supports through the use of some measurement tools.

Fig. 3.13 Thermal insulation activity of the prop with insulating material consisting of alkaline earth silicate wool

Fig. 3.14 Activity of protection of the radiative cracked cable

Fig. 3.15 Activity of positioning underprops through the use of a hydraulic basket

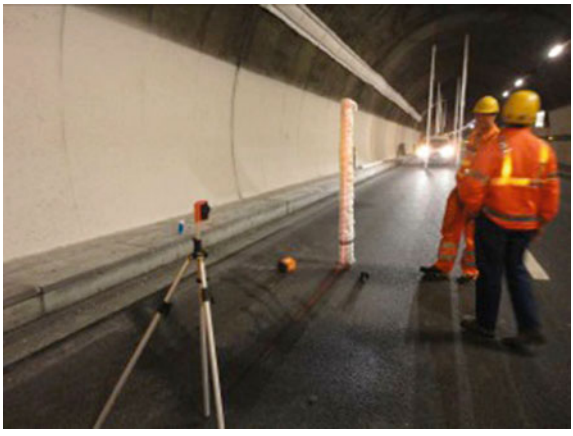

Fig. 3.16 Activity of positioning supports through the use of a laser measurement device

Fig. 3.17 Preparation of the accident scenario with the Morgex North tunnel open to traffic

Figure 3.17 shows the area of the accidental scenario, where it is possible to appreciate the construction site in the driving lane—choking of the driveway—in order to allow the preparation of the fire scenario. It can be moreover distinguished the first measurement section downstream of the fire and the roll-off container.

The road pavement protection has been realized through the use of insulation materials consisting of a first layer of gypsum plasterboards (Fig. 3.18), of a second layer of alkaline earth silicate wool (Fig. 3.19) and of a third layer of gypsum plasterboards (Fig. 3.20). The technical specifications of gypsum plasterboards and alkaline earth silicate wool are reported in Table 3.7.

The actual positioning of pans containing the fuel (diesel) was completed using firebricks capable of further ensuring the protection of the road surface, as illustrated in Fig. 3.21. Due to the insulation materials and the bricks, the final height of the pans from the road surface was increased of approximately 10 cm.

Fig. 3.18 First insulation layer with gypsum plasterboards

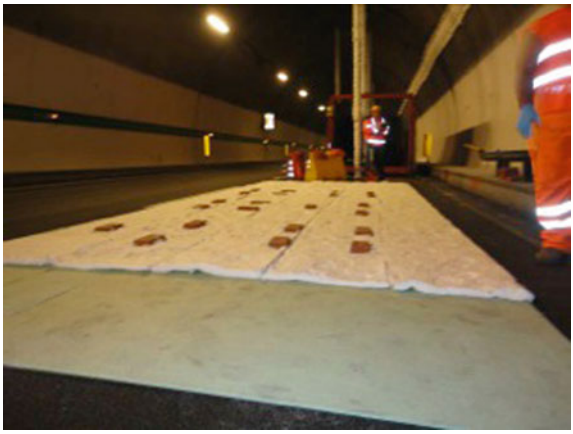

Fig. 3.19 Second insulation layer of alkaline earth silicate wool

Fig. 3.20 Third insulation layer with gypsum plasterboards

Fig. 3.21 Positioning of the fuel pans on the bricks

3.8 Measuring Instruments

This paragraph describes the measuring instruments used in the fire tests.

The acquisition of measured values during the test was supported by the Allemano Metrology Srl company, specialized in metrology of physical and chemical properties and certified for validation of equipment used (LAT ACCREDIA and UNI EN ISO/IEC 17025:2005).

Each measuring instrument was encoded using a unique alphanumeric code as a function of:

- type of instrument (i.e. thermocouple, anemometer, etc.);
- the position, as defined in Sect. 3.6.

According with the type of instruments, it was adopted the following code, where each letter is related to a type of instrument as follows:

- T = Thermocouple;
- A = Anemometer;
- G = Gas detector;
- P = PM detector;
- O = Opacimeter.

As an example, Fig. 3.22 shows the arrangement of thermocouples in the section L of the Morgex North tunnel.

Table 3.8 shows the number of instruments used during the two fire tests.

Depending on the sections of the tunnel, type J or type K thermocouples were used during the experiments. Both the devices and cables were shielded to avoid possible interferences especially due to thermal effects; they were connected to different data-loggers so as to have the real-time acquisition of the temperatures along the whole area of the experiments (with a length of about 125 m). The thermocouples position is summarized in Table 3.9.

Tables 3.10 and 3.11 report the positions of the anemometers and gas detectors, respectively, used to monitor the dynamics of the tunnel ventilation and the dispersion of the main species and pollutants produced by the diesel pool fires. In particular, the concentrations of O_2, CO and CO_2 were simultaneously measured with different on-line and portable gas analyzers, such as the Horiba PG-250 (Fig. 3.23).

As in a fire event, especially in a confined or a semi-confined environment, an abundant and dense smoke plume is generated and dispersed, some experimental data about the smoke were also collected; in particular, two optical particle counters (Table 3.12), provided by sampling probes, were used to monitor the PM concentration (Fig. 3.23) at a height above the ground of 1.6 m in order to gain some information about the smoke backlayering and its destratification, upstream and downstream the fire position, respectively. These instruments allowed also for the determination of the size distribution of the dispersed smoke particles, from $PM_{0.5}$ up to PM_{10} and the Total Particle Matter (TPM). In addition, it was possible to use

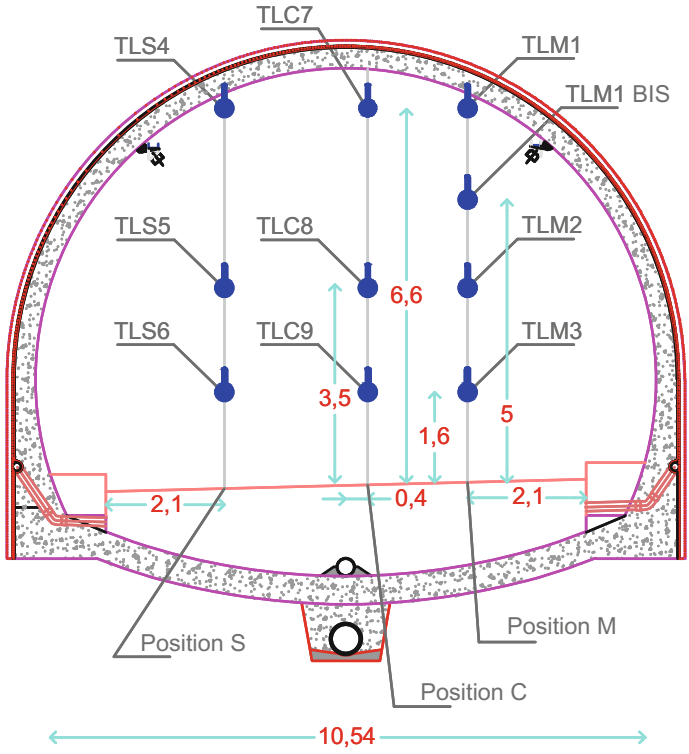

Fig. 3.22 Encoding measuring instruments. Example: thermocouples in section L

Table 3.8 Number of measuring instruments

Measuring instruments	Number
Thermocouples	42
Anemometers	6
Gas components detectors	7
PM detectors	2
Opacimeters	2
Load cells	4

the smoke opacimeters (Table 3.13), already present in the tunnel for safety reasons, installed on the tunnel walls at the edges of the test area (Fig. 3.24); this allowed to monitor the smoke opacity, expressed in terms of light attenuation coefficient k (m^{-1}).

Finally, a series of 4 load cells (Fig. 3.25) was used to detect the real-time weight loss of one of the diesel pool pans during the fire tests, as described in Fig. 3.4; due to the peculiar characteristics of the experimental setup, this was essential for estimating the fire HRR.

Table 3.9 List of thermocouples

	Thermocouples ID	Tunnel section	Total thermocouples per section	Position	Height (m)
1	TCM1	C	3	Lane	6.6
2	TCM2				3.5
3	TCM3				1.6
4	TDM1	D	3	Lane	6.6
5	TDM2				3.5
6	TDM3				1.6
7	TEM1	E	5	Lane	6.6
8	TEM2				3.5
9	TES4			Passing lane	6.6
10	TES5				3.5
11	TES6				1.6
12	TFM1	F	4	Lane	6.6
13	TFM1 BIS				5.0
14	TFM2				3.5
15	TFM3				1.6
16	TGM1	G	4	Lane	6.6
17	TGM1 BIS				5.0
18	TGM2				3.5
19	TGM3				1.6
20	TIM1	I	9	Lane	6.6
21	TIM1 BIS				5.0
22	TIM2				3.5
23	TIM3				1.6
24	TIS4			Passing lane	6.6
25	TIS6				1.6
26	TIC7			Centerline	6.6
27	TIC8				3.5
28	TIC9				1.6
29	TLM1	L	10	Lane	6.6
30	TLM1 BIS				5.0
31	TLM2				3.5
32	TLM3				1.6
33	TLS4			Passing lane	6.6
34	TLS5				3.5
35	TLS6				1.6
36	TLC7			Centerline	6.6
37	TLC8				3.5
38	TLC9				1.6
39	TNM1	N	4	Lane	6.6
40	TNM1 BIS				5.0
41	TNM2				3.5
42	TNM3				1.6

Table 3.10 List of anemometers

	Anemometers ID	Tunnel section	Total anemometers per section	Position	Height (m)
1	AARAV	A	1	Lane	5.0
2	ABPB	B	1	Lane	1.6
3	ACM1	C	2	Lane	6.6
4	ACM3	C		Lane	1.6
5	ANM3	N	1	Lane	1.6
6	AOM3	O	1	Lane	1.6

Table 3.11 List of gas components detectors

	List of gas components detectors	Tunnel sections	Total gas detectors per section	Position	Height (m)
1	GARAV	A	1	Lane	5.0
2	GBPB	B	3	Lane	1.6
3	GDM3	D	1	Lane	1.6
4	GHM3	H	2	Lane	1.6
5	GMM3	M	1	Lane	1.6
6	GNM3	N	3	Lane	1.6
7	GPRAV	P	1	Lane	5.0

Fig. 3.23 Gas detectors: (*left*) Horiba PG-250, (*right*) optical PM detector Lighthouse Handheld 3016

Table 3.12 List of PM detectors

	PM detectors ID	Tunnel section	Total PM detectors per section	Position	Height (m)
1	PCM3	C	1	Lane	1.6
2	PNM3	N	1	Lane	1.6

Table 3.13 List of opacimeters

	Opacimeters ID	Tunnel section	Total opacimeters per section	Position	Height (m)
1	OARAV	A	1	Lane	5.0
2	OPRAV	P	1	Lane	5.0

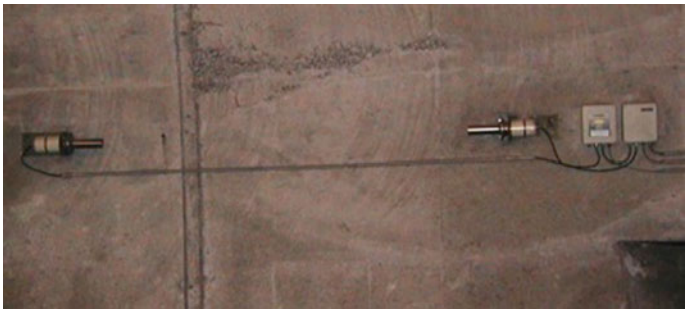

Fig. 3.24 Smoke opacimeter and CO detector located on the tunnel wall (model CODEL TunnelCraft AQM CO+VIS)

Fig. 3.25 Load cell LAUMAS model PV-Z/PPV used by the real time weighting system

References

1. Rew, P.J., Hulbert, W.G., Deaves, D.M.: Modeling of thermal radiation from external hydrocarbon pool fires. Process Saf. Environ. Prot. **75**, 81–89 (1997)
2. Chatris, J.M., Quintela, J., Folc, J., Planas, E., Arnaldos, J., Casal, J.: Experimental study of burning rate in hydrocarbon pool fires. Combust. Flame **126**, 1373–1383 (2001)
3. Babrauskas, V.: Estimating large pool fire burning rates. Fire Technol. **19**, 251–261 (1983)
4. Steinhaus, T., Welch, S., Carvel, R.O., Torero, J.L.: Large-scale pool fires. Therm. Sci. **11**, 101–118 (2007)
5. Ingason, H.: SP Technical Research Institute of Sweden Report P801596 (2008)
6. Li, Y.Z., Ingason, H.: Maximum Ceiling Temperature in a Tunnel Fire. SP Report 51 (2010)

Chapter 4
The Test Results

Abstract In this chapter are presented the experiments and experimental measurements obtained in the two full-scale fire tests performed in the Morgex North tunnel, where both the HRR and ventilation velocity were measured as a function of time. It is initially described how the fire scenarios were designed and operated, then the obtained experimental results are presented and compared to the numerical predictions of CFD simulations of the same fire scenarios. In this chapter the discussion is initially focused on the comparison with analytical models and empirical correlations based on theoretical analysis and literature measurements obtained in other tunnel fire tests. The Morgex fire tests allowed to collect different measurements (temperature, air velocity, smoke composition, pollutant species) useful for validating and improving new and existing CFD codes and for testing the real behaviour of a tunnel and its safety systems during a diesel oil fire with a significant Heat Release Rate (HRR).

4.1 The Experimental Measurements: Temperature Distribution

As already mentioned, two different fire scenarios were tested, one using 9 tail fans (Test #1 maximum air velocity $\sim$7.0 m/s), the other with 5 fans (Test #2 maximum air velocity $\sim$5.0 m/s).

The experimental activity involved measurements for air (smoke) temperature and velocity, exhausts and air composition (O_2, CO, CO_2), Particulate Matter (PM) concentration and size distribution.

On the basis of preliminary calculations, it was possible to identify different tunnel sections where thermocouples trees and other instruments were located. These sections cover a large part of the tunnel, upstream and downstream the fire zone. In particular, thermocouple trees were aimed to measure the vertical (from typical human height up to the tunnel ceiling) and transverse temperature profiles at several locations as summarized in Table 3.6 and Fig. 3.22.

F. Borghetti et al., *Tunnel Fire Testing and Modeling*,
PoliMI SpringerBriefs, DOI 10.1007/978-3-319-49517-0_4

Fig. 4.1 Fire pictures: single pan fire (*left*), initial smoke back-layering (*center*) and firefighters ensuring safety during the experimental activity (*right*)

Figure 4.1 shows some pictures taken during the first part of Fire Test #1. The smoke back-layering (visible in the central picture) completely disappeared after the activation of the emergency ventilation system which increased the air velocity. Furthermore, Fig. 4.2 highlights the effects of the presence of the obstacle on the dispersion of the smoke and its consequent deposition on the tunnel wall. Moreover, it is also possible to observe the strong thermal effects on the insulation material positioned below the fuel pans to protect the pavement.

Figure 4.3 shows some of the measurements made during the experimental campaign and the effect of the different ventilation strategy on the smoke dispersion dynamics.

Figure 4.3 shows that the critical ventilation velocity necessary to reduce the back-layering length to a value lower than 5 m was about 3 m/s for Fire Test #1, in agreement with what reported by [1, 2]. Using the correlation of [2], which is

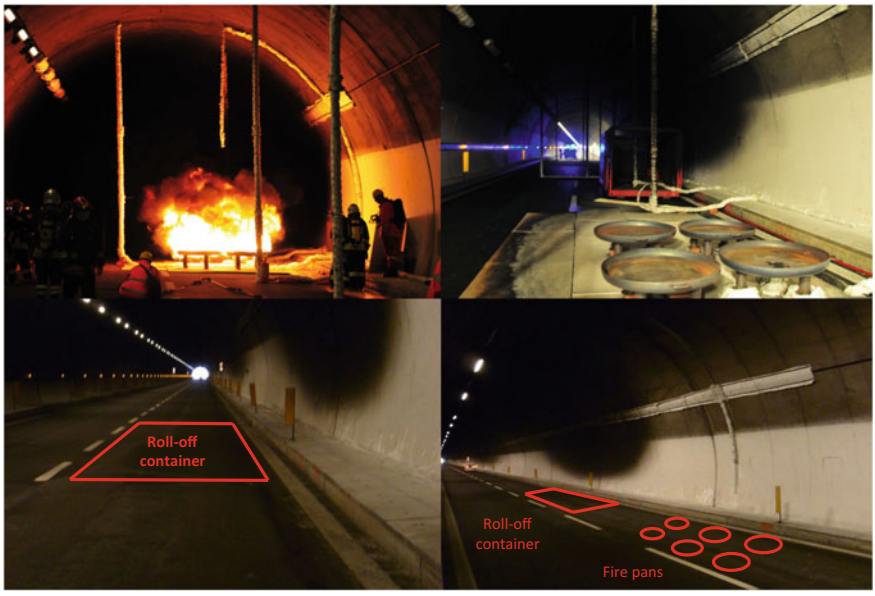

Fig. 4.2 Effect of obstacle on the smoke dispersion after the two fire tests

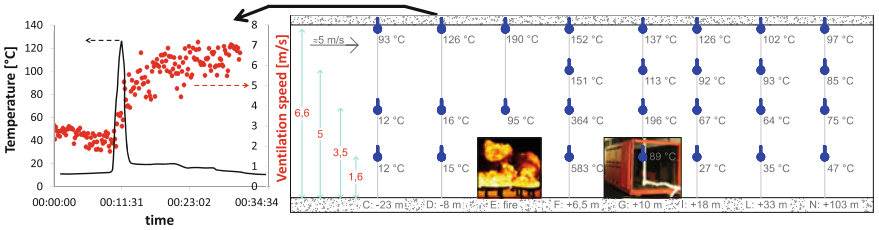

Fig. 4.3 Temperature and air velocity were measured in several locations during the fire test. *Left side* of the figure shows the temperature trend measured close to the ceiling 8 m upstream of the fire and the ventilation velocity. The *right side* of the figure shows the peak temperatures measured at the different locations during the entire Fire Test #1

applicable to large fires, it is possible to calculate that, at the initial ventilation conditions (V ~ 2.4 m/s) the expected back-layering length of the smoke (L_b) is about 40 m:

$$L_b^* = 17.3 \cdot \ln(0.4/V^*)$$

where $L_b^* = L_b/H$, $V^* = V/\sqrt{gH}$ are dimensionless back-layering length and longitudinal ventilation velocity and H is the tunnel height. From the same correlation, the ventilation velocity necessary to reduce the back-layering length to a value lower than 5 m is 3.25 m/s, also in agreement with the transient results of Fig. 4.3.

Figure 4.4 depicts the temperature distribution along the longitudinal mid-plane of the right lane (M devices) during the first fire scenario. It is important to notice

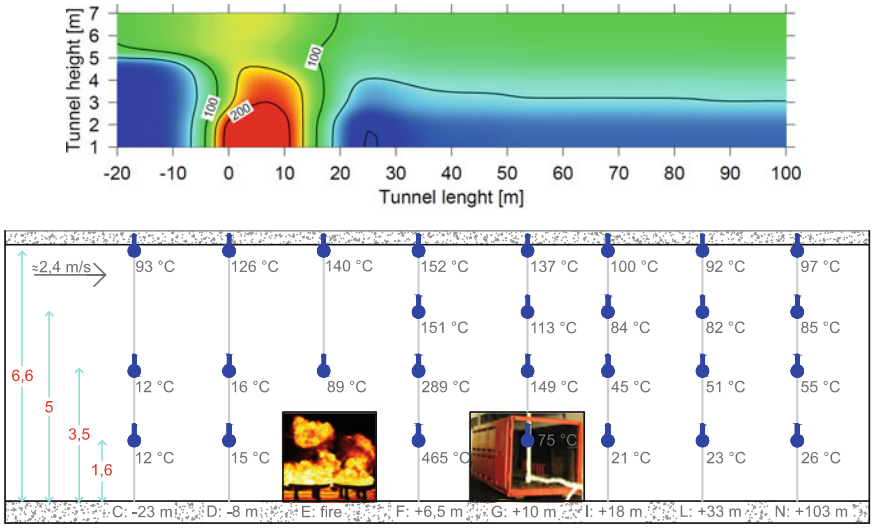

Fig. 4.4 Peak temperatures at several locations of the mid fire longitudinal plane during Fire Test #1 and low ventilation velocity (V ≅ 2.4 m/s)

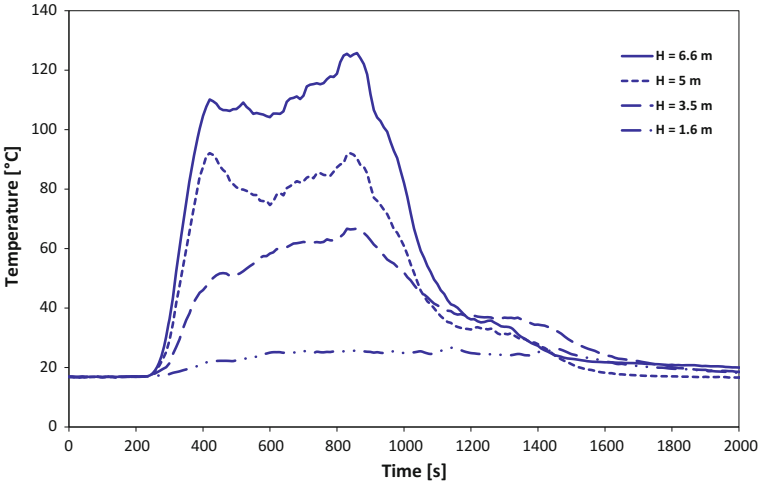

Fig. 4.5 Temperature profiles measured during Fire Test #1 by thermocouples located on the right lane of section I (M lane)

that the local maxima of temperature are measured at different times as a consequence of the ventilation change and the increasing HRR of the fire; an example of the temperature dynamics is reported in Fig. 4.5 which shows the temperature profiles measured by the thermocouples located on section I (thermocouples ID = TIM), 18 m downstream from the fire, for different heights above the ground. Moreover, Fig. 4.3 shows the temperature measured by the thermocouple close to the ceiling, 8 m ahead of the fire; it is possible to observe that initially, due to the low ventilation velocity, there is an initial temperature rise due to the back-layering of the smoke (also visible in Fig. 4.1), which is blown away when the emergency ventilation flow-rate is increased. To better understand the fire dynamics of this transient ventilation test, Figs. 4.4 and 4.6 show the analogous temperature distributions for low and high air velocities.

In particular, Fig. 4.4 shows the local temperature peaks measured after about 6 min and 30 s (when ventilation changes in the fire zone, see Fig. 4.3), while Fig. 4.6 shows the same values measured after about 9 min (when ventilation almost reached a steady value between 6 and 7 m/s). As expected, back-layering is visible in Fig. 4.4 and disappears in Fig. 4.6. The two figures also show the equivalent temperature contour plots, obtained from the measurements using a graphical interpolation technique based on the Barnes algorithm [4]. As the experimental data refer to a relatively small number of thermocouples to cover a very large area, these temperature plots are only illustrative and do not allow any quantitative analyses. Nevertheless, they are useful to support the discussion on the effect of ventilation on the fire dynamics.

Figures 4.7 and 4.8 show the transverse temperature distribution in the tunnel at two different distances from the fire (+18 and +33 m downstream of the fire).

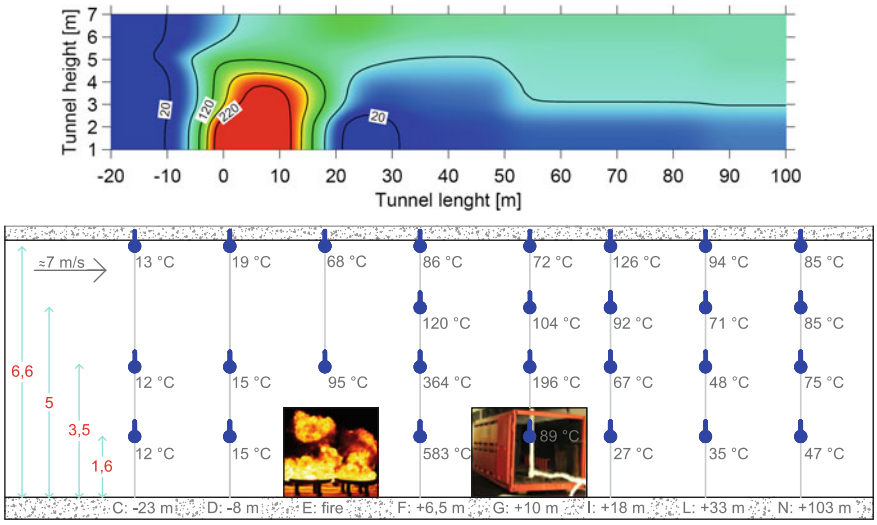

Fig. 4.6 Peak temperatures at several locations of the mid fire longitudinal plane during Fire Test #1 and high ventilation velocity (V ≅ 7 m/s)

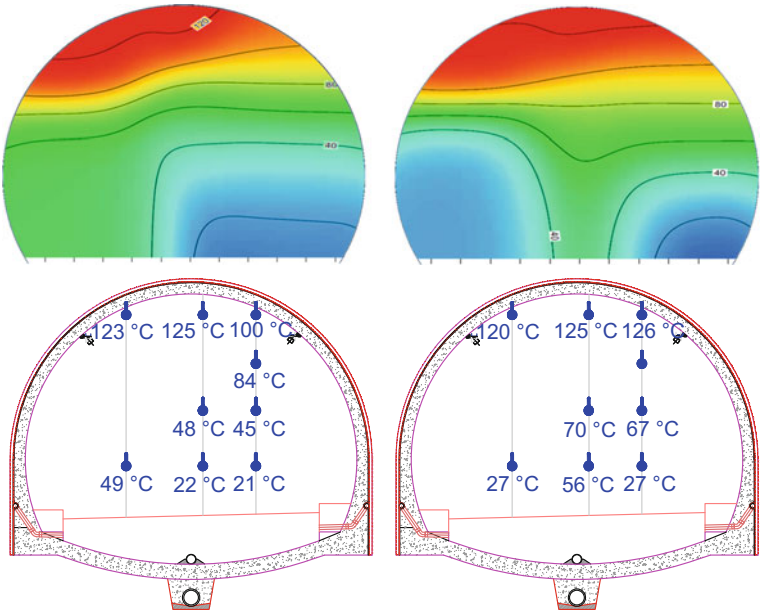

Fig. 4.7 Peak temperatures at several locations of the transverse plane I during Fire Test #1 with low (V ≅ 2.4 m/s, *left*) and high ventilation velocity (V ≅ 7 m/s, *right*)

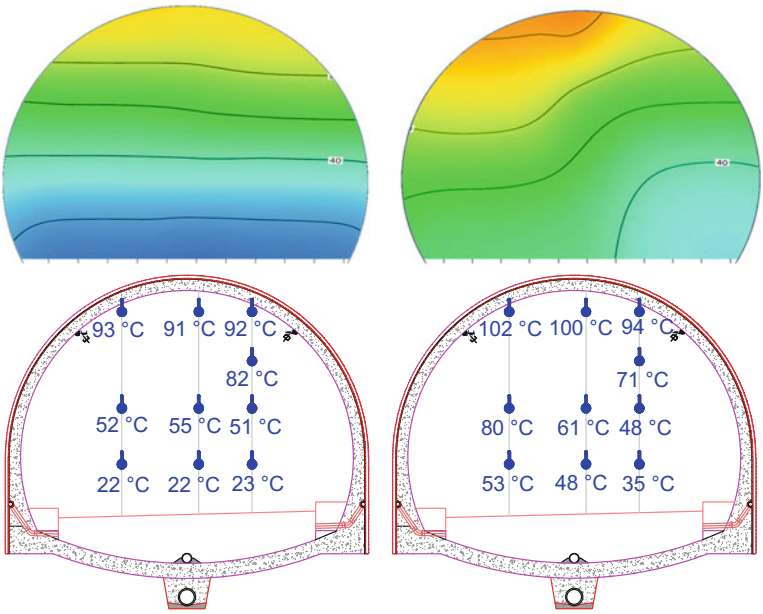

Fig. 4.8 Peak temperatures at several locations of the transverse plane L during Fire Test #1 and low (V ≅ 2.4 m/s, *left*) and high ventilation velocity (V ≅ 7 m/s, *right*)

The left panel refers to the initial period of the first test, with low ventilation velocity, while the right panel shows the peak temperatures during the second part of Fire Test #1, characterized by high ventilation velocity. It is possible to observe that the smoke distribution is characterized by a significant stratification and that the maximum temperature, as expected, diminishes with the increase of both distance from the fire and ventilation velocity. However, as can be seen from Figs. 4.5 and 4.9, the thermal stratification in the vertical direction is always present, independently of the ventilation velocity applied; similar qualitative trends were obtained in both the fire tests. It is also possible to observe the complex fluid dynamic behaviour induced by the wake of the semi-trailer which was observed in both fire tests.

Figure 4.10 compares the two fire tests using the transverse section of the tunnel at +18 m from the fire region. During Fire Test #1 a larger ventilation velocity was used (∼7 m/s), while in Fire Test #2 the velocity was ∼5 m/s. The figure shows the peak temperatures measured during the entire duration of the tests, 18 m downstream of the fire, i.e. the left panel of Fig. 4.10 is the combination of the values presented in the two panels of Fig. 4.7. Also in this figure it is possible to observe a colder region which is the effect of the wake of the semi-trailer (this colder region extends downstream up to about 30–50 m from the fire, depending on the ventilation velocity). Only a slight effect of the different ventilation conditions on the maximum ceiling temperature is evidenced; this is due to the fact that the temperature distribution is largely determined by the heat radiated by the fire, while

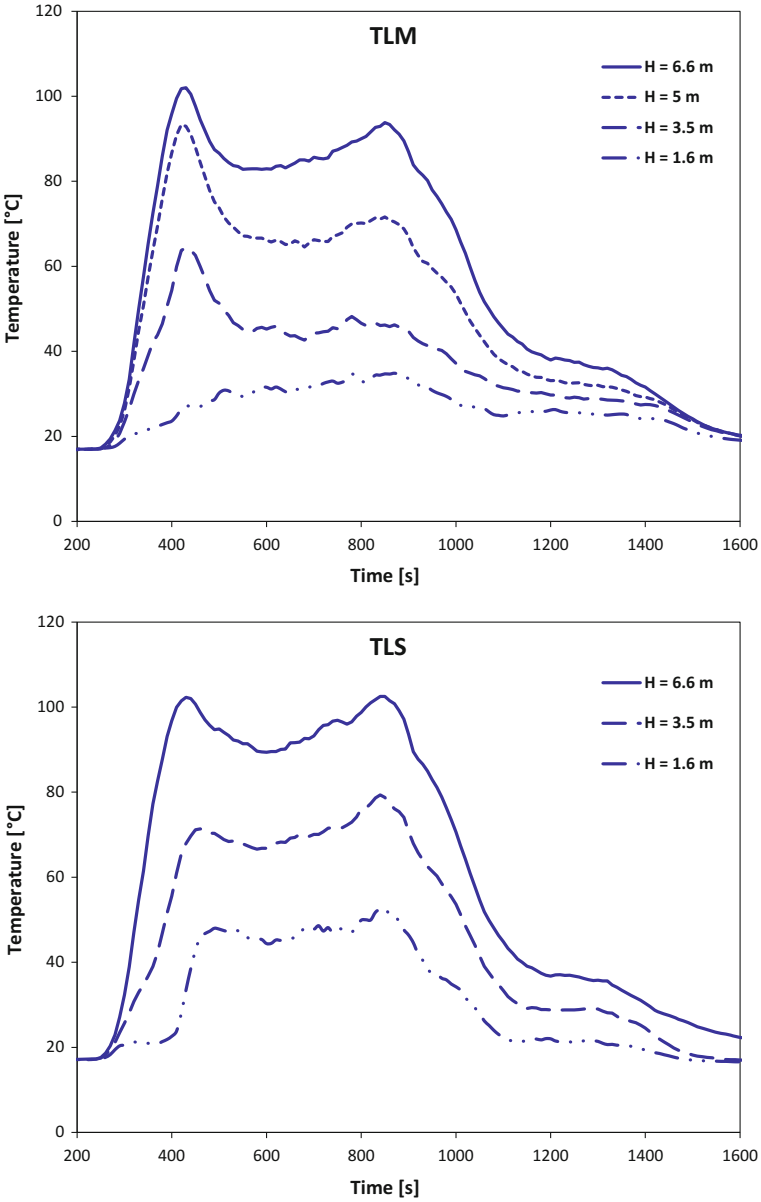

Fig. 4.9 Temperature profiles measured during Fire Test #1 by thermocouples located on the right lane (*top*) and passing lane (*bottom*) of section L

a small contribution can be ascribed to the heat dispersed by the hot combustion products. Different ventilation strategies can affect the rate of the temperature increase or decrease but for tests characterized by similar HRR comparable peak

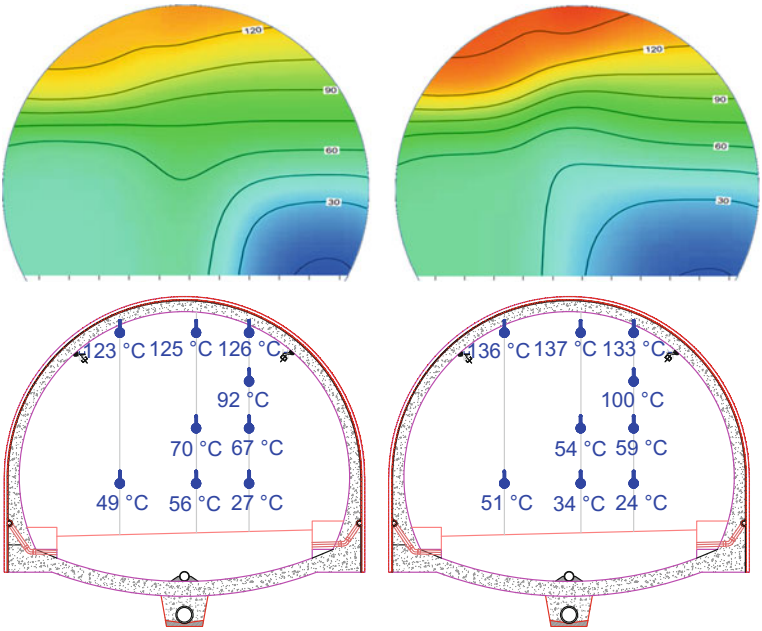

Fig. 4.10 Peak temperatures at several locations of the transverse plane I during the entire Fire Test #1 (V ≅ 7 m/s, *left*) and Fire test #2 (V ≅ 5 m/s, *right*)

temperatures can be always expected, as evidenced by the comparisons of Figs. 4.11 and 4.12.

However, the ventilation velocity can affect the smoke destratification. In particular, the obstacle used to reproduce a semi-trailer, especially at high air velocities,

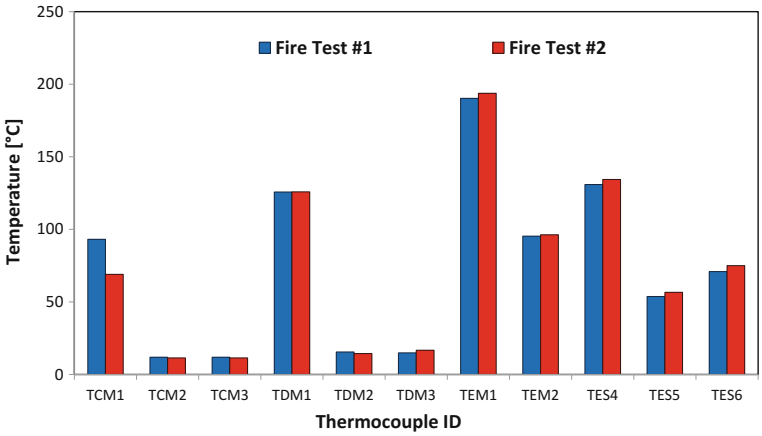

Fig. 4.11 Peak temperatures recorded in the Morgex fire tests at several locations upstream of the fire position

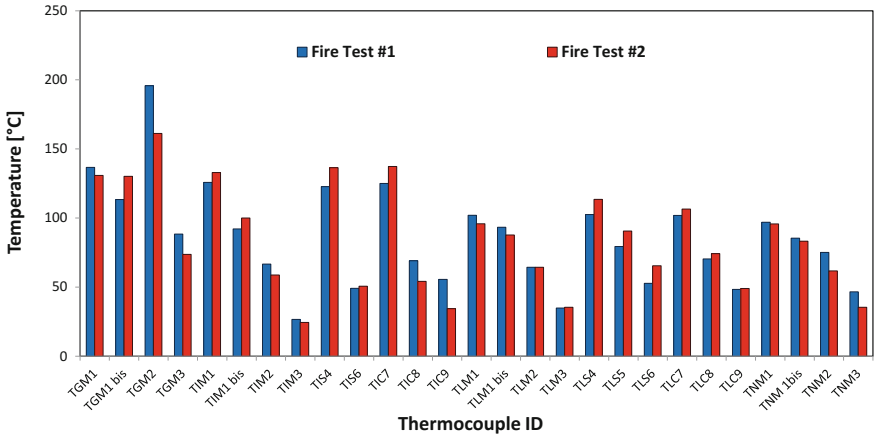

Fig. 4.12 Peak temperatures recorded in the Morgex fire tests at several locations downstream of the fire position

increases the turbulence and the air recirculation in its wake thus promoting the smoke destratification. This is confirmed by the CO trends measured at different locations downstream from the fire (Fig. 4.13). It is interesting to notice that Fire Test #1 was performed with an emergency ventilation velocity higher than the corresponding one used in the Fire Test #2, therefore it should be expected to have a

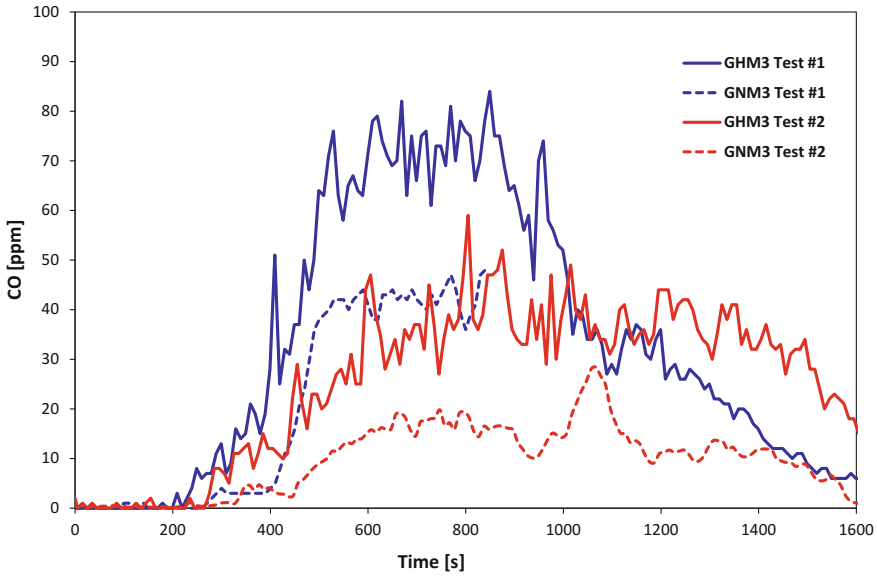

Fig. 4.13 CO profiles measured in the Morgex fire tests at sections H and N, 12 and 103 m far from the fire position, respectively

stronger dilution and consequently lower concentrations of the combustion products, such as CO and PM, during the first test, especially considering that these measurements were carried out at 1.6 m above the ground; on the contrary, as evidenced by Fig. 4.13, the maximum concentration reached by CO at any tunnel section downstream from the fire during Fire Test #1 was almost the double of the corresponding values recorded in Fire Test #2, thus underlining the presence of a strong turbulence, as well as a significant smoke and air recirculation, in the roll-off container wake which promoted the smoke destratification, in particular when the ventilation velocity was increased.

The effect of the turbulence on the smoke destratification can be seen also in the PM profiles measured far from the fire position (Figs. 4.14 and 4.15); similar concentration levels of the different PM size fractions were reached in the two fire tests but the experimental profiles of Fire Test #1 appear to be less regular, with huge fluctuations in the measured values even during the steady phase of the experiment (Fig. 4.14). However, the turbulence influenced the smoke dynamics promoting its destratification but did not affect the smoke composition for what concern the growth of the mean particles size or the aggregation among the particles; as evidenced by Fig. 4.16, the relative abundance of the different PM size fractions detected in the two tests was very similar, with a high amount of $PM_{2.5}$ and PM_{10} (that was about the 90% of the overall PM measured), thus confirming that all the growth and aggregation phenomena which involved the smoke particles

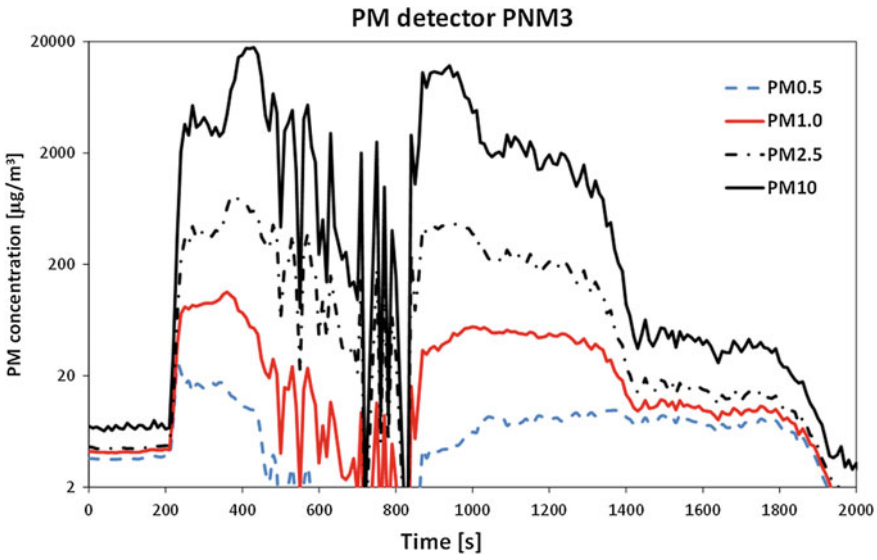

Fig. 4.14 Experimental trends of different PM size fractions measured in the Morgex North tunnel at section N, 103 m far from the fire position, during Fire Test #1

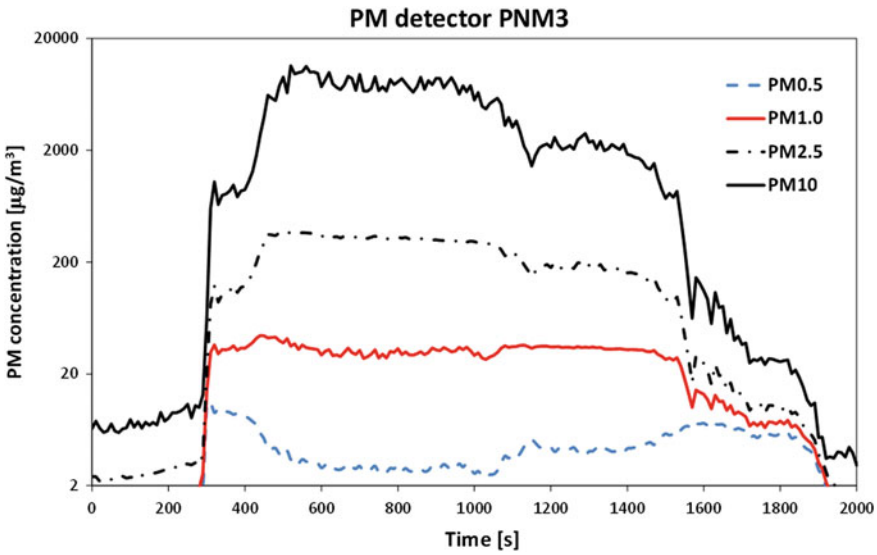

Fig. 4.15 Experimental trends of different PM size fractions measured in the Morgex North tunnel at section N, 103 m far from the fire position, during Fire Test #2

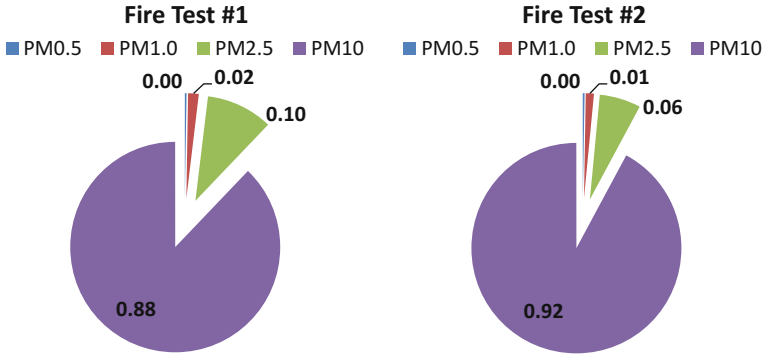

Fig. 4.16 Relative abundance of the different PM fractions detected at section N of the Morgex North tunnel in the two fire experiments

occurred closer to the fire source, before the beginning of the smoke destratification. These results, in turns, highlight a significant reduction of the visibility downstream of the fire, in the last part of the tunnel.

4.2 Temperature Measurements: Comparison with Literature Data and Theoretical 1D Correlations

According to Li and Ingason [5] the flame angle can be calculated as:

$$\sin\theta = \begin{cases} 1 & V' \le 0.19 \\ (5.26V')^{-\frac{3}{5}} & V' > 0.19 \text{ and } Q^* \le 0.15 \\ 0.5 \cdot H^{\frac{1}{2}}\left(b_{f_0} \cdot V^3\right)^{-\frac{1}{5}} & V' > 0.19 \text{ and } Q^* > 0.15 \end{cases}$$

In this definition θ is the angle between the horizontal line and the line connecting the fire source center and the position of the maximum ceiling temperature (θ = 90° in the case of a vertical fire). V′ is a dimensionless ventilation velocity and Q* a dimensionless HRR:

$$V' = \frac{V}{\sqrt[3]{\frac{g \cdot Q}{b_{f0} \cdot \rho_0 \cdot c_p \cdot T_0}}};\ Q^* = \frac{Q}{\rho_0 \cdot c_p \cdot T_0 \cdot g^{1/2} \cdot H^{5/2}}$$

b_{f0} [m] is the (equivalent) radius of the fire source, H the tunnel height [m], V the ventilation velocity [m/s] and Q the heat release rate [kW]. Cp is the heat capacity of air [kJ/kg K] and ρ_0 and T_0 are the ambient air density [kg/m^3] and temperature [K], respectively.

For a large and well ventilated fire, as in the case of the Morgex North experiments, $\sin\theta = 0.5 \cdot H^{\frac{1}{2}}\left(b_{f_0} \cdot V^3\right)^{-\frac{1}{5}}$. In this way, it is possible to calculate an angle of about 23° when the velocity is above 6 m/s and 51° when the velocity is 2.4 m/s. This means an expected location (downstream of the fire) of the temperature maxima at the height of 6.6 m (where thermocouples are located) of about 5.4 and 15.7 m for the two velocities, respectively.

Figure 4.6 shows that the maxima at high longitudinal ventilation velocity is measured at about 15 m, while Fig. 4.4 shows that, in the case of low longitudinal ventilation velocity, the temperature peak is approximately at about 3.5 m from the fire, a value which is consistent with the correlation. The effect of the air velocity on the deflection of fires has been studied also by other investigators [6, 7]. The American Gas Association (AGA) proposed an equation to determine the flame angle in open fires, for methane, which can be expressed as $\sin\theta = 1$ ($V' \le 0.19$) or $\sin\theta = (5.26\ V')^{-1/2}$ ($V' > 0.19$).

Figure 4.17 shows a comparison between the Li and Ingason correlation [5], the AGA equations and the experimental values measured during the Morgex North tests. Considering that the distance between the ceiling thermocouples in the vicinity of the fire were relatively large it is impossible to exactly determine the position of the maximum ceiling temperature. Despite this problem, a reasonable agreement among the measured values (the two points refer to the initial low ventilation velocity conditions and the final high ventilation velocity conditions, respectively)

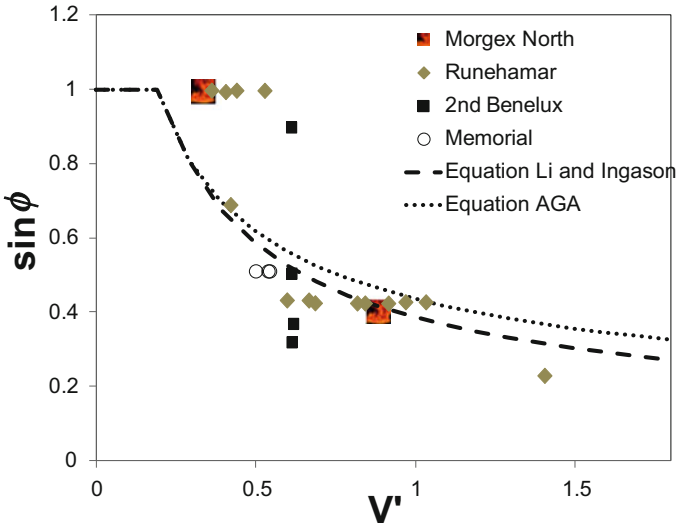

Fig. 4.17 Comparison of flame angles (based on maximum ceiling temperature) in the Morgex North experiments and in other full-scale tests. Lines refer to the predictions of the Li and Ingason [5] and American Gas Association [6] equations

and the models can be observed. Moreover, the comparison is extended to include relevant full scale experiments, such as the Memorial [8], Runehamar [9–11] and the 2nd Benelux [12, 13] tunnel fire tests. It is possible to observe that the measured values agree well with the theoretical models and with the new results measured during the Morgex fire tests. Both theoretical analysis and experimental data, including the Morgex ones, show that the flame angle is directly related to the dimensionless ventilation velocity.

Figure 4.18 shows the experimental data for the maximum gas excess temperature below the tunnel ceiling from the Morgex north experiments and compares these measurements with the corresponding results of several tunnel fire tests. As discussed by Li and Ingason [14], the maximum excess gas temperature can be divided into two clearly defined regions: a growth region, where the maximum excess temperature increases linearly with heat release and a region where the temperature remains relatively constant. They proposed the following criterion to describe the maximum temperature increase as a function of the fire HRR, ventilation velocity and geometry of the system (for the case of a well-ventilated fire, $V' > 0.19$).

$$\Delta T_{\max} = \begin{cases} \frac{Q}{V \cdot H_{ef}^{5/3} \cdot b_{fo}^{1/3}} & \Delta T_{\max} < 1350\ (^{\circ}\mathrm{C}) \\ 1350\ (^{\circ}\mathrm{C}) & \Delta T_{\max} \geq 1350\ (^{\circ}\mathrm{C}) \end{cases}$$

Figure 4.18 shows that the temperature increase measured during the Morgex North tests, due to the high ventilation velocity and the relatively low heat release

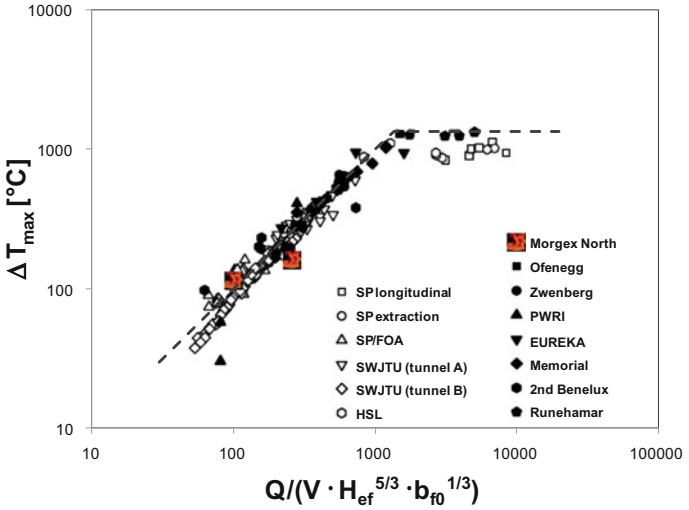

Fig. 4.18 The maximum excess temperature beneath the tunnel ceiling in the Morgex North fire test and other tunnel fire experiments, see [14] for references. Dashed line shows the equation proposed by [14]

rate, are in the first region, in reasonable agreement with model predictions and the other tunnel fire tests.

Figure 4.19 shows the dimensionless back-layering length L_b^* as a function of the dimensionless ventilation velocity V*. The experimental data of Ingason and Li [3] are also shown, as well as the correlation $L_b^* = 17.3 \cdot \ln(0.4/V^*)$. The experiments from the Morgex North tunnel, which refer to two different time instants during the dynamic fire test, agree well with the correlation and with other literature experimental data.

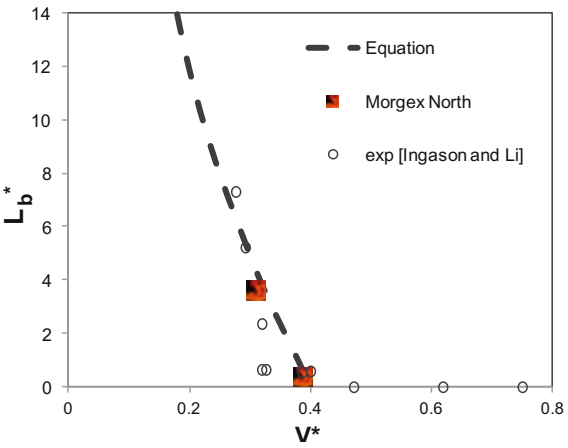

Fig. 4.19 Dimensionless back-layering length in the Morgex North experiment compared to the experimental values ant the correlation of [3]

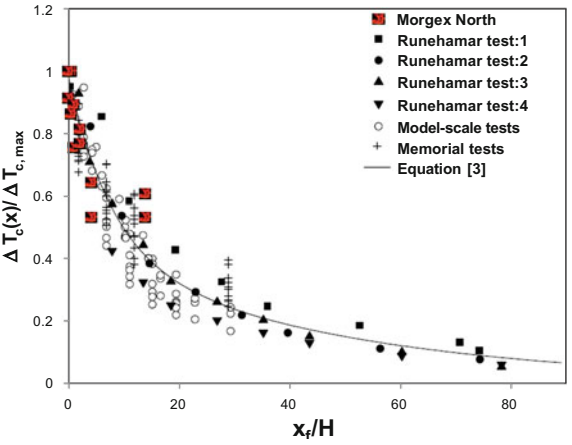

Fig. 4.20 Dimensionless excess gas temperature beneath the ceiling as a function of the dimensionless distance away from the fire xf/H. Comparison of Morgex North tests, other large tunnel fire tests (see [3] for references) and the equation proposed by Ingason and Li [3]

Figure 4.20 shows a comparison between the experimental data of Morgex North experiments and large-scale tunnel fire tests in terms of dimensionless excess gas temperature beneath the ceiling as a function of the dimensionless distance away from the fire x_f/H. Also in this case the agreement with predictions of empirical models and other literature experiments is satisfactory.

In the next section the Morgex tests will be compared to model predictions using the CFD code FDS following the same methodology described by Tavelli et al. [15], with special emphasis on transient ventilation velocity and smoke composition. The CFD simulation allows also to evaluate the effectiveness of the ventilation system in the presence of large fires (with HRR up to 100 MW), which cannot be studied experimentally in a tunnel which is normally open to traffic.

4.3 CFD Modeling of the Morgex Fire Tests

The behaviour of an accidental fire developing in a tunnel is intrinsically dynamic, and key parameters from the user's safety point of view vary continuously in time. CFD models must be validated against full-scale, transient experimental data in order to assess their reliability [16] before being deployed in risk assessment, which is becoming a fundamental element in designing and upgrading tunnels according to national and international guidelines [17, 18]. Much of the experimental data regarding full-scale tunnel fire tests in literature focused on quasi-steady state conditions [14] and empty tunnels [19].

In this section, model predictions of the Fire Dynamics Simulator (FDS) are compared with experimental measurements of the fire tests performed in the Morgex experiments. The successful comparison of the predictions to the experimental results further confirm the use of this code for the simulation of fire dynamics and to support the evaluation of the risk associated with fires in road tunnels.

The Fire Dynamics Simulator (FDS) [20], developed at NIST, is a CFD model of fire-driven fluid flow. FDS solves numerically a form of the Navier-Stokes equations appropriate for the low-speed, thermally-driven flow with an emphasis on the smoke and heat transport from fires. FDS model solves the equations for the conservation mass, species, and momentum, taking into account conductive and radiative heat fluxes. The overall computation is treated as a Large Eddy Simulation (LES).

The description of how the fire scenario was designed and operated, presented in the previous chapters, is here followed by the simulations setup and the discussion of the results of the comparison between experimental data and numerical predictions. Finally, in the following chapter, a sensitivity analysis is presented to highlight the effect of the peculiar geometry and congestion, as well as to study the benefits of the emergency ventilation procedure on the consequences for the user safety, relying on a methodology derived from ISO 13571 [21].

The tunnel geometry and its main characteristics were already presented in Chap. 3. In this section, only the boundary conditions adopted for the CFD simulations are presented.

4.3.1 Ventilation

As already discussed, the rationale behind the experiments was to assess the performance of the emergency ventilation system in a realistic fire scenario.

The two different tests implemented two different emergency ventilation strategies: during the first one nine fans (five before and two couples of fans located +375 and +475 m after the fire position, respectively) were activated during the emergency operations, while during the second test only five of them were activated (one before and four after the fire position, respectively). The ventilation velocity profiles recorded by anemometer AMO3 for the different tests are presented in Fig. 4.21. These values were used as transient boundary conditions for the simulations with the FDS code.

4.3.2 Pool Fires Burning Dynamics

As already discussed in the previous chapters, the development of a diesel fuel pool fire is a dynamic process: after an initial growth period at the beginning (fire development), there is a fully developed phase of fire, with a duration limited by the amount of fuel available, and then an extinguishment phase. Moreover, the pool fire behavior is quite complex, as from the initial stages of the fire there are a number of non-steady effects which tend to enhance the burning rate [22]: heat losses to the sides and the base of the pan, heating of the fuel itself. Other non-steady effects are experienced when the fuel level diminishes, as well as during the last stages of the

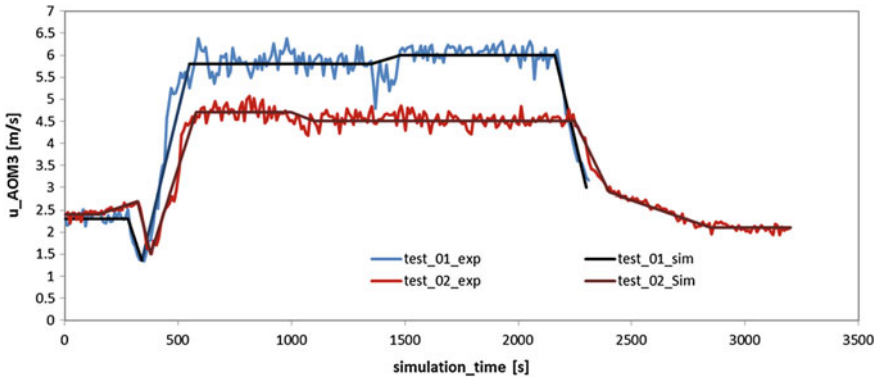

Fig. 4.21 Velocity profiles obtained from anemometer AOM3 during the experimental tests and the corresponding curves used as an input boundary condition for the FDS simulations

fire, when the fuel is consumed, the fuel layer becomes very thin and the heat transfer is greatly enhanced. Moreover, during the test the ventilation velocity was modified, and this is expected to affect the evolution of both the burning velocity and the HRR. Finally, the fuel mixture varies its composition during the combustion process, leading to complete absence of steady-state burning condition [22]. During the experiments four of the six pools—pools #3 to #6 (see Fig. 3.4)—highlighted a significant interaction, a more intense fire burning and a shorter duration, being completely extinguished due to fuel consumption after about 15 min. Conversely, the burning rate of the two pools located upstream was noticeably less intense and more consistent with the values of isolated pools predicted by means of the correlation of Fig. 3.5. These two pans extinguished after about 20 min, a duration close to the value obtained from an isolated pan experiment during a preliminary open-field test realized as a part of the setup phase of the tunnel tests.

During the experiment, the pools were ignited manually, with approximately 30 s delay between each aligned couple. Pool fires #1 and #2 behaved approximately as independent fires, while the behaviour of pool fires number #3 to #6 (Fig. 3.4) was similar to a single, bigger fire with higher burning rate.

The input for the simulation was provided as HRR-prescribed source terms with transient dynamics. To account for the different behaviour of the pools during the simulation, different HRR curves were used for the different pools. The dynamics of the four pools burning together was derived from the mass loss rate curve obtained from the load cell measurements (Fig. 3.6). The HRR input of the simulations of both tests is shown in Fig. 4.22.

The two independent-like pools upstream, with the longer burning dynamics, were described with a simplified isolated pool correlation with growth phase similar to the other four and a linear decay phase. The overall heat balance was coherent with the amount of fuel burnt in each fire test.

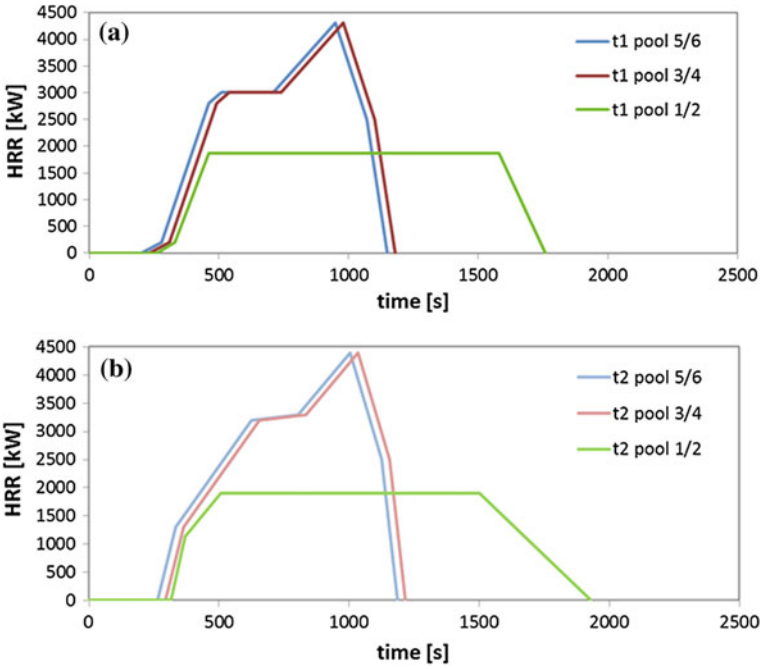

Fig. 4.22 Heat Release Rate profiles used as input for the CFD simulations of the experimental tests; Plot **a** reproduces the profiles for the different pools (numbered #1 to #6 coherently with Fig. 3.4) in Fire Test #1, Plot **b** the ones in Fire Test #2

4.3.3 Computational Domain and Boundary Conditions

The computational domain for the fire simulation is shown in Fig. 4.23 and comprised the portion of tunnel from 70 m before the fire to the tunnel end, some 200 m downstream from the fire location. In particular, the bypass located 50 m ahead of the fires was included in the simulation domain in order to assess its influence on the air flow inside the tunnel, as well as the large obstacle downstream the fire to account for the effect of a vehicle on the smoke dynamics. Since the metal container was cooled with water during the experiments, its walls were considered isothermal at 40 °C during the simulation. The thermal properties of the tunnel walls were set equal to that of concrete. Details of the boundary conditions are shown in Table 4.1.

The computational grid selection over the fire source was made coherently with the criterion of Ma and Quintiere [23] applied to a single pool, and corresponds to cubic cells of 10 cm size. The results of the variation in the cell size over the fire source are shown in Fig. 4.24 below a certain cell dimension the results are

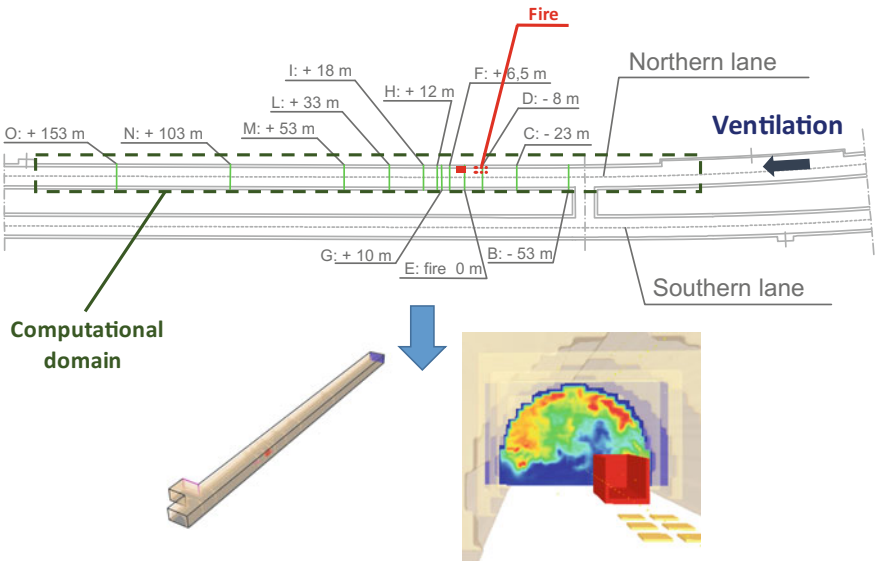

Fig. 4.23 Smokeview and FDS visualizations of the Morgex tunnel geometry analyzed

Table 4.1 Boundary conditions and material properties used in the tests

External boundaries:		Passive opening to the outside		
Inlet:		Passive opening to the outside		
Outlet:		Velocity profile according to Fig. 4.21		
Surfaces	Walls	Floor	Container, fuel pans	
Materials	Concrete	Asphalt	Steel	
Conductivity	1.67	0.06	45.0	[kW m^{-1} K^{-1}]
Specific heat	0.940	0.940	0.46	[kJ kg^{-1} K^{-1}]
Density	2585	1300	7800	[kg m^{-3}]
Emissivity	0.95	0.93	0.3	[–]
Thickness	1.0	1.0	0.05	[m]
Roughness	0.01	0.01	0.001	[m]
No slip	True	True	True	
Fixed temperature	No	No	40	[°C]

comparable, and decreasing the cell dimension to 10 cm the agreement with the experimental value improves compared to that for coarser meshes. The cells away from the fire source were modeled of 20 cm size, while downstream along the tunnel cell dimension was further increased. The total number of cells was close to five millions.

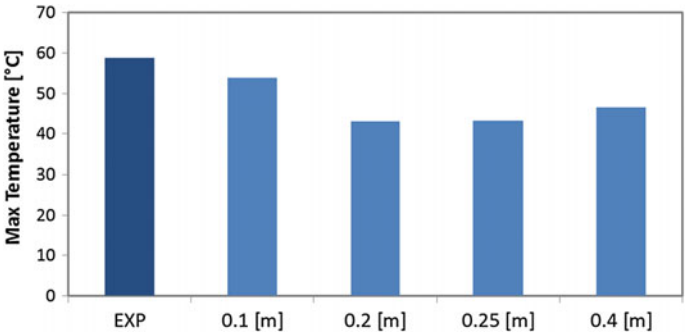

Fig. 4.24 Effect of the variation of the grid cell size over the fire source on the maximum temperature values recorded by thermocouple TIM2, located downstream, behind the trailer

4.3.4 Simulation Results and Discussion

The dynamics of the two tests is quite similar. After the sequential ignition of the six pools, the fires burning rate increased in intensity until reaching the fully developed state, with smoke and hot gases produced in large quantity moving both up and downstream.

As previously mentioned, during the tests the emergency ventilation was activated 90 s after the fire ignition, and the time span required to the ventilators to achieve regime conditions was large enough for some smoke backflow. Figure 4.25 shows the transient smoke dynamics and the qualitative agreement between the experimental and simulated transient back-layering behaviour. Figure 4.26 shows the temperature measurements recorded close to the ceiling 20 m upstream from the fire: the temperature increases after being reached by the hot gases and then decreases when the increased value of longitudinal velocity was enough to move the smoke further downstream. It is possible to notice that both the transient smoke dynamics and the temperature profile are correctly predicted by the FDS simulations.

The effect of the ventilation on the evolution of the hot gases can be seen clearly in the thermocouple profiles. In Fig. 4.27 it is reported a profile obtained from a thermocouple located on the fire axial plane, 3.5 m after the pool fires and behind the ceiling (monitor TFM1-bis). At first, the temperature increases as the fire grows in intensity and the hot gases reach the thermocouple. Then, when the emergency ventilation sets in, the larger airflow leads to a sharp decrease in the temperatures; only after a while the temperature started to rise again as the increased airflow enhanced the fire burning rate outweighing the cooling effect.

The experimental trend is correctly reproduced by the simulation, which predicts both the double peak behaviour (due to the airflow dynamics) and the absolute temperature values with reasonable agreement. The same is true for the thermocouple located at 1.6 m height on the part of the tunnel section opposite the fire

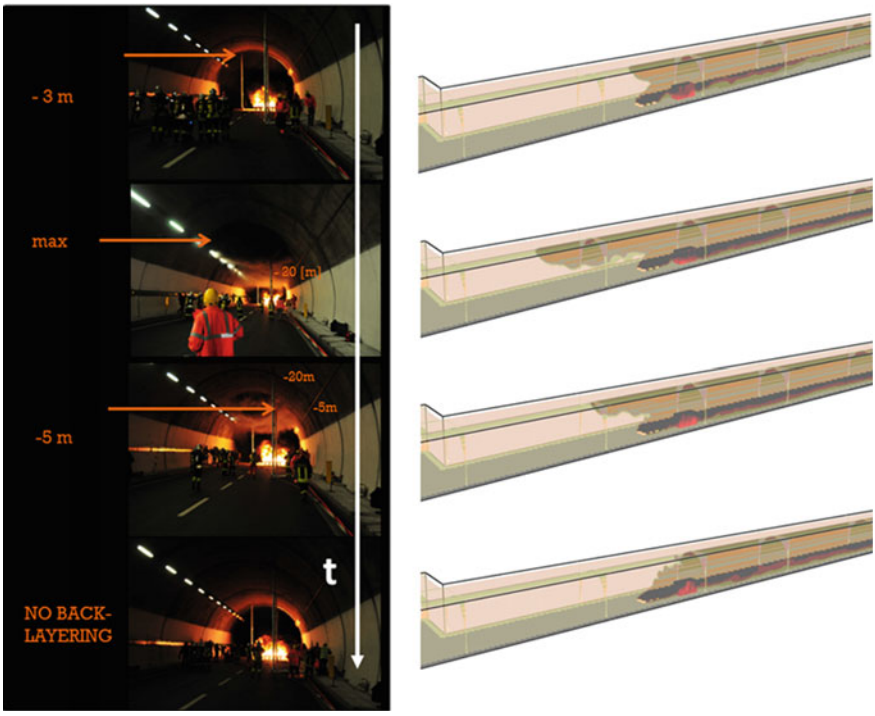

Fig. 4.25 Transient behaviour of smoke layer: experimental evidences (*left*) and FDS predictions (*right*). The arrows indicate the extent of the smoke layer upstream at different times after the fire ignition

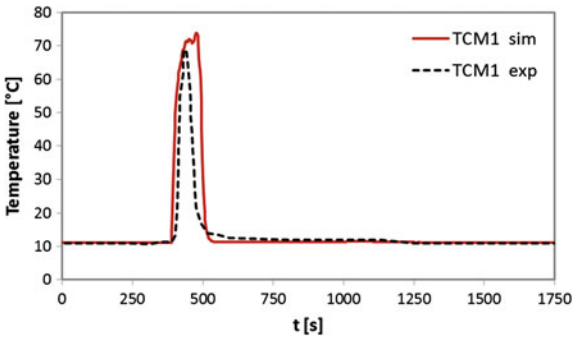

Fig. 4.26 Measured (*dashed lines*) and predicted (*red lines*) temperature values at thermocouple TCM1 during Fire Test #2. See Fig. 3.12 and Table 3.6 for the thermocouple position

(monitor TSL6, also shown in Fig. 4.27). The temperatures here are lower as the area was not directly affected by the hot gases plume.

A similar agreement was found for the dynamic behaviour of the hot gases along the tunnel axis, as shown in Fig. 4.28. In particular, model predictions show a good

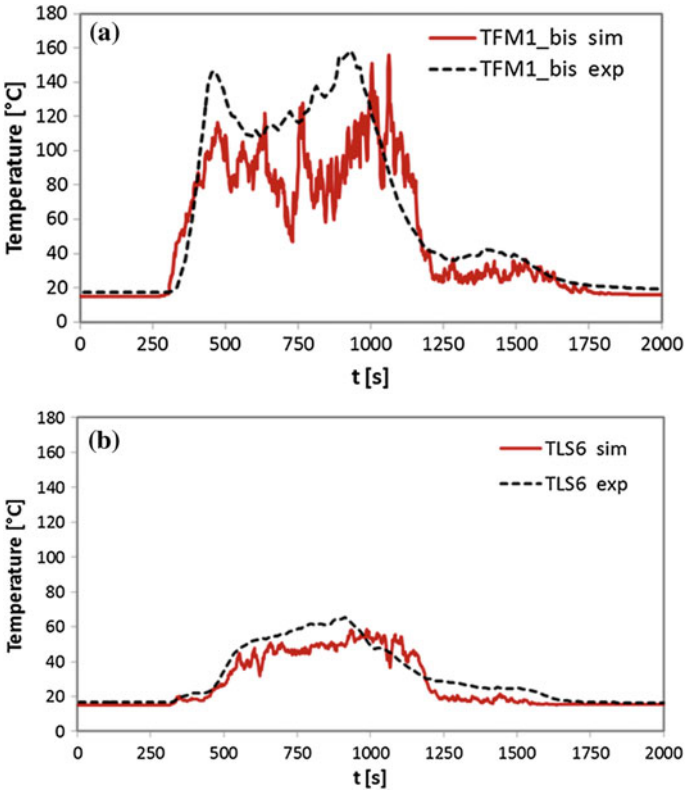

Fig. 4.27 Experimental (*dashed lines*) and simulated (*red lines*) temperature profiles recorded at monitor points TFM1bis (**a**) and TLS6 (**b**)

agreement with the experimental data in terms of capturing the qualitative dynamics of both the fire evolution and the smoke dispersion: recirculations around the obstacle, the back-layering of hot gases for normal-operation conditions, as well as the plume tilt and smoke destratification after the emergency ventilation activation.

Moreover, also the experimental profiles and the simulation results of CO concentrations agree quite well, as shown in Fig. 4.29. No tuning was performed on the parameter, and a CO yield of 0.037 was assigned to the code according to the literature [24]. Only few measurement devices were used during the tests to measure CO concentrations (GDM3, GHM3, GMM3, GNM3), and the corresponding parity plot are shown in Fig. 4.30. The average percentage error is equal to about 30% for Fire Test #1 and 24% for Fire Test #2.

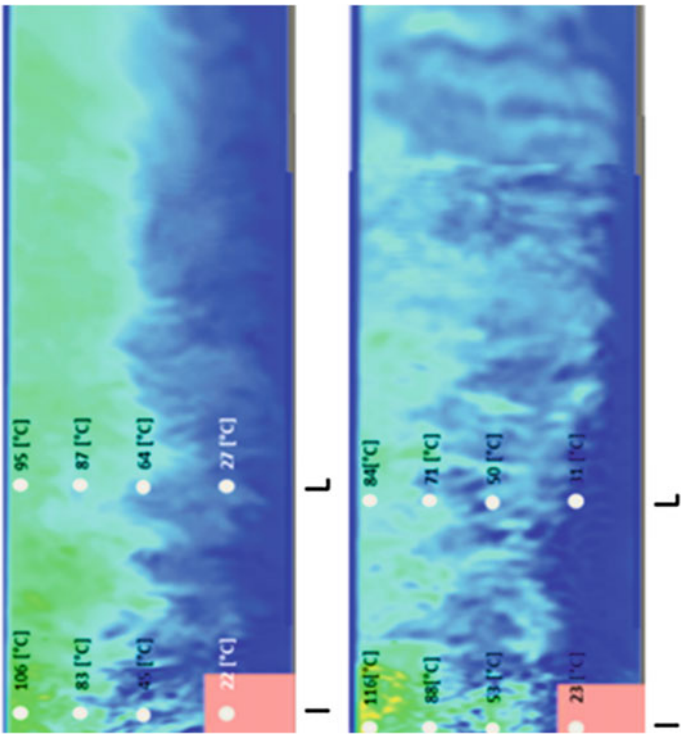

Fig. 4.28 Fire Test #2: simulated temperature profiles before (*left panel*) and after (*right panel*) the activation of the emergency ventilation, with the corresponding experimental values (included as numbers in correspondence to the monitor points) on the longitudinal section across the fire source

A synthesis of the FDS performance in predicting the temperature values is shown in Fig. 4.31, where the maximum temperature values recorded during each of the two experiments are plotted against the corresponding simulated values. It is possible to see that both tests show a reasonable agreement with the experimental data, especially considering the complex dynamics evidenced by the Morgex fire experiments. On average, there is a slight tendency to underpredict the experimental data; the average percentage error is equal to 24% for Fire Test #1 and 22% for Fire Test #2. However, apart from a few outliers, almost all the data are inside the ±30% range.

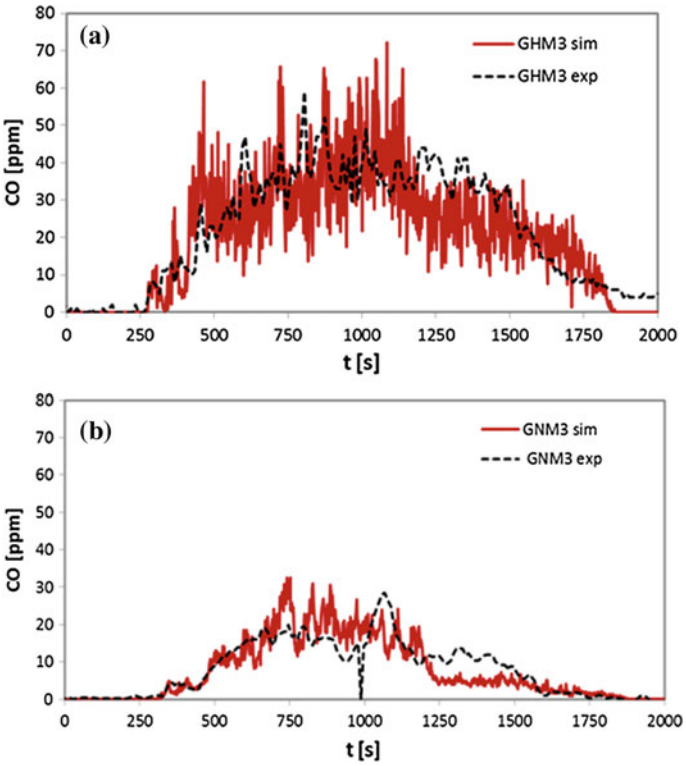

Fig. 4.29 Carbon monoxide values recorded during the experiment (*dashed lines*) and simulated (*red lines*) during Fire Test #2 at monitor GHM3 (**a**) and GNM3 (**b**)

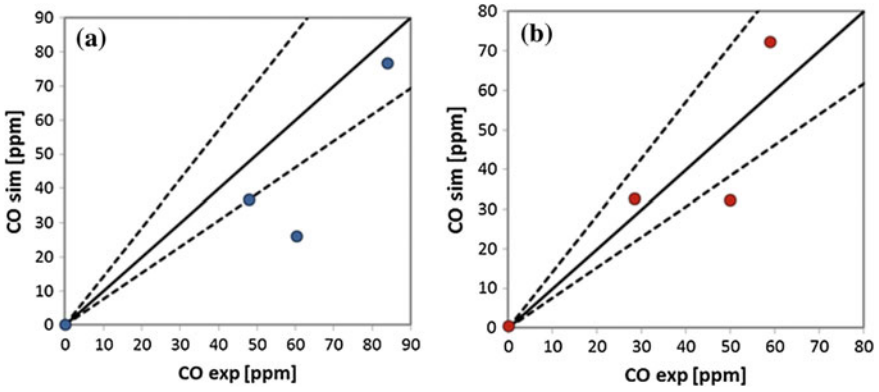

Fig. 4.30 Experimental versus predicted maximum carbon monoxide concentration values recorded during Fire Test #1 (**a**) and Fire Test #2 (**b**). The *dashed lines* correspond to ±30% error bands

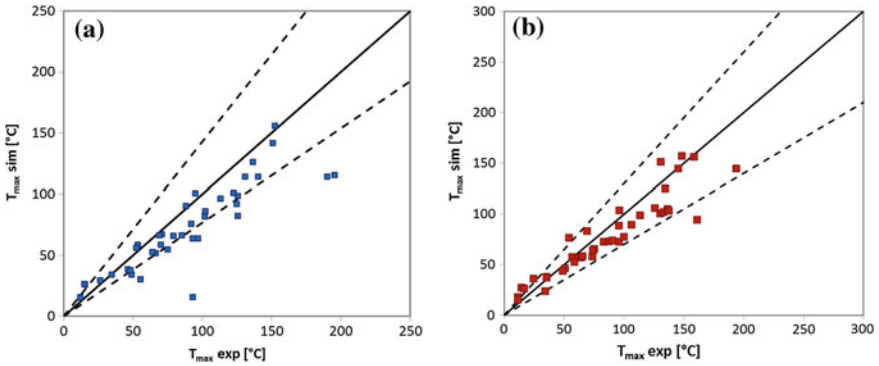

Fig. 4.31 Experimental versus predicted maximum temperature values recorded during Fire Test #1 (**a**) and Fire Test #2 (**b**). The *dashed lines* correspond to ±30% error bands

References

1. Carvel, R., Rein, G., Torero, J.L.: Ventilation and suppression systems in road tunnels: Some issues regarding their appropriate use in a fire emergency. Proceedings of the 2nd International Tunnel Safety Forum for Road and Rail, pp. 375–382 (2009)
2. Hwang, C.C., Edwards, J.C.: The critical ventilation velocity in tunnel fires—A computer simulation. Fire Safety J. **40**, 213–244 (2005)
3. Ingason, H., Li, Y.Z.: Model scale tunnel fire tests with longitudinal ventilation. Fire Safety J. **45**, 371–384 (2010)
4. Koch, S.E., DesJardins, M., Kocin, P.J.: An interactive Barnes objective map analysis scheme for use with satellite and conventional data. J. Clim. Appl. Meterol. **22**, 1487–1503 (1983)
5. Li, Y.Z., Ingason, H.: Position of maximum ceiling temperature in a tunnel fire. Fire Technol. **48**, 38–48 (2012)
6. American Gas Association LNG safety research program, report IS3–1. American Gas Association, Washington, DC (1974)
7. Kurioka, H., Oka, Y., Satoh, H., Sugawa, O.: Fire properties in near field of square fire source with longitudinal ventilation in tunnels. Fire Safety J. **38**, 319–340 (2003)
8. FHWA: Memorial tunnel fire ventilation test program—test report, Massachusetts Highway Department and Federal Highway Administration, Massachusetts (1995)
9. Ingason, H., Lönnermark, A.: Heat release rates from heavy goods vehicle trailers, in tunnels. Fire Safety J. **40**, 646–668 (2005)
10. Lönnermark, A., Ingason, H.: Gas temperatures in heavy goods vehicle fires in tunnels. Fire Safety J. **40**, 506–527 (2005)
11. Lönnermark, A., Ingason, H.: Fire spread and flame length in large-scale tunnel fires. Fire Technol. **42**, 283–302 (2006)
12. Lemaire, T., van de Leur, P.H.E., Kenyon, Y.M.: Safety proef: TNO metingen beneluxtunnel-meetrapport, TNO-rapport 2002-CVB-R05572. TNO, Amsterdam (2002)
13. Lemaire, T., Kenyon, Y.: Large scale fire tests in the second Benelux tunnel. Fire Technol. **42**, 329–350 (2006)
14. Li, Y.Z., Ingason, H.: Maximum ceiling temperature in a tunnel fire. SP Rep. **51** (2010)
15. Tavelli, S., Derudi, M., Cuoci, A., Frassoldati, A.: Numerical analysis of pool fire consequences in confined environments. Chem. Eng. Trans. **31**, 127–132 (2013)

16. Kim, E., Woycheese, J.P., Dembsey, N.A.: Fire dynamics simulator (version 4.0) simulation for tunnel fire scenarios with forced, transient, longitudinal ventilation flows. Fire Technol. **44**, 137–166 (2008)
17. European Union, Directive 2004/54/CE: Minimum levels of safety in European road tunnels (2004)
18. Repubblica Italiana, D.Lgs. 5 ottobre 2006, n. 264: Attuazione della direttiva 2004/54/CE in materia di sicurezza per le gallerie della rete stradale transeuropea (2006) (in Italian)
19. Beard, A., Carvel, R.: The Handbook of Tunnel Fire Safety. Thomas Telford Publishing (2005), ISBN 0727731688
20. McGrattan, K., McDermott, R., Hostikka, S., Floyd, J.: Fire Dynamics Simulator (Version 5). User's Guide. National Institute of Standards and Technology Special Publication 1019-5 (2010)
21. ISO 13571:2012: Life-threatening components of fire—Guidelines for the estimation of time to compromised tenability in fires. International Standardization Organization, Switzerland (2012)
22. Steinhaus, T., Welch, S., Carvel, R.O., Torero, J.L.: Large-scale pool fires. Therm. Sci. **11**, 101–118 (2007)
23. Ma, T.G., Quintiere, J.G.: Numerical simulation of axi-simmetric fire plumes: Accuracy and limitations. Fire Safety J. **38**, 467–492 (2003)
24. Köylü, Ü.Ö., Faeth, G.M.: Carbon monoxide and soot emissions from liquid-fueled buoyant turbulent diffusion flames. Combust. Flame **87**, 61–76 (1991)

Chapter 5
Evaluation of the Consequences on the Users Safety

Abstract In this chapter it is introduced a simple methodology for the quantitative assessment of the severity of the expected consequences of a tunnel fire that can be applied in any complex environment. The proposed methodology was applied to the Morgex North tunnel to show its potentiality for evaluating the effect of different geometric characteristics on the safety performances of a tunnel in the event of an unwanted fire.

5.1 Methodology for the Evaluation of Tunnel Fire Consequences

The quantitative assessment of the severity of the expected consequences of a tunnel fire, even in complex environments, can be supported by a simple, generic, extensible methodology which could be useful for the analysis of specific scenarios, for comparing different configurations and for highlighting qualitative trends when varying some design parameters.

The intrinsic complexity of the fire phenomena and their interactions in geometrically complex environments imply that predicting the consequences in terms of users' safety requires to account for several interacting parameters, such as the presence of toxic gases, heat and smoke in a specific location inside the tunnel. These, in turn, depend upon the specific characteristic of the fire source, of the tunnel geometry, and of the ventilation system.

The idea on which the methodology is based is to identify an overall parameter related to the severity of the consequences of a tunnel fire, that is the length of the tunnel interested by values of some suitable Key Hazard Indicators (KHIs) larger than a given threshold value.

The relevant KHIs arise from a comprehensive evaluation of the effects of a tunnel fire on human tenability, that is, the ability to perform cognitive and motor skill functions at an acceptable level when exposed to fire environment [1]. Several combined hazards, such as combustion products toxicity, heat and thermal damage,

F. Borghetti et al., *Tunnel Fire Testing and Modeling*,
PoliMI SpringerBriefs, DOI 10.1007/978-3-319-49517-0_5

visual obscuration due to smoke, must be taken into account, as these parameters influence the occupants ability to reach safety exits and thus to survive the fire.

The effects of those parameters are different both in severity and in mechanism of action, and the tunnel users' response depends upon their physical well-being and their specific location inside the tunnel environment.

Therefore, different KHIs were considered based on the ISO 13571 standard [2], which identifies a few comprehensive parameters aimed at measuring the effect of the exposure to heat and toxic effluents from a fire on the user's ability to possess enough cognitive and motor skills to escape the fire.

5.2 Key Hazard Indicators

The comparison of the effects of some of the different parameters is based upon the concept of fractional effective dose, FED, which is the ratio of the actual exposure dose to the exposure dose which is enough to produce a specified harmful effect on a person of average susceptibility, i.e. is critical for their survival.

The FED_T, that is, the toxic gases FED contribution, can be estimated through the following expression [2]:

$$FED_T = \sum_i \frac{\varphi_{CO}}{35{,}000} v_{CO_2} \Delta t_i + \sum_i \frac{\varphi_{HCN}{}^{2.36}}{1.2 \cdot 10^6} v_{CO_2} \Delta t_i$$

where φ_{CO} [ppm] and φ_{HCN} [ppm] are the average concentrations of CO and HCN over the discrete time increment Δt_i [min] in which the overall time span is divided. The coefficient v_{CO2} takes into consideration the role of CO_2 in increasing the ventilation rates, and can be linked to the CO_2 concentration φ_{CO2} [%vol] as follows:

$$v_{CO_2} = exp\left[\frac{\varphi_{CO_2}}{5}\right]$$

FED_H, that is the FED contribution of human body exposure to heat, radiant energy and high temperatures can be estimated through the following relation [2]:

$$FED_H = \sum_i \left(\frac{1}{t_{rad}} + \frac{1}{t_{conv}}\right) \Delta t_i$$

where t_{rad} [s] and t_{conv} [s] represent the time to compromised tenability due to exposure to radiant and convective heat, while Δt_i [s] is the time increment over which the measurements are taken.

The radiative time contribution is the smallest between the time to second degree burning ($t_{rad\text{-}II\text{-}burn}$) and the time to pain experience due to radiant heat ($t_{rad\text{-}pain}$),

while the convective contribution is the time to pain experience due to convective heat (t_{conv}); they can be estimated as follows:

$$t_{rad-Ilburn} = 6.9\, q^{-1.56} \cdot 60[\mathrm{s}]$$

$$t_{rad-pain} = 4.2\, q^{-1.9} \cdot 60[\mathrm{s}]$$

$$t_{conv} = (5 \cdot 10^7)\, T^{-3.4} \cdot 60[\mathrm{s}]$$

where q [kW/m^2] is the radiant heat flux, while T [°C] is the temperature in the location of interest.

FED values are integral in nature because they account for the cumulative effect of heat and toxic gas exposure over time. The threshold value for FED_T and FED_H was defined accordingly with the ISO standard [2] equal to one, which corresponds to half of the population exposed experiencing compromised tenability.

Exposure to heat and high temperatures can lead to significant damage to the structural resistance of the tunnel itself, posing an ulterior indirect threat to the occupants. In this analysis the work of Johnson and Herrera [3] was considered to link the risk of concrete spalling to its heating dynamics, as shown in Table 5.1.

In this case the KHI is built by analyzing the ceiling temperature and its heating rate, and considering as threshold values 440 °C and 20 °C/min.

Smoke affects the visibility and thus the ability of the tunnel user to reach a safe place. The distance L_{smoke} up to which the user can identify objects can be estimated from the following correlation [2]:

$$L_{smoke} = -\frac{\ln(c_v)}{\sigma \cdot \rho_{smoke}} = -\frac{\ln(0.02)}{10[\mathrm{m}^2 \cdot \mathrm{g}^{-1}] \cdot \rho_{smoke}}$$

where σ is the mass specific extinction coefficient for the smoke aerosol (σ = 10 m^2/g for well-ventilated fires), c_v the visual contrast (the standard assumes the value c_v = 0.02 as the value corresponding to minimum detectable contrast) is and ρ_{smoke} [g/m^3] is the mass concentration of the smoke aerosol.

In contrast with the previous parameters, L_{smoke} gives an instantaneous indication which can be affected by the fluctuating intrinsic behaviour of the smoke plume. Consequently, together with a threshold value of L_{smoke} = 1 m, the obtained

Table 5.1 Key Hazard Indicators and corresponding thresholds

j	KHI_j	Threshold
1	FED_T	1 [−]
2	FED_H	1 [−]
3	L_{smoke}	5 m
4	$T_{ceiling}$ $dT_{ceiling}/dt$	440 °C 20 °C/min
5	$O_{2,warn}$	17% vol.
6	$O_{2,crit}$	11% vol.

results were preliminarily compared with those computed using threshold values of L_{smoke} = 0.9 m and L_{smoke} = 1.1 m. This was made in order to assess the sensitivity of the extent of tunnel length over which smoke impairs the visibility to the chosen threshold value.

It should be stressed that the threshold value of L_{smoke} = 1 m is arbitrary; larger values such as 5 m or even 10 m can be used for safety assessment when evaluating survivability in realistic situations [4].

As a further KHI, the O_2 concentration was used with two distinct threshold values, namely 17% by vol., which represents a warning level in breathable atmospheres, and 11% by vol., which is the critical level of O_2 below which asphyxiation is assumed to occur almost immediately [5].

To summarize, 6 KHIs were used, as reported in Table 5.1 together with their threshold values.

For a given tunnel fire configuration, the values of KHIs at a representative height were analysed along the tunnel. The length of the portion of tunnel interested by values of each KHI larger than its threshold value, Δ (expressed in m), was computed. As an indicator of the severity of the consequences, the largest value of such lengths was used, which can be considered as a Key Performance Indicator (KPI) of the resilience of a given tunnel configuration:

$$KPI = \max(\Delta(KHI_j)) \quad j = 1, \ldots, 6$$

where $\Delta(KHI_j)$ (m) is the tunnel length over which the KHI_j value is larger than its corresponding threshold value. The lower the value of the KPI is, the larger the resilience of the tunnel configuration is.

5.3 Evaluation of the Consequences for the Morgex Tunnel

After verifying that the simulations were in good agreement with the experiments, as discussed in the previous chapter, in this section a sensitivity analysis on the Morgex North fire tests was performed: different simulations were performed to study how a variation in the configuration would have affected the evolution of the fire and its consequences on the tunnel users.

Apart from a point to point comparison of the measured data and FDS predicted values, the previously mentioned methodology for the identification of the consequences of a tunnel fire was applied to the investigated fire scenarios. Since the hazard associated to a fire event in a tunnel derives from a combination of effects (direct and indirect thermal damage, exposure to toxic gases, oxygen depletion, visual impairment due to smoke), the different Key Hazard Indicators (KHIs) previously proposed and discussed can be used to account for the exposure to each factor in a specific location inside the tunnel, and their maximum value can be

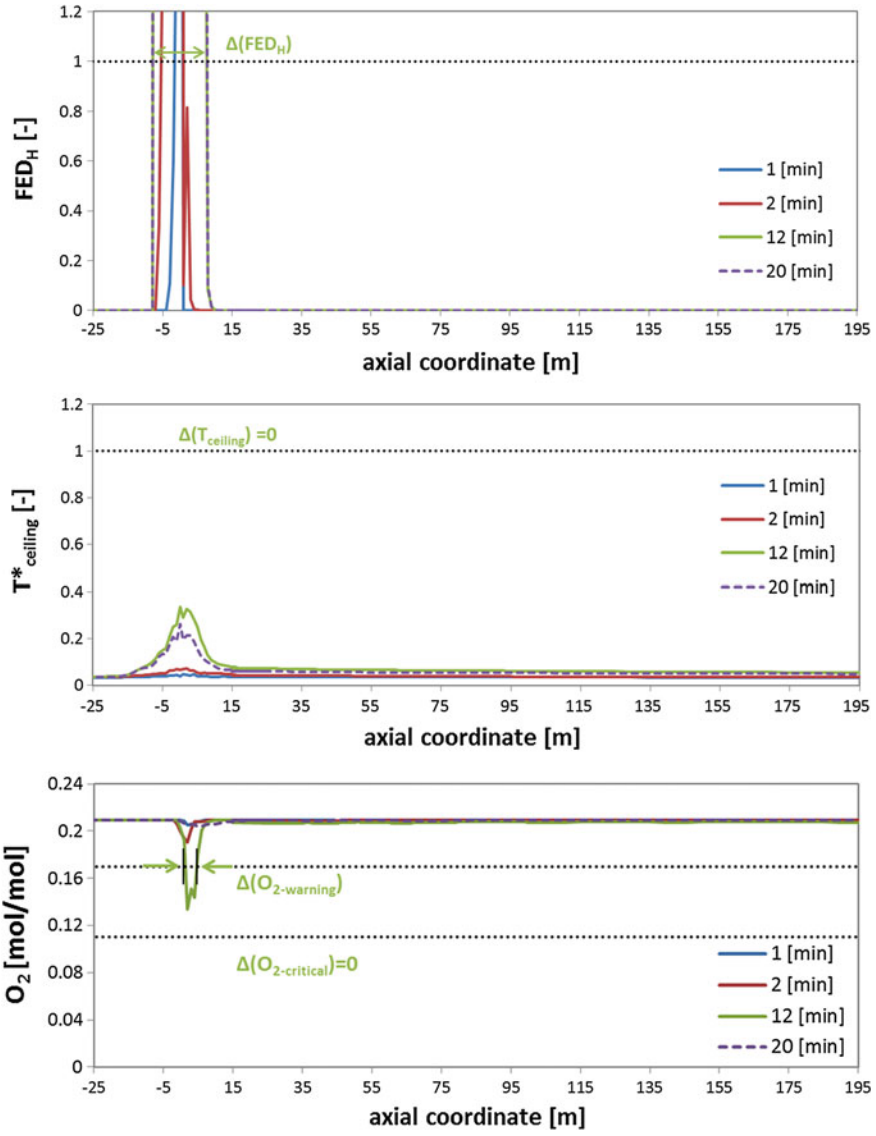

Fig. 5.1 KHI profiles along the tunnel, evaluated at different times after ignition, on the fire axial plane at 1.6 m height, for the reference configuration corresponding to Fire Test #2: from *top* to *bottom*: FED_H, $T_{ceiling*}$, (actual ceiling temperature divided by the threshold value), O_2 concentration levels, FED_T, L_{smoke}. The areas corresponding to values above the critical values are highlighted for the curves representative of the most severe conditions, 12 min after the fire ignition

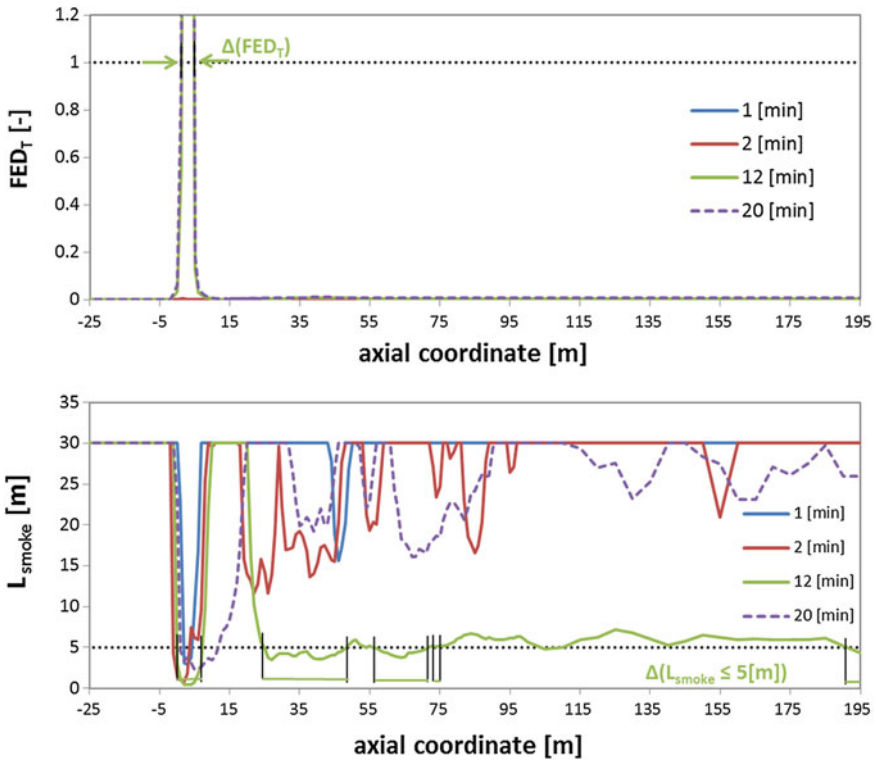

Fig. 5.1 (continued)

considered as an overall Key Performance Indicator of the resilience of the given tunnel configuration.

The most severe conditions were found in correspondence to 12 min after the fire ignition, when all six pools were still burning steadily and the visibility downstream was very low. The profiles obtained at different times after the fire ignition at 1.6 m height for the various KHIs are shown in Fig. 5.1.

The length of the tunnel section in which the KHIs are above the critical values is equal to 48 m, which is quite a small value when compared to the tunnel length. In this case, the controlling parameter is represented by the smoke visibility. Its threshold was set to 5 m, as it is a requirement normally asked for in risk assessment practice [4]. The overall KPI value is relatively low, showing that a critical situation for survival is expected only around the fire source, therefore controlling that the emergency ventilation procedure was effective in the dilution and removal of hot gases and smoke. This was confirmed by the fire brigades taking part in the tests in order to ensure safety and test their equipment and procedures, who testified that the visibility downstream was not completely compromised.

5.4 Parametric Analysis: The Effect of Geometry and Congestion

The presence of an obstacle 6 m downstream the fires had an effect on the smoke and hot gases movement, with lateral canalization and recirculation as shown in Fig. 5.2. In addition, some 50 m before the fire zone the tunnel is linked to the other lane through a bypass.

In order to assess the effect of each of these geometrical characteristics on the fire consequences, the results previously discussed were compared to that computed considering both the same tunnel fire scenario without the presence of the obstacle and then a scenario characterized by the presence of the obstacle but the absence of the bypass. The KHIs values computed for these scenarios are summarized in Table 5.2.

It can be noticed that the presence of both the by pass and the obstacle has a clear effect, leading to an increase in the hazardous area. However, considering that the real situation was not too warning thanks to the presence of the emergency ventilation, also the KPI variations cannot be too large. The longitudinal velocity contours in Fig. 5.3 show that the presence of the bypass enhances the turbulence and recirculation upstream. However, the smoke stratification and the back-layering length are not affected significantly, leading to consequences in terms of KHIs quite similar to that of the reference scenario.

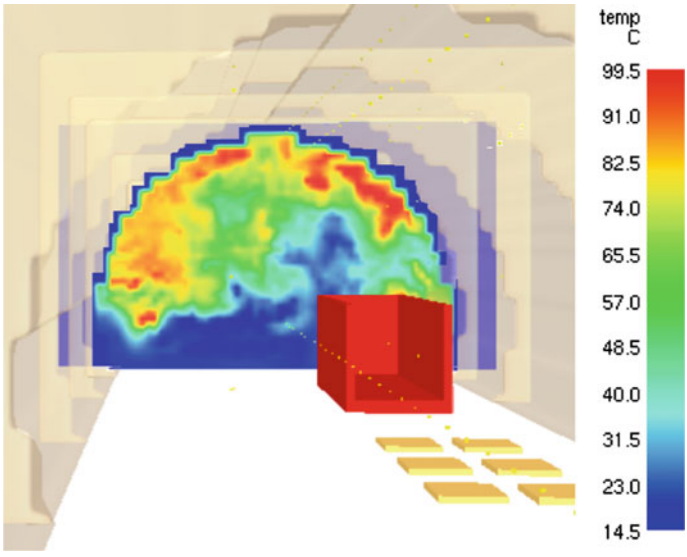

Fig. 5.2 Temperature contours immediately downstream of the obstacle, where the asymmetrical profile of the hot gases is shown

Table 5.2 Comparison of the KHI [m] and KPI [m] values for the reference (REF) configuration corresponding to the experimental setup, the tunnel without the bypass and the tunnel without the obstacle

	Δ (FED_H)	Δ (FED_T)	Δ ($O_{2,warning}$)	Δ (L_{smoke} = 5 m)	Δ ($T_{ceiling}$)	KPI
REF	14	2	2	48	0	48
NO Bypass	14	1.5	1	43	0	43
NO Obst	14	1.5	1	36	0	36

In the experimental setup a container was placed immediately downstream the fires. The obstacle is 6.0 m long, 2.6 m high and 2.5 m wide, and only its rear end was closed by a panel (see Fig. 5.2); the ratio α between its cross-flow area and the tunnel cross-section is equal to 0.1.

The absence of the obstacle lowers the overall KPI from 48 to 36 m. Similarly to the reference configuration, also in this case the major role is played by the visibility impairment due to smoke destratification. The simulations performed pointed out that obstacles located downstream from the fire influence the overall KPI of the tunnel only if placed very close to the fire. In this case, the obstacle creates a recirculation pattern (see Fig. 5.3) which promotes the smoke destratification compared to the empty scenario.

The results prove the importance of an accurate representation of the geometrical configuration as well as the evaluation of the effect of vehicles for a realistic assessment of the consequences in tunnel fires.

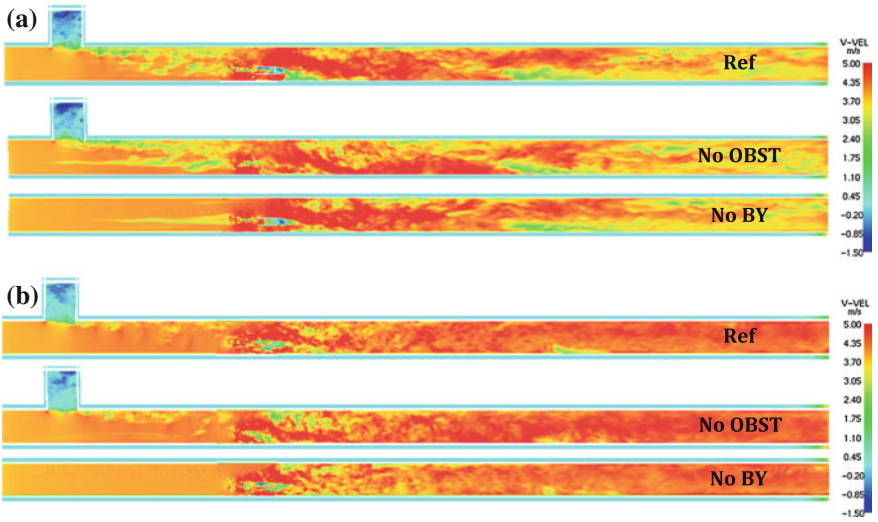

Fig. 5.3 *Top view* of the longitudinal velocity contours at z = 1.6 m (**a**) and z = 3.0 m (**b**) for (from *above*) the reference configuration, the one without obstacle and the one without bypass

5.5 Effect of the Ventilation

In order to assess the consequences in case of a failure in the emergency ventilation system, the reference scenario was compared to a configuration in which only the ordinary ventilation was activated throughout the fire test. The effect of this variation in the airflow input over the fire burning rate was neglected, and the HRR input was maintained equal to the real case scenario. The simulation results are shown in Figs. 5.4 and 5.5.

As shown in Fig. 5.4, the temperatures values upstream in the ordinary ventilation scenario are higher than in the emergency ventilated scenario. The ordinary ventilation is not enough to suppress the smoke back-layering, which expands in time backwards until reaching the upstream boundary of the computational domain (Fig. 5.5). The reduced airflow of the ordinary ventilated scenario, however, does not result in a complete destratification of the smoke layer, which remains close to the ceiling. This trend is confirmed by the KPI analysis, as in this case the smoke KHI (and thus the overall KPI), is equal to 25 m. The apparently counterintuitive conclusion that the emergency ventilation leads to worse situation from the safety point of view was the object of further analysis.

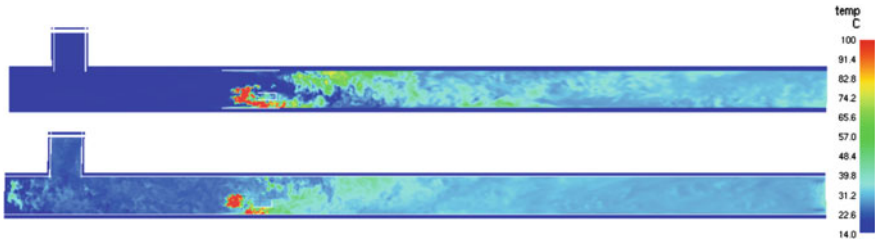

Fig. 5.4 Temperature contours at z = 1.6 m for the reference case, with V = 4.7 m/s (*top*) and the ordinary ventilation simulation (*bottom*), where V = 2.4 m/s, at t = 800 s after the fire ignition

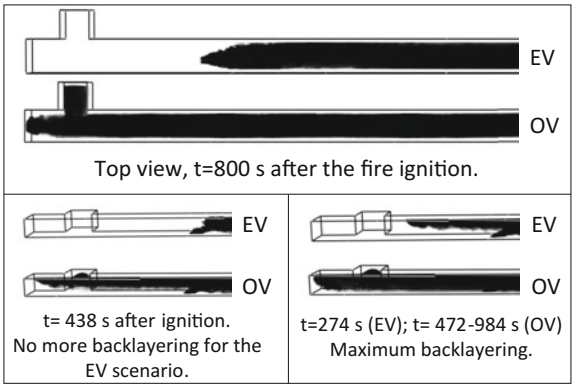

Fig. 5.5 Smoke profiles for the reference case (EV) and the ordinary ventilation simulations (OV) at various times after the fire ignition

The overall source term HRR used, approximately 15 MW at its peak, was motivated by safety constraint during the actual experimental tests and the need to preserve the structural integrity of the tunnel, which needed to be fully operative a few hours after the tests. However, there is evidence [6, 7] that in a real tunnel fire scenario an HGV fire can reach significantly higher values, up to 100 MW and more.

In order to further analyze the effect of HRR and ventilation simultaneously, a series of simulations were performed on an analogous but simplified scenario, a 500 m long empty tunnel, with 12 m width, 7.5 m height and semi-circular section. The boundary conditions were comparable, the domain symmetrical and a single source term was used for the analysis. The grid choice was performed coherently with the criterion proposed by Ma and Quintiere [8] over the fire source, and the total number of cells over half the computational domain was of about 500,000 cells.

The study focused on the effect of the increase in the source term HRR over some of the KHIs both in absence of ventilation and in presence of ventilation corresponding to the critical velocity u_{cr}.

Figure 5.6 shows that for HRR = 15 MW the area affected by compromised tenability conditions is limited to the immediate proximity of the fire, even in the absence of any forced ventilation. In order to obtain significant thermal damage the

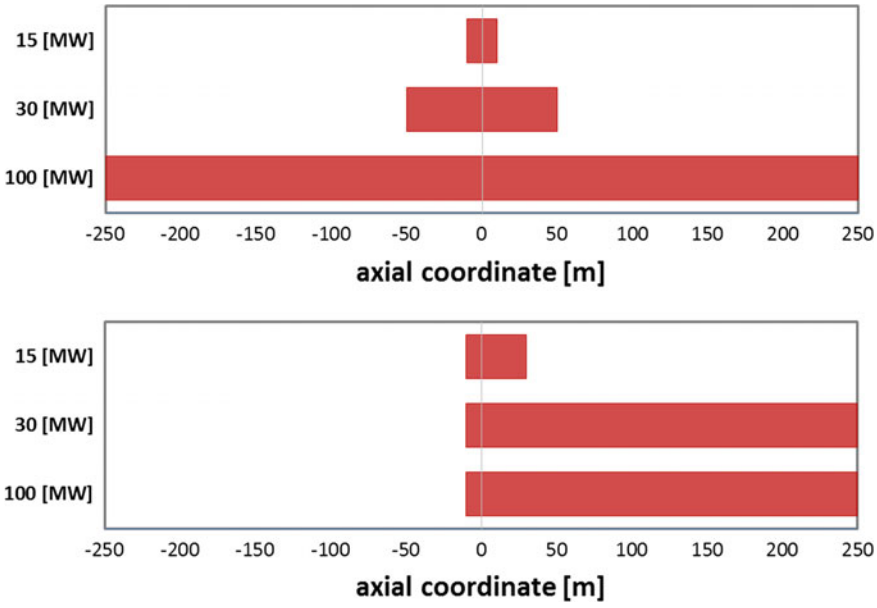

Fig. 5.6 KPI—corresponding to $\Delta(FED_H)$—values at z = 1.6 m height for the non-ventilated (*left*) and ventilated (*right*) tests for different heat release rates 15 min after the fire ignition: for HRR of 15, 30 and 100 MW the longitudinal velocity values corresponded to V = 2.5, 3 and 3.8 m/s, respectively

HRR values need to be at least 30 MW; in this case the benefits of mechanical ventilation are clearly evidenced, as the area upstream the fire is kept in tenable conditions even when increasing the HRR to 100 MW.

References

1. ISO 13943:2008: Fire Safety Vocabulary. International Standardization Organization, Switzerland (2008)
2. ISO 13571:2012: Life-Threatening Components of Fire—Guidelines for the Estimation of Time to Compromised Tenability in Fires. International Standardization Organization, Switzerland (2012)
3. Jönsson, J., Herrera, F.: HGV traffic—consequences in case of a tunnel fire. In: Proceedings of 4th International Symposium on Tunnel Safety and Security, Frankfurt am Main, Germany (2010)
4. CmR Gexcon: MARLIN Platform CFD Fire Analysis. Internal Report (2014)
5. Occupational Safety and Health Standards: OSHA Standard 29 CFR 1910.146. Permit-Required Confined Spaces. USA (1993)
6. Carvel, R.O., Beard, A.N. (eds.): The Handbook of Tunnel Fire Safety. Thomas Telford Publishing, London (2005)
7. Ortolani, C.: Casi di combustioni accidentali. Maggioli Editore, Italy (2007). (in Italian)
8. Ma, T.G., Quintiere, J.G.: Numerical simulation of axi-symmetric fire plumes: accuracy and limitations. Fire Safety J. **38**, 467–492 (2003)

Chapter 6
Conclusions

In this book new full-scale tunnel fire experimental results are presented and discussed. The tests took place in the Morgex North tunnel of the A5 highway (Italy). The first part of the book describes how to set up full-scale fire tests inside an existing tunnels. Indications are given about fire scenarios and their preparation, safety issues, materials and equipment, preparation of tunnel sections and measuring instruments.

Two transient diesel oil fire tests were performed with variable ventilation strategies and a peak HHR of about 15 MW was observed. The measurements are first compared to empirical models in terms of flame angle, maximum temperature increase and back-layering length as a function of the ventilation velocity. The results are found to agree well with model predictions as well as with analogous full scale tunnel fire experiments found in the literature. A peculiar aspect of this new test case refers to the geometry of the tunnel and the accidental scenario: the presence of a bypass zone ahead of the fire region and an obstacle, representing a semi-trailer, located immediately downstream of the fire zone makes this experiment a challenging test case for CFD modeling of tunnel fires with longitudinal ventilation.

Finally, the two full-scale, transient fire tests were simulated using the FDS code. The comparison between simulated and experimental results proved to be satisfactory for both temperature and CO profiles, as well as for characterizing the dynamics of the smoke and hot gases layer.

A sensitivity analysis was performed to assess the effect of the presence of the bypass and the obstacle, as well as of the emergency ventilation procedure on the consequences for the users safety. The bypass has an influence in enhancing the turbulence upstream the fire, however its net effect was not relevant in terms of immediate danger to people. The presence of the obstacle downstream of the pool fires led to an enhanced destratification of the hot gases compared to the empty tunnel configuration. This confirms the importance of an accurate representation of

F. Borghetti et al., *Tunnel Fire Testing and Modeling*,
PoliMI SpringerBriefs, DOI 10.1007/978-3-319-49517-0_6

both the geometry of the system and the evaluation of the effect of vehicles for a realistic assessment of the consequences. Finally, thanks to a series of comparisons with scenarios of different HRRs and ventilation conditions, it has been confirmed that the emergency ventilation procedure plays a fundamental role in tunnel fire safety.

Annex A
Sections of Encoded Measuring Instruments

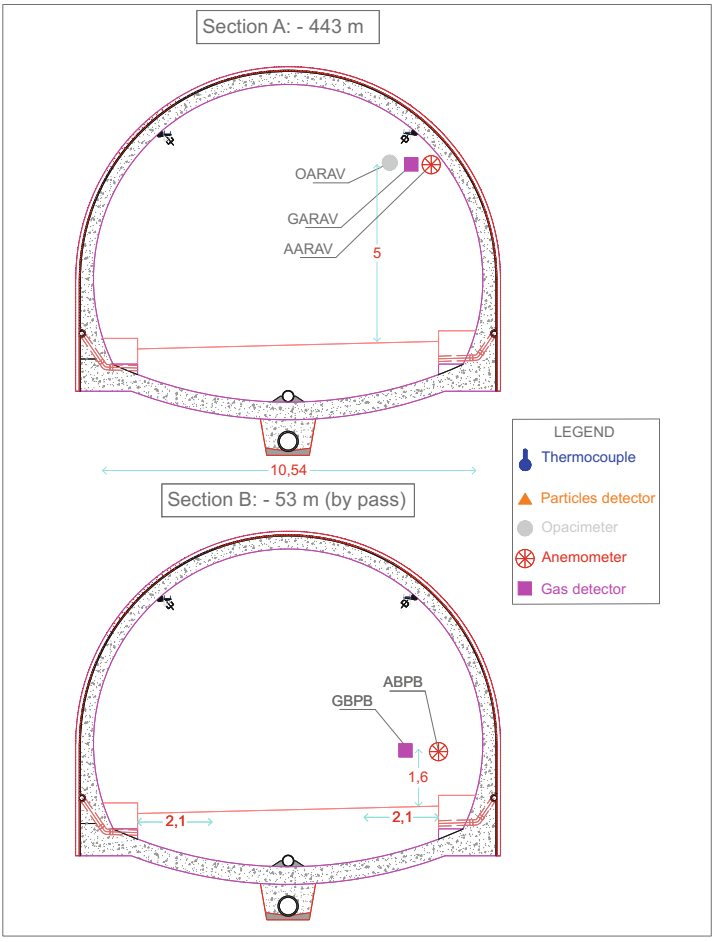

F. Borghetti et al., *Tunnel Fire Testing and Modeling*,
PoliMI SpringerBriefs, DOI 10.1007/978-3-319-49517-0

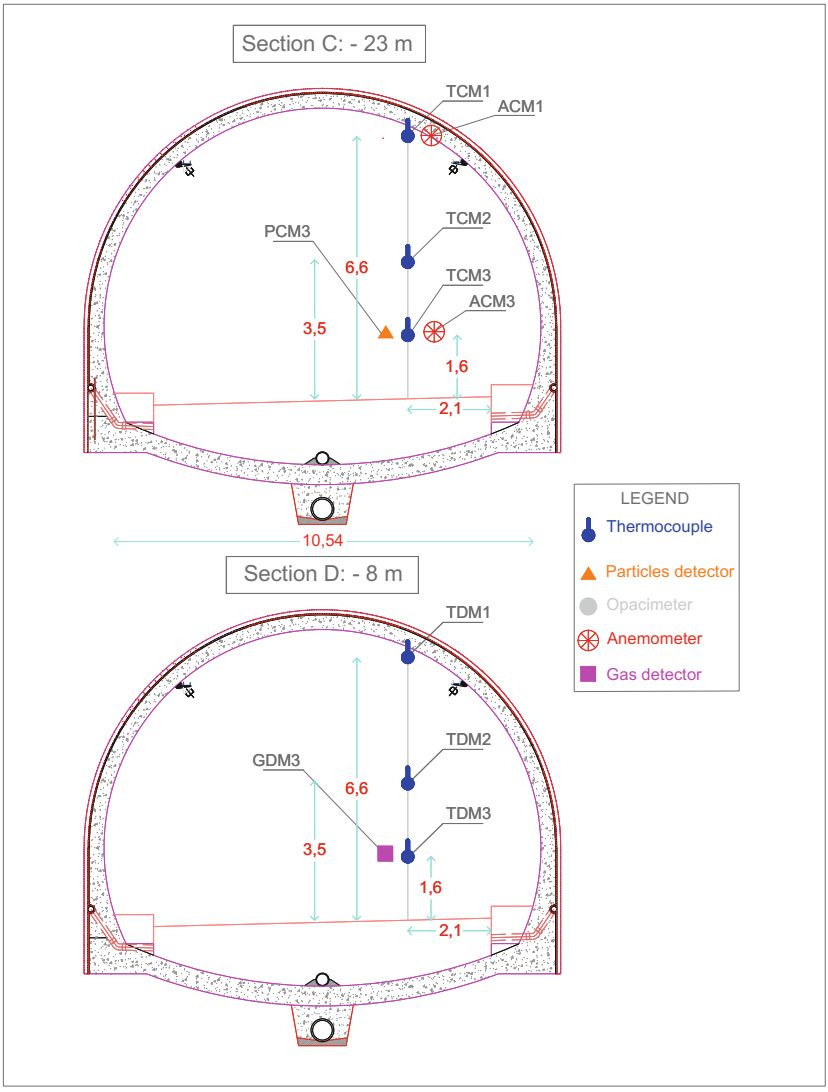
Section C: - 23 m
TCM1
ACM1
PCM3
TCM2
6,6
TCM3
ACM3
3,5
1,6
2,1
10,54
LEGEND
Thermocouple
Particles detector
Opacimeter
Anemometer
Gas detector
Section D: - 8 m
TDM1
GDM3
TDM2
6,6
TDM3
3,5
1,6
2,1

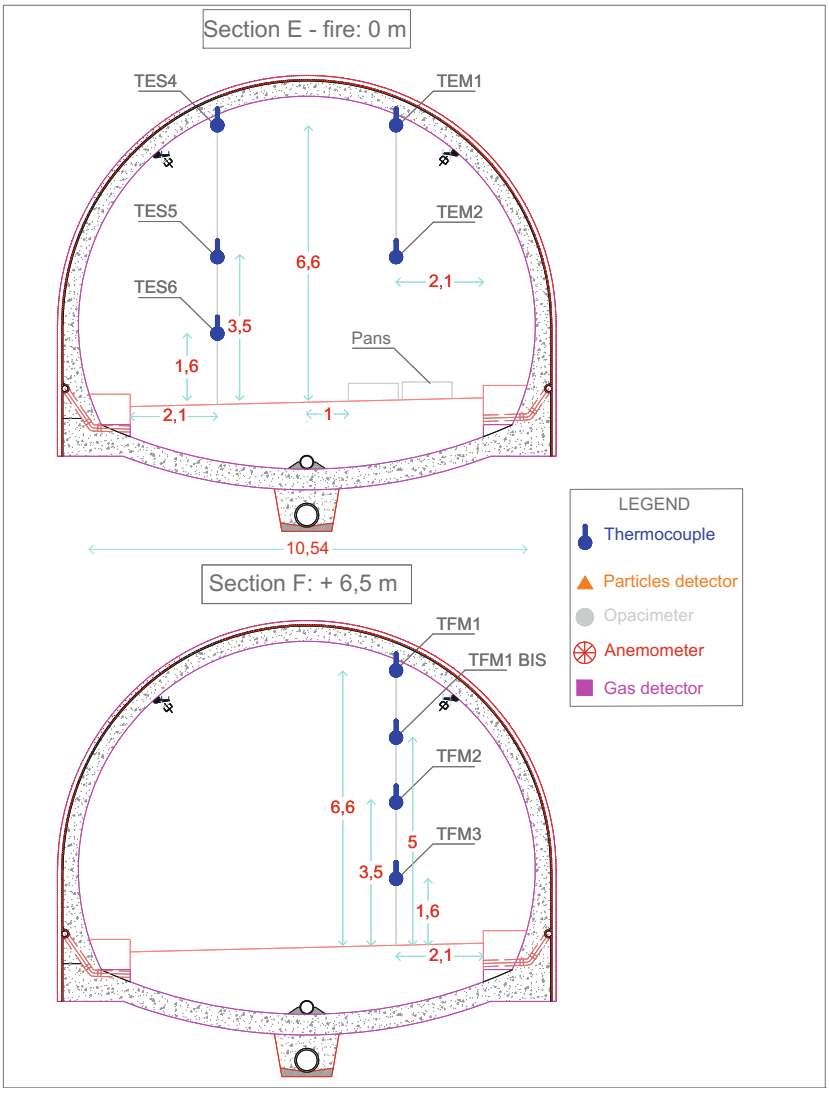
Section E - fire: 0 m
TES4
TEM1
TES5
TEM2
6,6
2,1
TES6
3,5
Pans
1,6
2,1
1
10,54
LEGEND
Thermocouple
Particles detector
Opacimeter
Anemometer
Gas detector
Section F: + 6,5 m
TFM1
TFM1 BIS
TFM2
6,6
5
TFM3
3,5
1,6
2,1

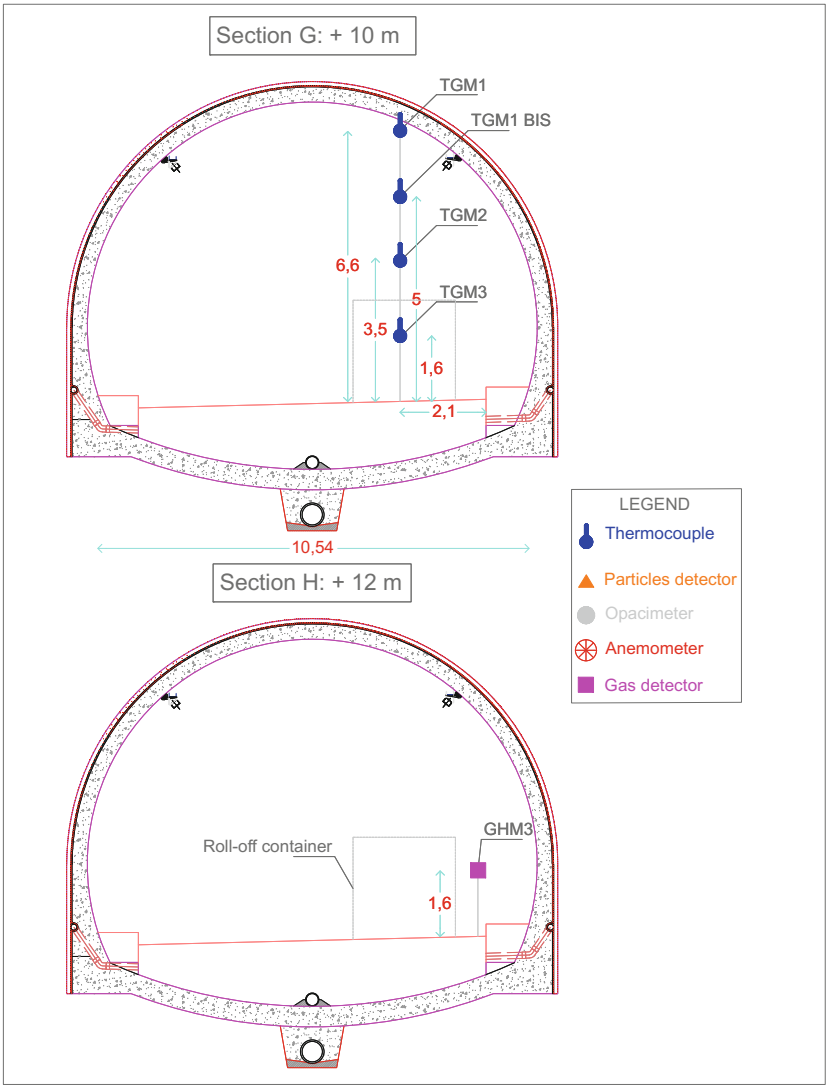
Section G: + 10 m
TGM1
TGM1 BIS
TGM2
TGM3
6,6
5
3,5
1,6
2,1
10,54
Section H: + 12 m
Roll-off container
GHM3
1,6
LEGEND
Thermocouple
Particles detector
Opacimeter
Anemometer
Gas detector

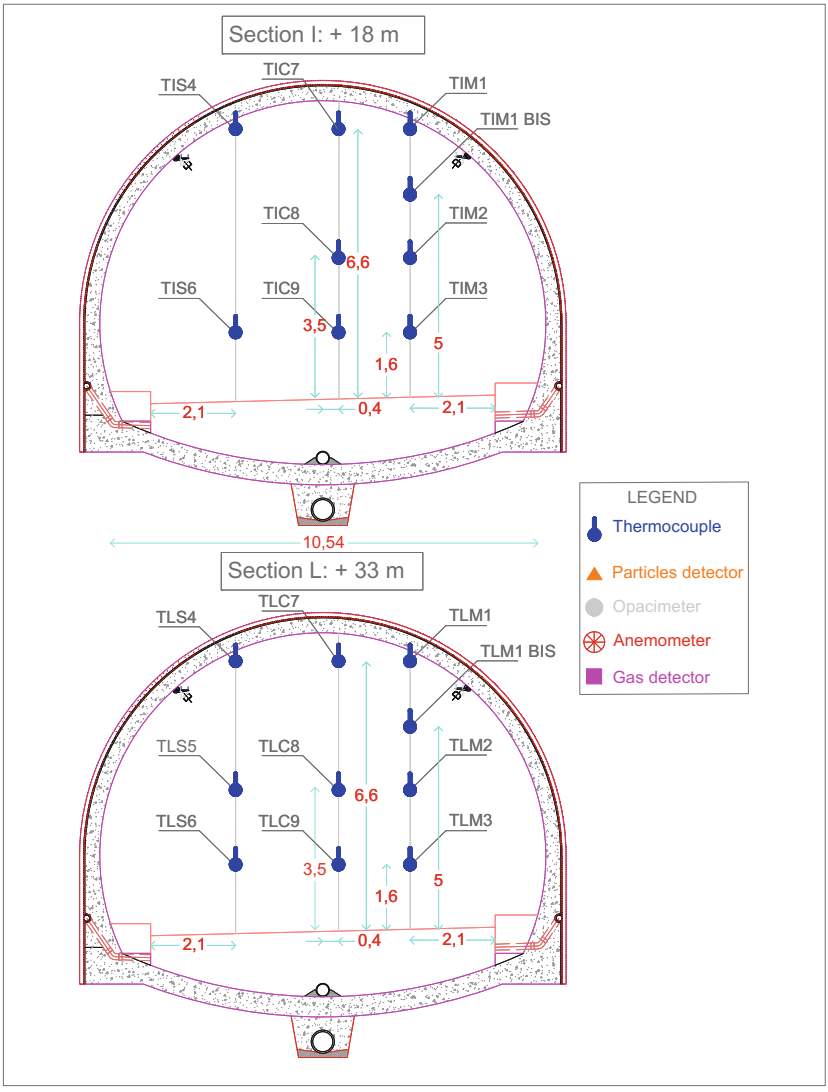
Section I: + 18 m
TIS4
TIC7
TIM1
TIM1 BIS
TIC8
TIM2
TIS6
TIC9
TIM3
6,6
3,5
5
1,6
2,1
0,4
2,1
10,54
Section L: + 33 m
TLS4
TLC7
TLM1
TLM1 BIS
TLS5
TLC8
TLM2
TLS6
TLC9
TLM3
6,6
3,5
5
1,6
2,1
0,4
2,1
LEGEND
Thermocouple
Particles detector
Opacimeter
Anemometer
Gas detector

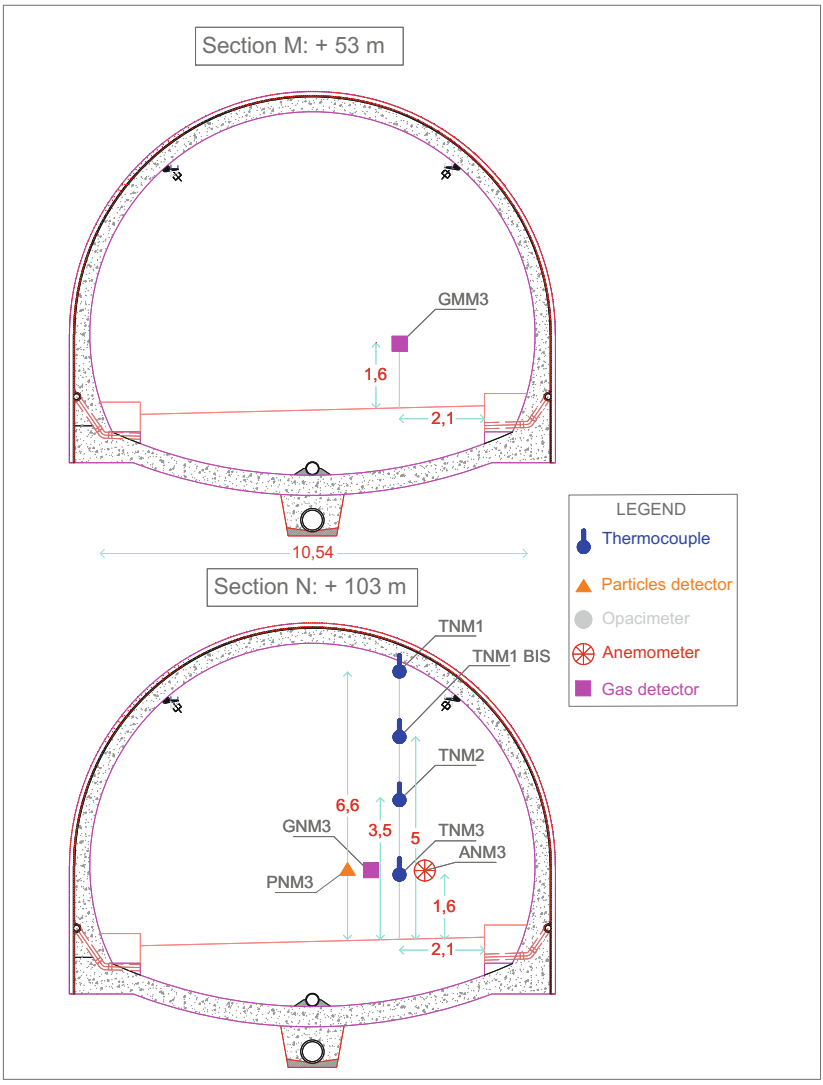
Section M: + 53 m
GMM3
1,6
2,1
10,54
Section N: + 103 m
TNM1
TNM1 BIS
TNM2
6,6
GNM3
3,5
5
TNM3
ANM3
PNM3
1,6
2,1
LEGEND
Thermocouple
Particles detector
Opacimeter
Anemometer
Gas detector

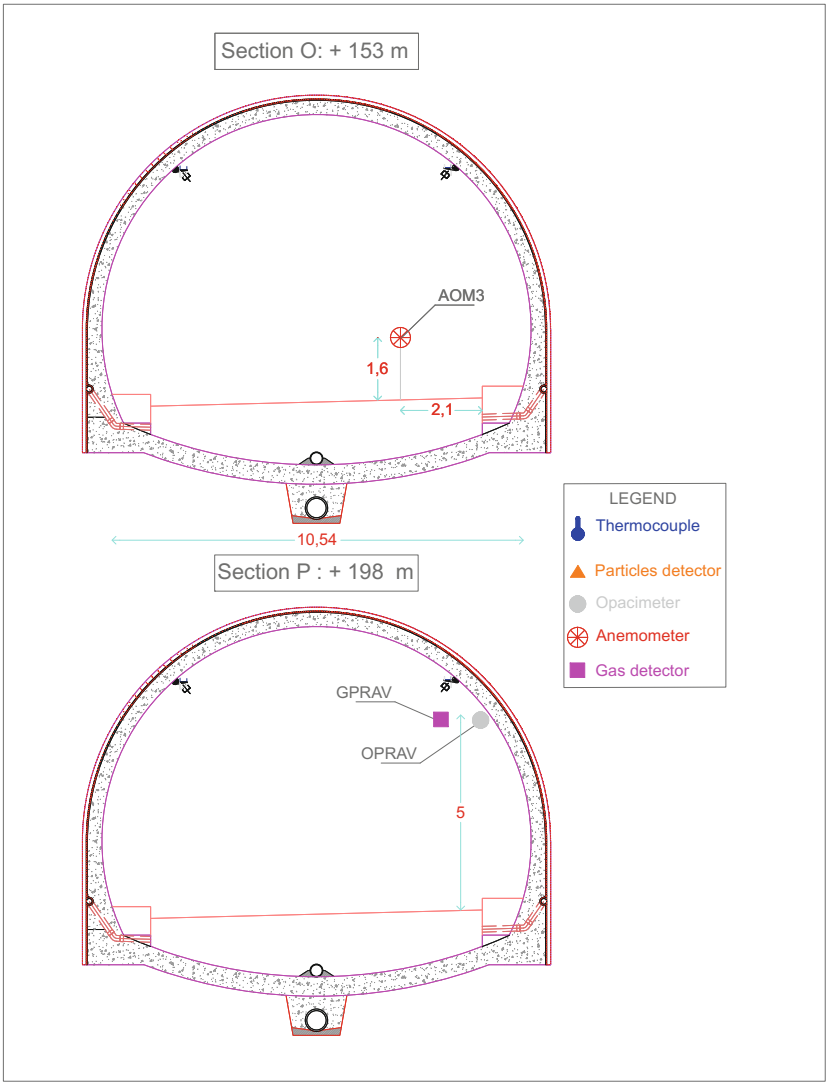
Section O: + 153 m
AOM3
1,6
2,1
10,54
Section P : + 198 m
GPRAV
OPRAV
5
LEGEND
Thermocouple
Particles detector
Opacimeter
Anemometer
Gas detector

Annex B
Selected Experimental Results of the Morgex Fire Tests

In the following some of the relevant temperature profiles measured in the two Morgex fire tests are reported. Details about the location of the devices inside the tunnel can be found in Table 3.9 as well as in the Annex 1.

Temperature measurements: Fire Test #1

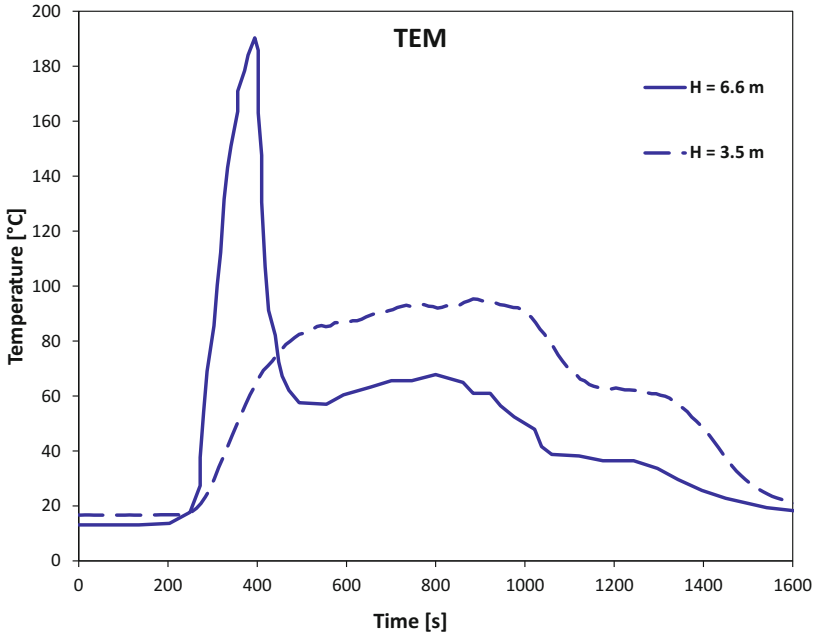

F. Borghetti et al., *Tunnel Fire Testing and Modeling*,
PoliMI SpringerBriefs, DOI 10.1007/978-3-319-49517-0

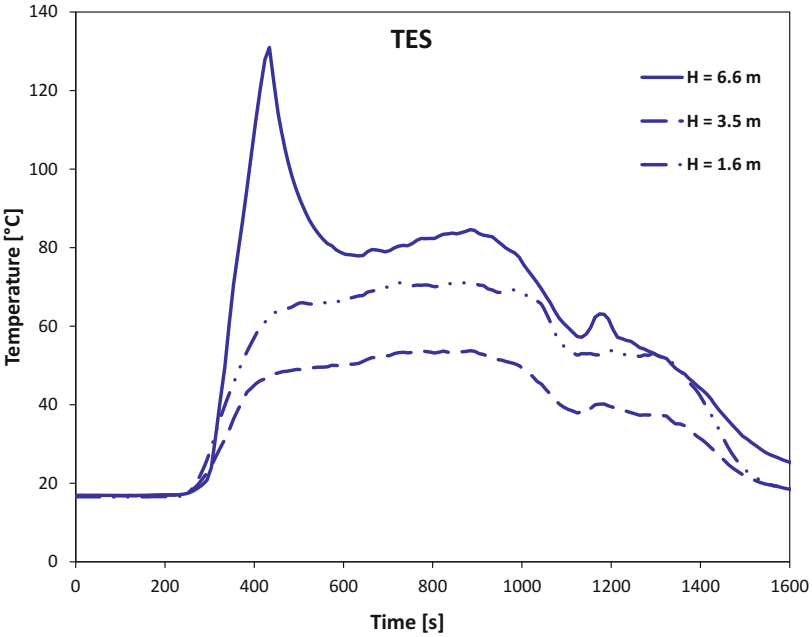
TES
H = 6.6 m
H = 3.5 m
H = 1.6 m
Temperature [°C]
Time [s]
0
20
40
60
80
100
120
140
0
200
400
600
800
1000
1200
1400
1600

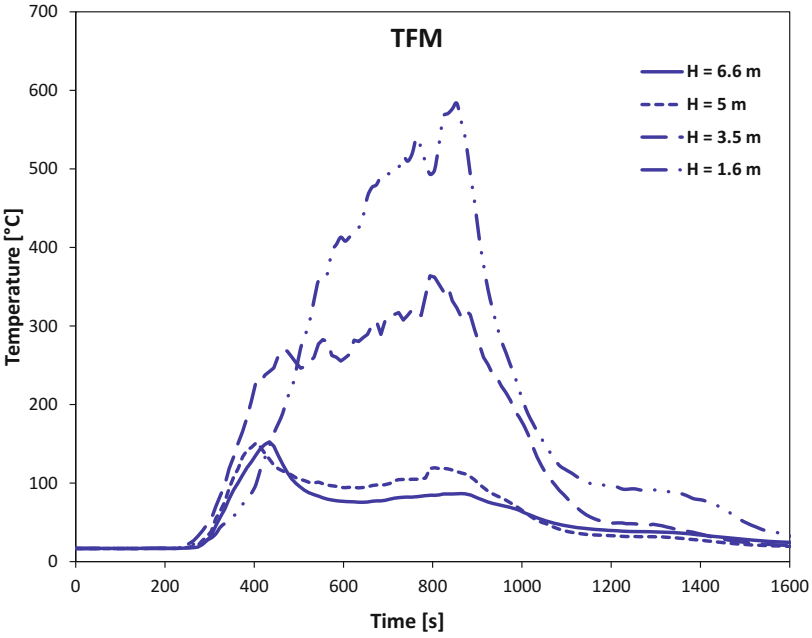
TFM
H = 6.6 m
H = 5 m
H = 3.5 m
H = 1.6 m
Temperature [°C]
Time [s]
0
100
200
300
400
500
600
700
0
200
400
600
800
1000
1200
1400
1600

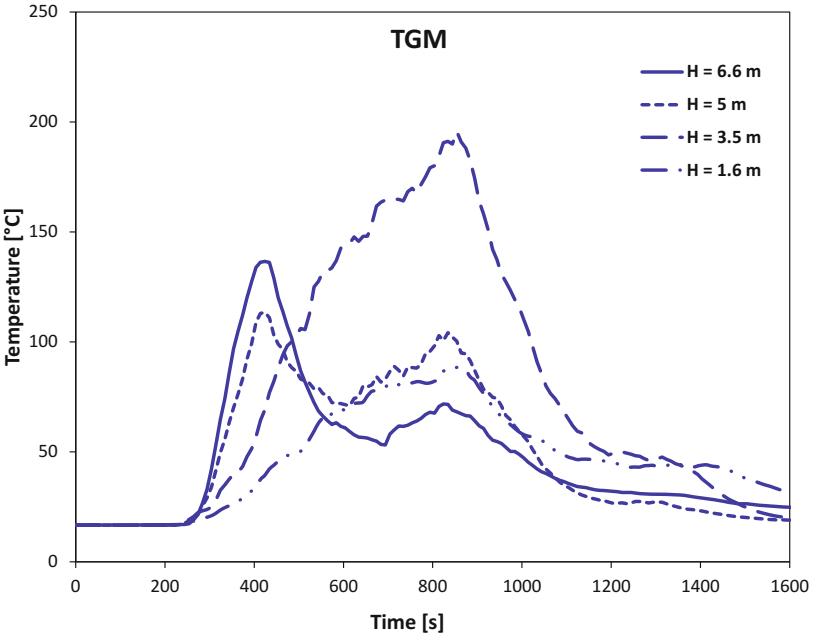
TGM
H = 6.6 m
H = 5 m
H = 3.5 m
H = 1.6 m
Temperature [°C]
Time [s]
0
50
100
150
200
250
0
200
400
600
800
1000
1200
1400
1600

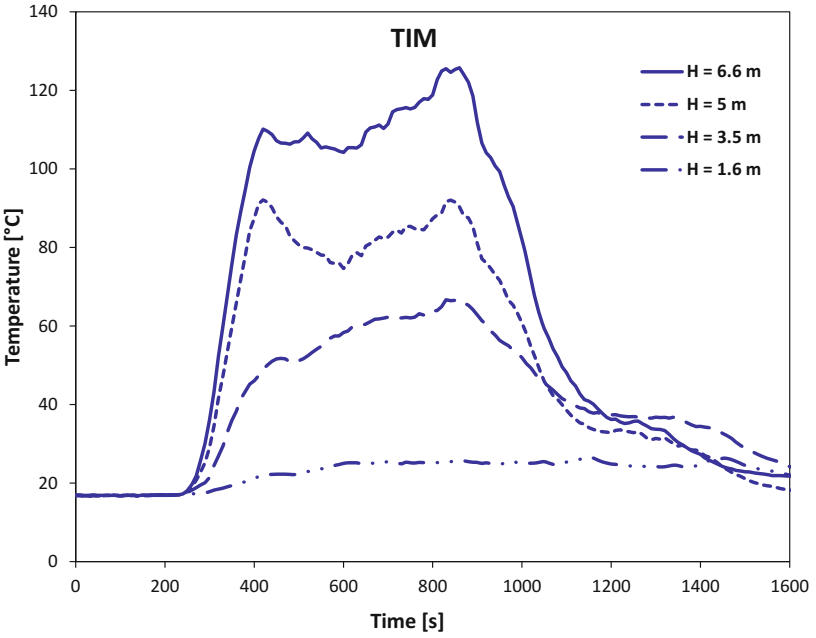
TIM
H = 6.6 m
H = 5 m
H = 3.5 m
H = 1.6 m
Temperature [°C]
Time [s]
0
20
40
60
80
100
120
140
0
200
400
600
800
1000
1200
1400
1600

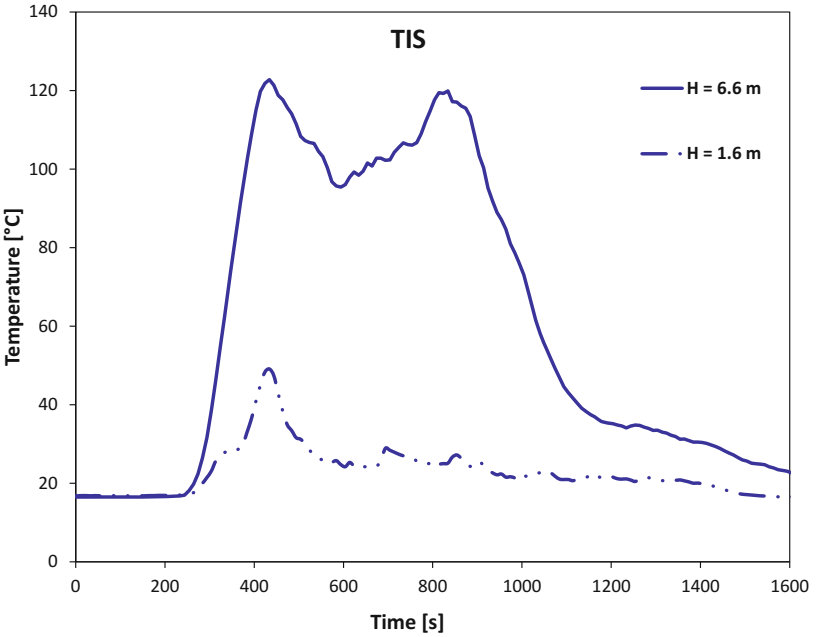
TIS
H = 6.6 m
H = 1.6 m
Temperature [°C]
Time [s]
0
20
40
60
80
100
120
140
0
200
400
600
800
1000
1200
1400
1600

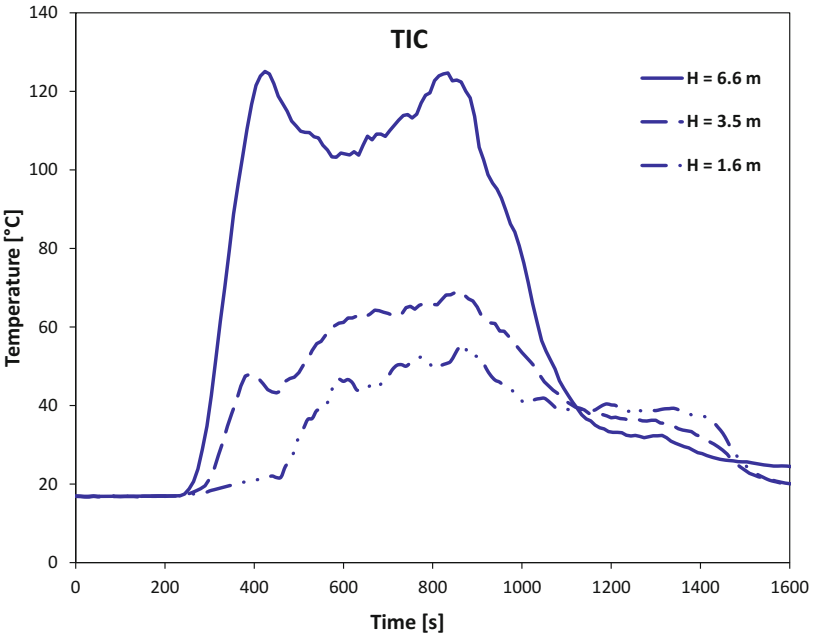
TIC
H = 6.6 m
H = 3.5 m
H = 1.6 m
Temperature [°C]
Time [s]
0
20
40
60
80
100
120
140
0
200
400
600
800
1000
1200
1400
1600

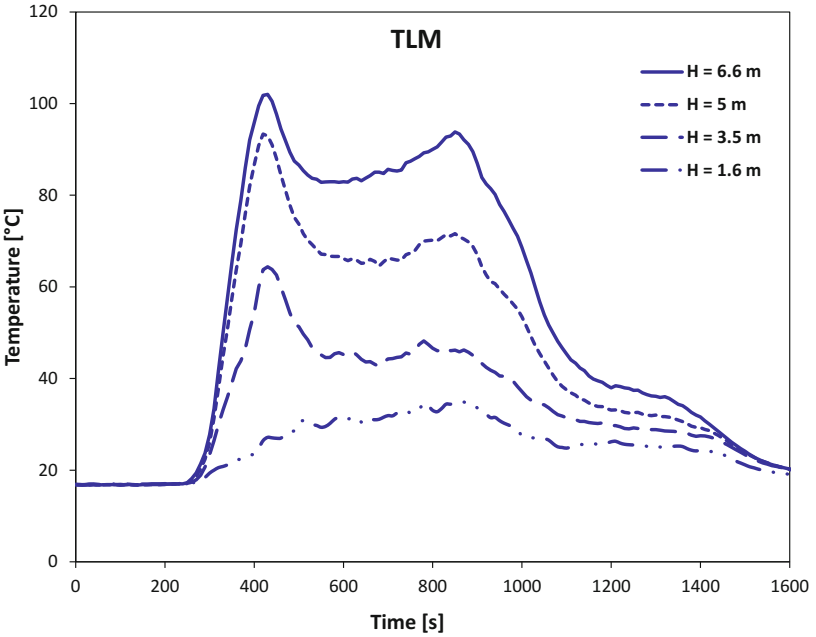
TLM
H = 6.6 m
H = 5 m
H = 3.5 m
H = 1.6 m
Temperature [°C]
Time [s]
0
20
40
60
80
100
120
0
200
400
600
800
1000
1200
1400
1600

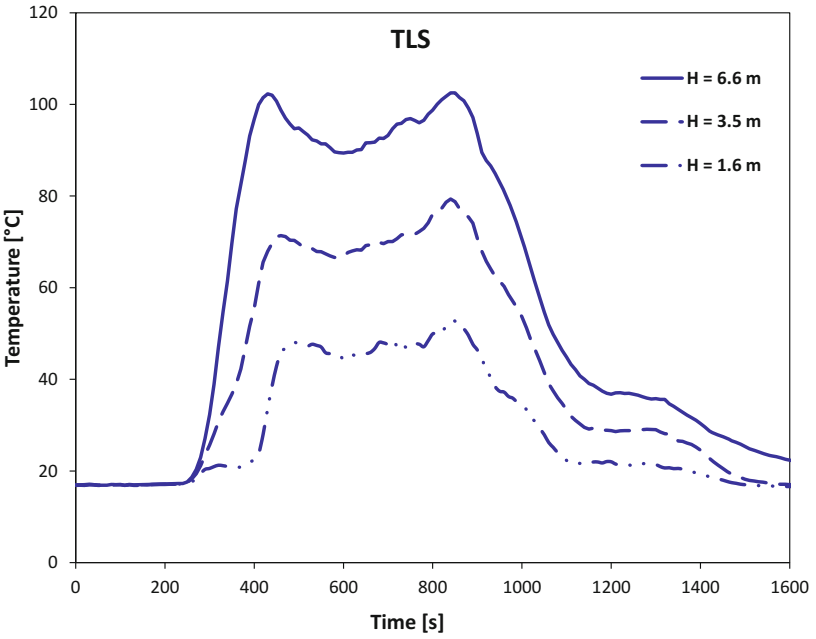
TLS
H = 6.6 m
H = 3.5 m
H = 1.6 m
Temperature [°C]
Time [s]
0
20
40
60
80
100
120
0
200
400
600
800
1000
1200
1400
1600

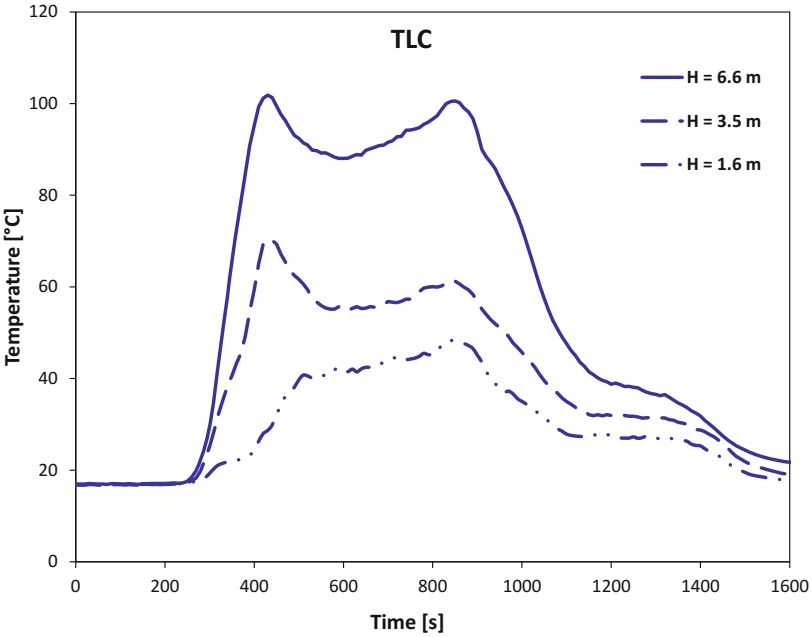
TLC
H = 6.6 m
H = 3.5 m
H = 1.6 m
Temperature [°C]
Time [s]
0
20
40
60
80
100
120
0
200
400
600
800
1000
1200
1400
1600

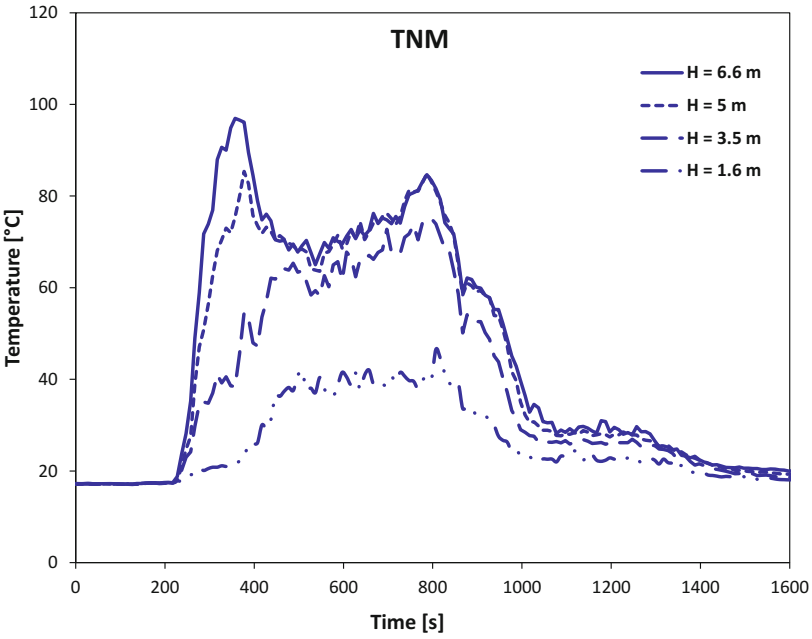
TNM
H = 6.6 m
H = 5 m
H = 3.5 m
H = 1.6 m
Temperature [°C]
Time [s]
0
20
40
60
80
100
120
0
200
400
600
800
1000
1200
1400
1600

Temperature measurements: Fire Test #2

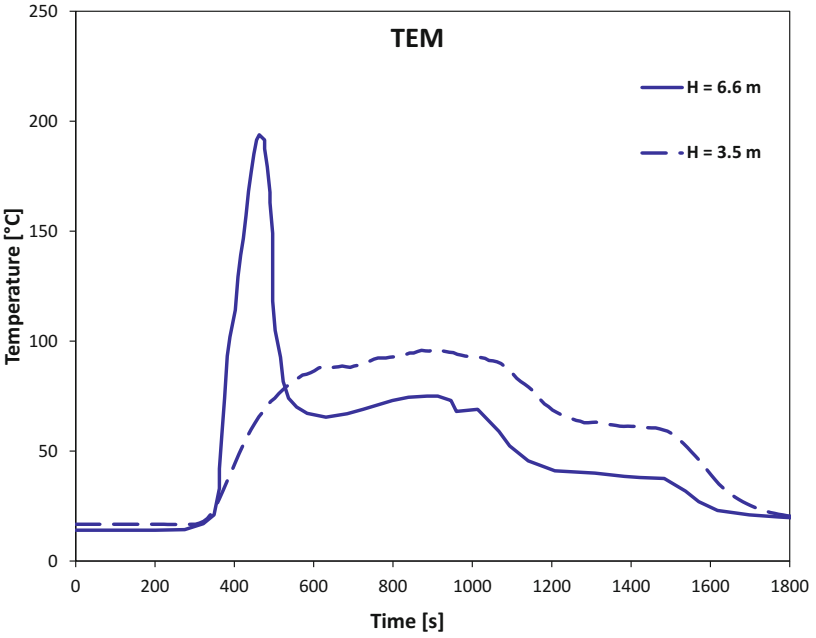

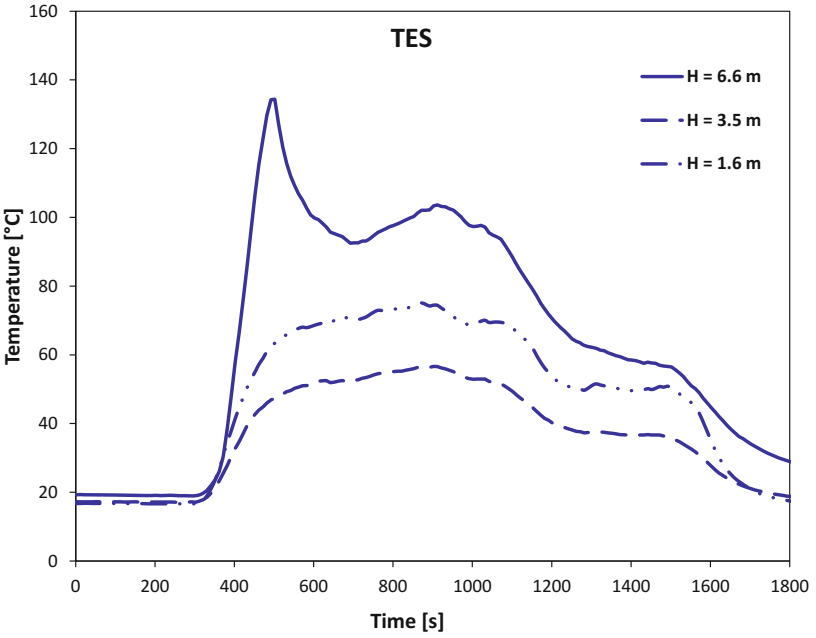

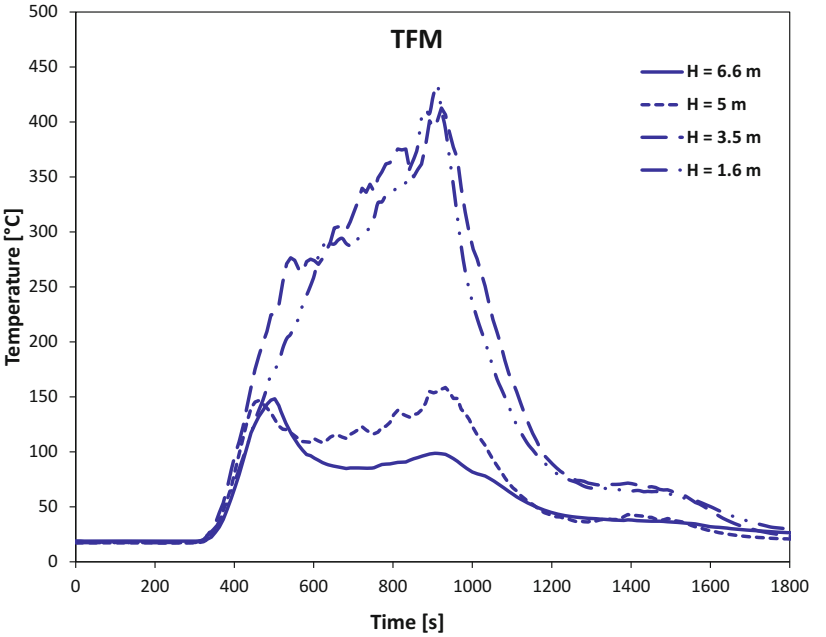
TFM
H = 6.6 m
H = 5 m
H = 3.5 m
H = 1.6 m
Temperature [°C]
Time [s]
0
50
100
150
200
250
300
350
400
450
500
0
200
400
600
800
1000
1200
1400
1600
1800

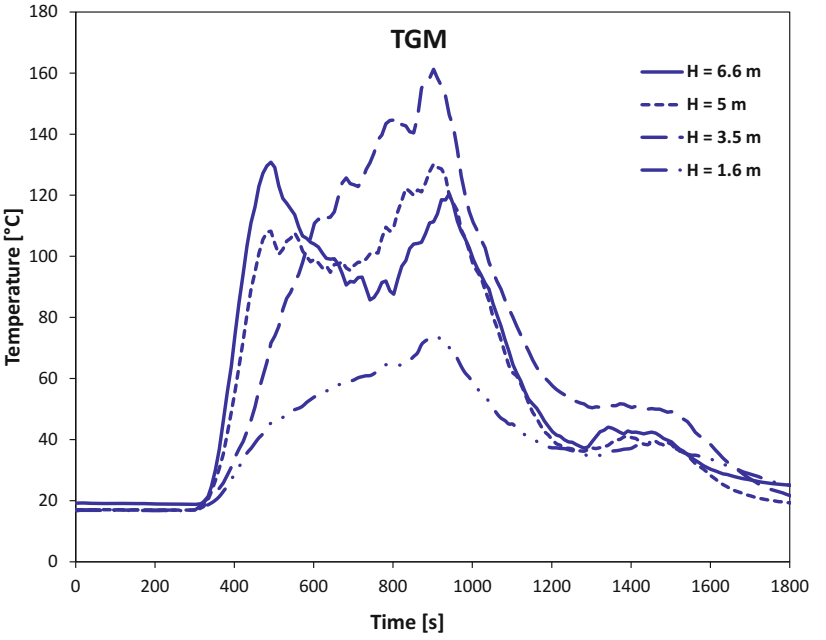
TGM
H = 6.6 m
H = 5 m
H = 3.5 m
H = 1.6 m
Temperature [°C]
Time [s]
0
20
40
60
80
100
120
140
160
180
0
200
400
600
800
1000
1200
1400
1600
1800

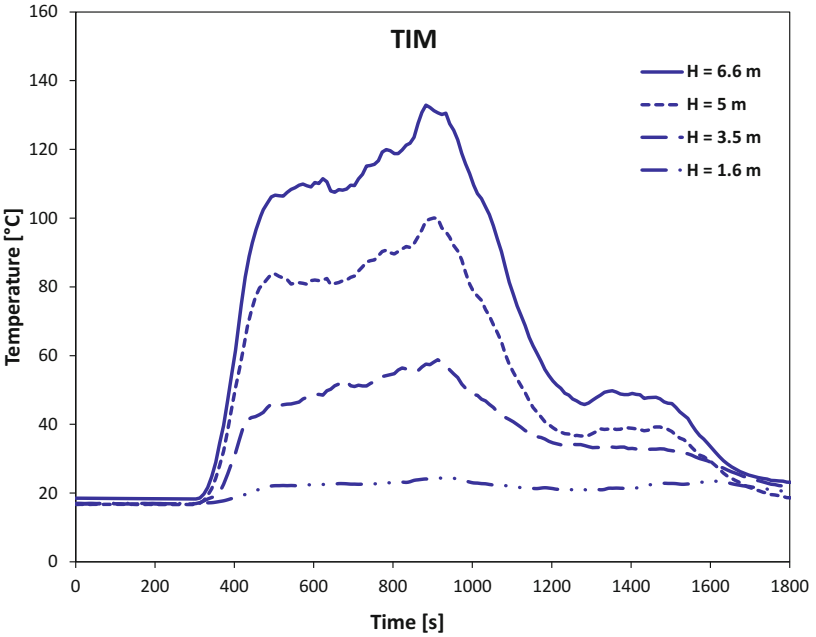
TIM
H = 6.6 m
H = 5 m
H = 3.5 m
H = 1.6 m
Temperature [°C]
Time [s]
0
20
40
60
80
100
120
140
160
0
200
400
600
800
1000
1200
1400
1600
1800

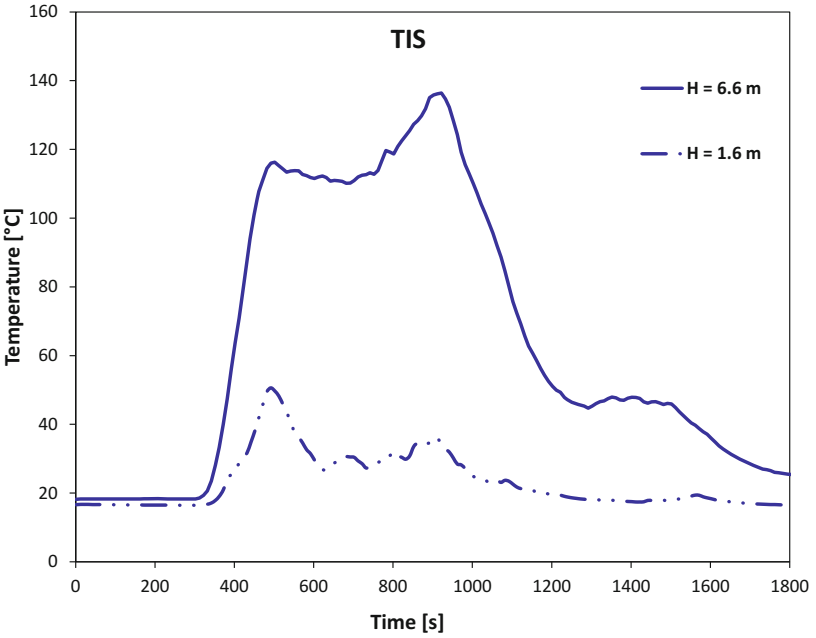
TIS
H = 6.6 m
H = 1.6 m
Temperature [°C]
Time [s]
0
20
40
60
80
100
120
140
160
0
200
400
600
800
1000
1200
1400
1600
1800

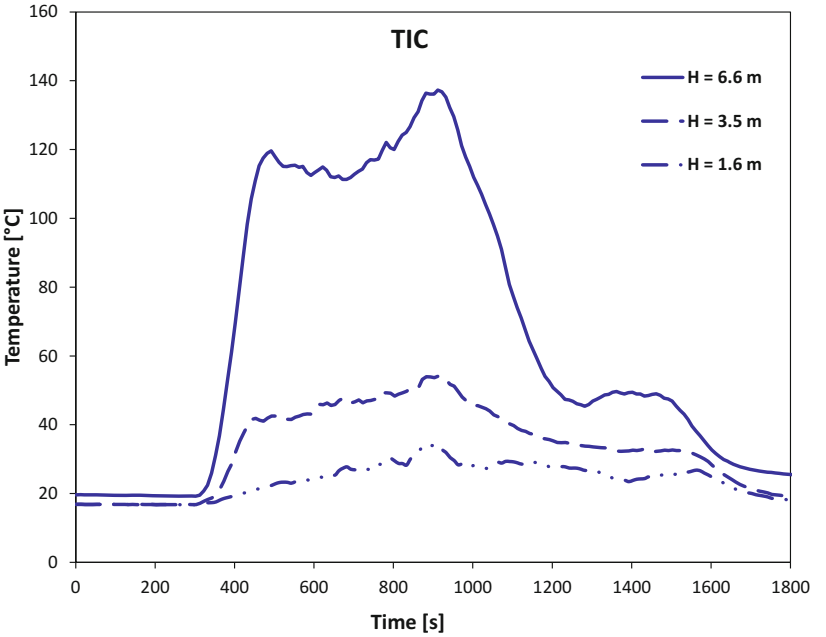
TIC
H = 6.6 m
H = 3.5 m
H = 1.6 m
Temperature [°C]
Time [s]
0
20
40
60
80
100
120
140
160
0
200
400
600
800
1000
1200
1400
1600
1800

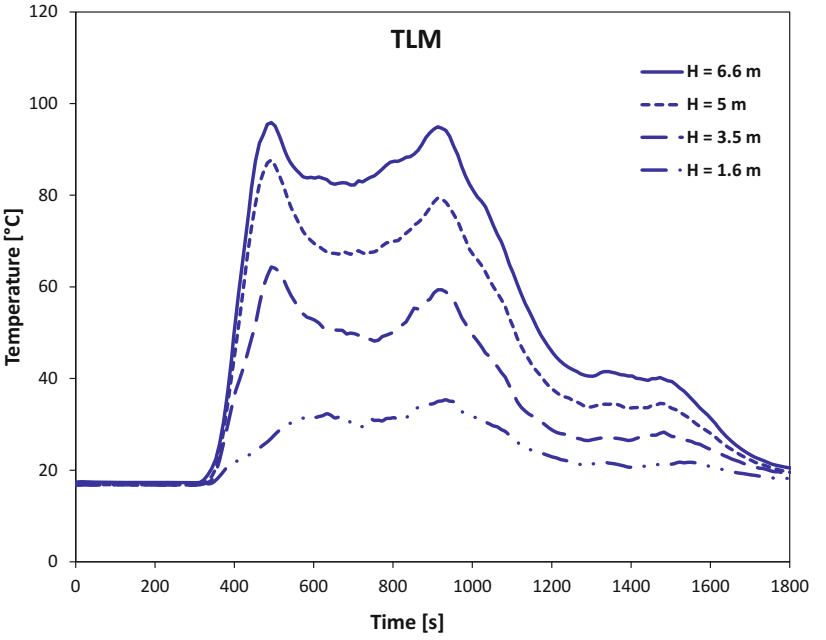
TLM
H = 6.6 m
H = 5 m
H = 3.5 m
H = 1.6 m
Temperature [°C]
Time [s]
0
20
40
60
80
100
120
0
200
400
600
800
1000
1200
1400
1600
1800

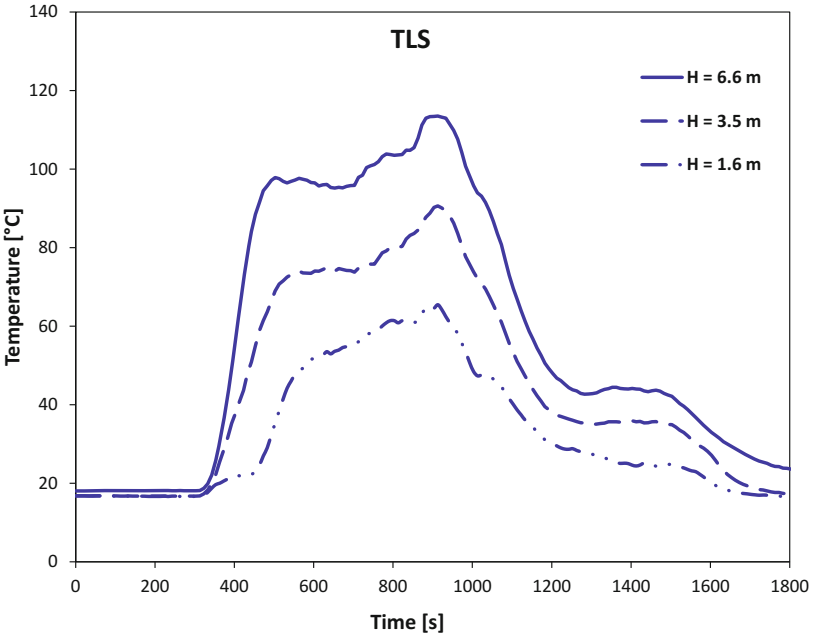
TLS
H = 6.6 m
H = 3.5 m
H = 1.6 m
Temperature [°C]
Time [s]
0
20
40
60
80
100
120
140
0
200
400
600
800
1000
1200
1400
1600
1800

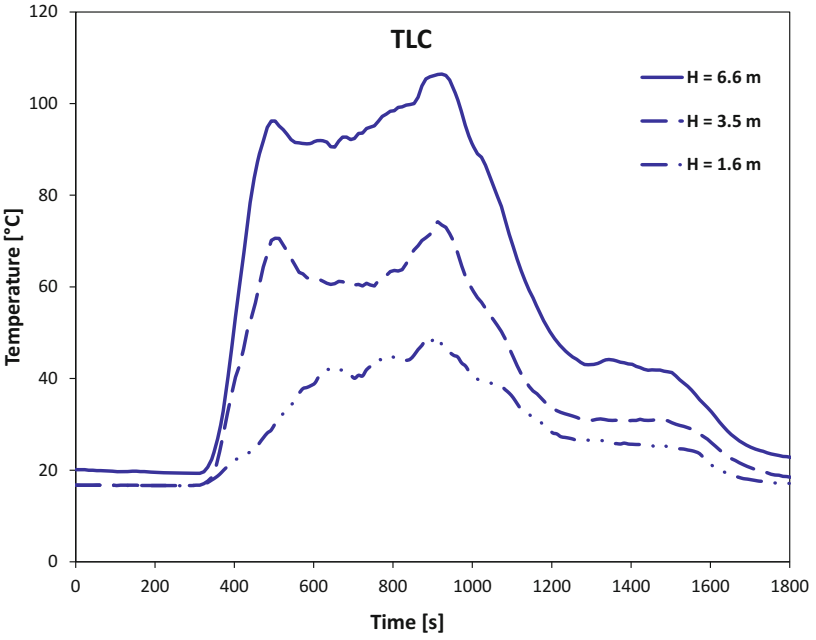
TLC
H = 6.6 m
H = 3.5 m
H = 1.6 m
Temperature [°C]
Time [s]
0
20
40
60
80
100
120
0
200
400
600
800
1000
1200
1400
1600
1800

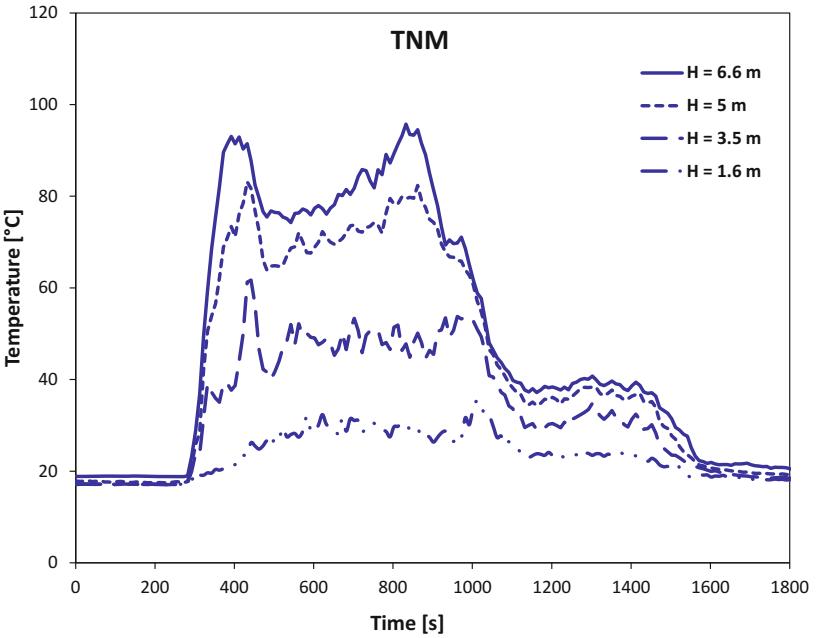
TNM
H = 6.6 m
H = 5 m
H = 3.5 m
H = 1.6 m
Temperature [°C]
Time [s]
0
20
40
60
80
100
120
0
200
400
600
800
1000
1200
1400
1600
1800